uOttawa

L'Université canadienne
Canada's university

FACULTÉ DES ÉTUDES SUPÉRIEURES ET POSTOCTORALES

uOttawa

L'Université canadienne
Canada's university

FACULTY OF GRADUATE AND POSDOCTORAL STUDIES

Silu Chen

AUTEUR DE LA THÈSE / AUTHOR OF THESIS

M.A.Sc. (Electrical and Computer Engineering)

GRADE / DEGREE

School of Information Technology and Engineering

FACULTÉ, ÉCOLE, DÉPARTEMENT / FACULTY, SCHOOL, DEPARTMENT

Improving Algorithms for Oscillometric Blood Pressure Estimation by Suppressing Breathing Effects

TITRE DE LA THÈSE / TITLE OF THESIS

Miodrag Bolic

DIRECTEUR (DIRECTRICE) DE LA THÈSE / THESIS SUPERVISOR

Voicu Groza

CO-DIRECTEUR (CO-DIRECTRICE) DE LA THÈSE / THESIS CO-SUPERVISOR

Milmi Dajami

Adrian Chan

Gary W. Slater

Le Doyen de la Faculté des études supérieures et postdoctorales / Dean of the Faculty of Graduate and Postdoctoral Studies

Improving Algorithms for Oscillometric Blood Pressure Estimation by Suppressing Breathing Effects

By
Silu Chen

A Thesis
Presented to School of Graduate Studies and Research
In partial fulfillment of the
Requirements for the degree of

Master of Applied Science

Electrical and Computer Engineering
University of Ottawa

Your file Votre référence
ISBN: 978-0-494-73865-8
Our file Notre référence
ISBN: 978-0-494-73865-8

I hereby declare that I am the sole author of this document. I authorize the University of Ottawa to lend this document to other institutions for the purpose of scholarly research.

Silu Chen

I further authorize the University of Ottawa to reproduce this document by photocopying or by any other means, in total or in part, at the request of other institutions or individuals for the purpose of scholarly research.

Silu Chen

The University of Ottawa requires the signatures of all persons using or photocopying this document. Please sign below, and give address and date.

Abstract

Blood pressure estimation by the oscillometry is a practice growing in popularity. Algorithms for blood pressure estimation are diverse, however little effort has been put forth to assess their performance. This thesis first surveys and assesses the algorithms used for oscillometric blood pressure estimation. Of all the known algorithms, the results of this work revealed one procedure which performed the best. These algorithms were evaluated by readings from two trained nurses. Next, we developed algorithms for extracting and suppressing breathing effects on blood pressure estimation. Breathing causes fluctuation in blood pressure and current oscillometric devices do not account for these effects. Extracting breathing signals extends the capabilities of existing oscillometric devices, such as reporting respiratory sinus arrhythmia, without the need for hardware changes. Suppression of these effects is performed by homomorphic and adaptive filtering. Results show improvement in that estimated pressure after suppression was closer to the nurse readings.

Acknowledgments

This thesis would not have been completed without the help and support I received. I would like to acknowledge all those who have provided me with the opportunity to complete this thesis and my graduate studies.

First, I would like to thank my supervisors at the School of Information Technology and Engineering at the University of Ottawa, Dr. Miodrag Bolic and Dr. Voicu Groza. I am deeply grateful for both the guidance and support they have provided me during the course of my research.

I would also like Biosign Technologies Inc. and the Ontario Centres of Excellence (OCE) for their collaborative research support and funding. I wish to further thank Biosign Technologies Inc. for providing the samples and equipment to use for my research.

The work here could also not have been completed without the support and aid of fellow research team members including Professor Dr. Hilmi Dajani and research collaborators Dr. Izmail Batkin and Dr. Sreeraman Rajan. To their countless hours of guidance and support, I am extremely grateful. I would also like to thank and acknowledge postdoctoral fellows Dr. Saif Ahmad, Dr. Soojeong Lee, Dr. Balakumar Balasingam, fellow graduate students Karen Soueidan, Mohamad Forouzanfar, Majid Mafi and past undergraduate students Aly Shoukry and Mukul Tewary. It has been a pleasure collaborating with each member of the team.

And finally I would like to express my gratitude and appreciation to my family and friends for their understanding and encouragements for the period of my graduate studies.

Table of Contents

List of Figures

List of Tables

List of Acronyms

ALE: Adaptive line enhancer - An adaptive filter scheme that uses a reference signal.

AM: Amplitude modulation - Embedding information of a carrier onto the envelope of a message wave

ANC: Adaptive noise canceller - An adaptive filter scheme that does not use a reference signal.

CP: Cuff pressure - Name of one of two curves returned by the Biosign UFIT that contains information on the cuff deflation.

DBP: Diastolic blood pressure - Minimum pressure produced in the arteries at the end of the cardiac cycle.

ECG: Electrocardiogram - Noninvasive recording of the electrical activity of the heart.

FM: Frequency modulation - Embedding information of a carrier onto the instantaneous frequency of a message wave

HF: High frequency - One of three frequency ranges that are known to contain part of the physiological variability of blood pressure (between 0.15 to 0.5 Hz), known to be caused by breathing effects.

HRV: Heart rate variation - The natural tendency of the fluctuation in the time intervals between heart beats.

LAA: Linear approximation algorithms - Height based algorithm to find blood pressure in oscillometry that is based on approximation linear lines of best fit.

LF: Low frequency - One of three frequency ranges that are known to contain part of the physiological variability of blood pressure, known to be caused by the Mayer wave.

MAA: Maximum amplitude algorithm - Height based algorithm to find blood pressure in oscillometry that is based on characteristic ratios.

MAE: Mean absolute error - Quantity to measure error by finding the absolute error between an estimated value and a reference value, then computing the mean.

MAP: Mean arterial pressure - Average arterial blood pressure of a person.

mmHg: Millimeters Mercury - Commonly used unit adopted in blood pressure to measure pressure.

Chapter 1 - Introduction

1.1 Blood Pressure Estimation

Blood pressure provides a measure of a subject's state of health and is one of the most commonly measured physiological parameters. High blood pressure is a dangerous condition that if left untreated, can lead to heart disease, stroke and other health problems. One in three adults in the USA has high blood pressure, but nearly a third of them are unaware of it [1].

Blood pressure is typically reported in terms of millimetres of mercury (mmHg) and two values are estimated: systolic and diastolic blood pressure (SBP and DBP). Physiologically, SBP is the pressure pushing blood flow in the arteries near the beginning of a cardiac cycle, when the heart contracts, or systole. This is the maximum pressure in the arteries. DBP occurs at the opposite end of the cardiac cycle, when the heart relaxes in between beats. Here, the heart reaches diastole and the pressure produced in the arteries is at its minimum level [2].

Methods of measuring blood pressure vary between invasive and noninvasive methods. An intra-arterial measurement, the most common invasive method, is recognized as the most accurate [3], but has obvious disadvantages in complexity and inconvenience. Noninvasive methods, like oscillometric, palpitation or auscultation are preferred in common situations such as home monitoring or at health check clinics. One of the most popular noninvasive methods is oscillometry, which is widely used in the home blood pressure monitoring market due to its simplicity and ease of use [4].

Oscillometric measurements are based on sensing the pressure pulsations from a cuff wrapped around a subject's bicep or wrist. This method was first discovered by Marey in 1876, who detected oscillations imposed on an arm cuff by arterial pulsations [5]. The oscillometric method works by inflating a cuff to a pressure above SBP and then deflating to a pressure below DBP. Deflating the cuff produces a decreasing curve which represents the pressure as it drops from a high to low value. Along with the cuff deflation, pressure oscillations induced by the beat-to-beat pulsations in the subject's artery are superimposed

onto this curve. From these pressure oscillations, numerous existing algorithms to estimate the SBP and DBP have been proposed [4].

Blood pressure values are also known to fluctuate over time. These natural fluctuations create variability in SBP and DBP and have been previously studied and quantified spectrally [6]. A large part of this variation is attributed to respiration, or breathing [7], whose effects were first discovered by Hales [8]. Subjects who breathed normally were found to have a variation of about 3 to 6 mmHg in SBP, while subjects who breathed deeply exhibited a variation of about 15 to 20 mmHg [9]. In both cases, this fluctuation is quite large and is a potential cause for inaccuracy in the estimation of blood pressure.

1.2 Motivation and Problem Statement

Studies regarding the performance of the oscillometric method have shown mixed results in its estimates of SBP and DBP [10]-[14]. Some show that oscillometric readings agree with intra-arterial and Korotkoff sound measurements [10], whereas others have shown a large deviation in readings between commercially available devices [11], [12] or large error when measuring subjects in uncontrolled situations [13] or for unhealthy subjects [14]. These studies criticize the performance of these devices but do not focus on the underlying basis of all these devices, the algorithms.

Blood pressure measurements by the method of oscillometry is defined by the physical procedure of deflating a cuff wrapped around a subject's arm, but methods to harvest information from these measurements are not rigidly defined. After an oscillometric blood pressure measurement has taken place, estimating blood pressure is strictly based on the operations of algorithms to find the SBP and DBP. From a literature review, a large variety of methods were discovered that estimate blood pressure but these methods were scattered around many different publications or sources. Considering that oscillometric devices dominate the home blood pressure monitoring market, surprisingly little effort has been put forth to assess the underlying algorithms which are actually used to estimate blood pressure.

Inaccuracies in estimation can come from the natural fluctuations that are inherent in blood pressure, which include breathing, or artifactual or physiological phenomena. In this case, the term inaccuracy corresponds to blood pressure estimates which may not be truly representative of a subject's actual blood pressure, but instead is heavily influenced by some other natural physiological processes. Breathing is a natural, automatic process that everyone must engage in, yet can also induce fluctuations in SBP and DBP estimates. Breathing effects on blood pressure are already quite well known, but to the best of our knowledge, no work found has attempted to reduce these effects in oscillometric waveforms. Breathing effects leads to alterations in the signal recorded during an oscillometric measurement. Proper suppression of these effects could yield SBP and DBP estimations that are more representative of a subject's blood pressure than algorithms that do not account for these effects.

1.3 Prior Art

Prior work on oscillometric blood pressure recordings is scattered around a variety of works. After an oscillometric recording, a deflation curve is returned. Estimation of SBP and DBP is performed based on an algorithm composed of several steps that processes this deflation curve. The individual steps of this algorithm have been proposed in many independent studies, but there exists a lack of unification between the existing methodologies. Generally, the procedure that composes the algorithm is as follows:

1. Extract an oscillometric waveform (OMW) from the deflation curve
2. Choose an oscillometric pulse index (OPI)
3. Perform envelope cleaning
4. Find the SBP and DBP points on the envelope
5. Locate the corresponding actual SBP and DBP points on the deflation curve

Existing methods for steps 1 to 4 are quite diverse and varying. In the first step, extracting an OMW is necessary to identify pulsations that are caused by blood flow. The OMW should contain only the pulsations caused by the artery as it reacts to the decreasing cuff pressure. The downward trend relating to the cuff deflation should be removed to create the OMW. This can be performed by digital filtering (band pass [16], [17] or high pass [18]), analog filtering [9] or detrending [19], [20]. From the OMW, a definition of an OPI is then required

as part of step 2. The OPI forms an envelope where points which correspond to SBP and DBP are located in later steps. The OPI can be taken as the height from baseline-to-peak, peak-to-peak, or area of each pulse [4], [19], [21], [22]. The OPI should form a locus, or envelope, for which cleaning techniques in step 3 are employed. This step is aimed at cleaning the envelope from any possible disturbances caused by noise or interference and is necessary for the algorithms later on in step 4 that estimate SBP and DBP values. Methods here include frequency domain filtering [16], [18] median filtering [23], moving average filtering [24]-[25], fuzzy logic [26], [27], curve fitting [27], [28], [29] and methods that identify and replace corrupted pulses heuristically [9], [20], [30]. These methods are intended to be a general purpose way rid the envelope formed by the OPI from noise or other interference. Afterwards, step 4 is performed where points that correspond to the SBP and DBP are found on the now cleaned envelope. Four known algorithms have been surveyed for this: the maximum amplitude algorithm (MAA) [9], [16]-[18], [21], [22], [24], [25], linear approximation algorithm (LAA) [31], points of maximum/minimum slope algorithm (MMSA) [21], [22], [32], [33], and slope change algorithm (SCA) [34]. Variations of these algorithms also exist, but these four represent the fundamental algorithms which others are based on. Finally, step 5 is locating the SBP and DBP points on the cuff deflation curve to provide proper estimates of SBP and DBP in terms of mmHg.

Although a number of algorithms exist for estimating SBP and DBP, to the best of the author's knowledge nobody has assessed or evaluated these different algorithms against each other. Some work that address the current state of oscillometric measurement techniques exist [4], [22], [35], [36], but the underlying algorithms behind these devices lack a more critical assessment. One objective of this work to fulfill this need and compare the different algorithms in each step of the procedure. This is important because further work on oscillometry requires an algorithmic procedure for oscillometric blood pressure estimation.

Envelope cleaning methods in step 4 of the algorithm are performed to reduce irregularities caused by noise or other interference in the OMW in a general way; that is they try to capture the useful information in the envelope while removing all other irregularities. However, breathing, one source for irregularities in the envelope, is known to be a major influence and

cause of large variations in blood pressure estimation. These effects are taken into more consideration in this work. Existing studies have shown that the presence of breathing in blood pressure recordings can lead to larger error when estimating SBP and DBP values [9], [37]. Currently, studies on the effects of breathing have been performed using intra-arterial blood pressure recordings. From this, breathing information is known to manifest itself through amplitude modulation, frequency modulation and additive effects [38].

Demodulation has been applied to estimate the subject's breathing signal [8] and adaptive filtering with a reference signal has been used to remove breathing effects from the intra-arterial waveform [40]. The use of demodulation has been adapted from popular methods that derive breathing from ECG signals [41]-[44]. To the best of the author's knowledge, methods that investigate or reduce breathing effects in oscillometric recordings have never been published before.

1.4 Contributions

Major contributions of this work are listed below:

- Provide a comparison of most popular oscillometric algorithms and sub-algorithms
- Extract breathing signals from oscillometric measurements and study there effects on blood pressure estimation
- Suppress breathing effects in blood pressure to improve SBP and DBP estimates
- Extract respiratory sinus arrhythmia, a quantity not typically returned by oscillometric devices

Different algorithms to estimate SBP and DBP from oscillometric recordings exist. These algorithms need to be properly evaluated. The contribution of the work performed here is to first provide a critical assessment of many of these algorithms. First, existing algorithms are surveyed and then implemented. Second, their performance is assessed based on comparing the estimated SBP and DBP values produced by the algorithms with some reference blood pressure readings. No development of any new algorithms is claimed but this work does provide meaningful contribution in surveying the current oscillometric algorithms and assessing their performance. This also helps to determine which algorithm is most accurate

for estimating SBP and DBP in comparison to nurse readings. The work in Sections 3.1 to 3.9 and the partial results of Chapter 4 have led to a publication in IEEE Instrumentation and Measurement Conference [45].

Breathing effects have been investigated and reduced in other cardiac recordings such as the ECG and intra-arterial blood pressure signals. These effects have never been studied in oscillometric recordings before. Another contribution of this work is to provide an analysis of breathing in oscillometric recordings and the suppression of its effects to provide better SBP and DBP estimates is a third contribution of this work. Existing studies also all require a reference breathing signal to be explicitly provided for the operation of the cancellation scheme. This work will show that breathing effects may be suppressed in oscillometric recordings without the need of any additional reference signal, reducing cost and complexity compared to other studies which require an additional signal [39],[40],[72]. The results of this study led to a publication in [46]. This includes Sections 5.1 to 5.8, 6.1 and 6.3. An extension of this work has also submitted for publication in a special issue of IEEE Transactions on Instrumentation and Measurement [47], which also includes Section 5.9 to 5.11, 6.4 and 6.5. Currently, this publication [47] is in the revision process.

In addition to the aforementioned two publications, the contribution of this work has also led to the publication of an additional three conference proceedings which used the algorithms developed here [48]-[50]. In [48] and [49], two statistical analyses on the fluctuations in blood pressure are presented. The blood pressure estimation algorithms assessed here in Chapter 3 are used in these two studies. A prototype system which uses National Instruments hardware and LabView software was published in [50]. This system is used to acquire synchronous ECG and blood pressure data and incorporates the breathing extraction algorithms developed in Chapter 5.

1.5 Analysis

Figure 1.1 shows a block diagram of the overall work performed in this thesis. The ultimate goal is to provide a system where the inputs are the oscillometric recordings and the outputs are the accurately estimated SBP and DBP values. The implemented algorithms presented as

solid blocks in this figure (extract OMW, define OPI, envelope cleaning and SBP/DBP algorithms) rely on existing published algorithms. Blocks inside the large dashed block of this figure represent how breathing effects are dealt with and are newly developed algorithms for the purpose of this work. ECG signals are used here to assist development of the algorithms that deal with breathing. However, the developed algorithms for suppression of breathing effects may also operate without ECG as well. Breathing suppression algorithms are specific type of envelope cleaning and operate just before general envelope cleaning methods are implemented. Breathing signal extraction also leads to estimation of respiratory sinus arrhythmia (RSA) values. Extracted RSA can provide information that is correlated to other physiological mechanisms such as stress, obesity, diabetes, and more [15]. A major contribution of this work is to extract this information using only oscillometric recordings as this can greatly extend the capabilities of existing oscillometric devices without having to change existing hardware or add new hardware. The methods employed for these two blocks are new and have never been applied to oscillometric recordings before.

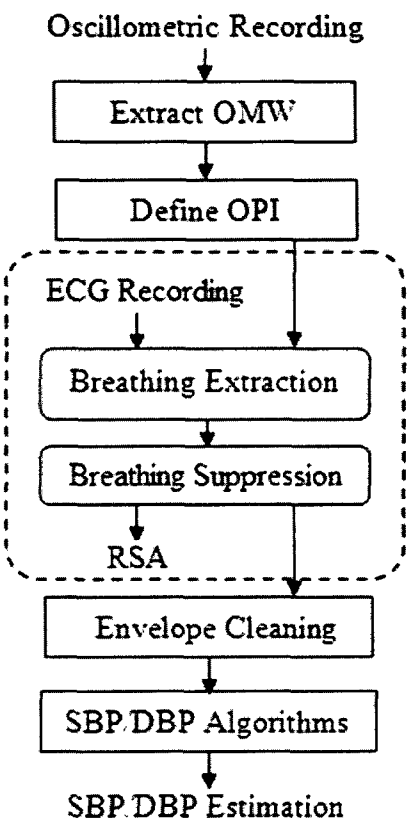

Figure 1.1. General outline for work proposed in this thesis.

To create the system shown in Figure 1.1, the analysis performed in this work will be completed as shown in Figure 1.2. Oscillometric algorithms were surveyed first and implemented in MATLAB. They were evaluated using a data set of 85 subjects provided by Biosign Technologies Inc. The performance of each algorithm was assessed with some defined metrics which use reference SBP and DBP readings that are also provided. The second step of this analysis is developing algorithms to suppress the effects of breathing in oscillometric measurements. These algorithms use some of the oscillometric algorithms to assist in detecting and extracting breathing. Performance metrics to assess these algorithms are defined and the algorithms are again applied on the data set provided by Biosign Technologies Inc. For breathing signal extraction, ECG recordings are also used to help develop these algorithms because of existing knowledge of the breathing effects on ECG. These ECG recordings are obtained by a BioHarness by Zephyr Technology. Recordings were performed in the room 3010 of SITE building at the University of Ottawa. Approval of these experiments was granted by a local ethics approval board. The approval notice is shown in Appendix A. The use of ECG signals here is to add different sources for extracting breathing and is optional, as oscillometric blood pressure estimates are improved with and without it. All work here was performed using Mathworks MATLAB version 7.10.0.499.

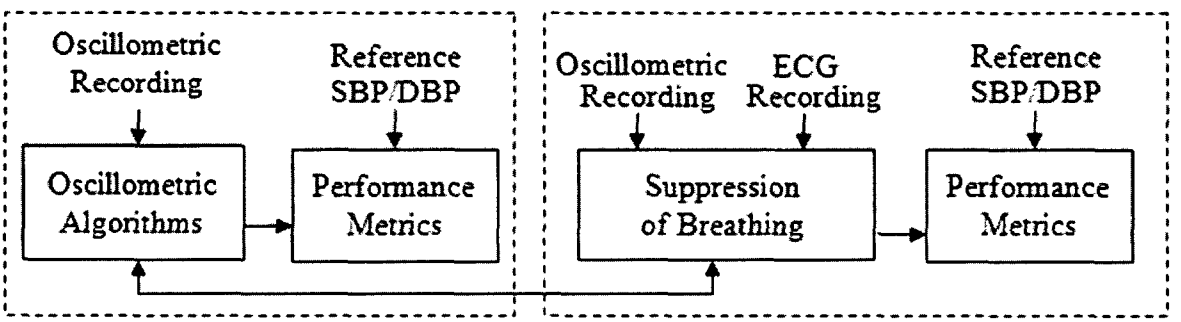

Figure 1.2. Block diagram of the analysis procedure.

1.6 Assumptions and Limitations

Algorithms for oscillometric recordings here are validated by comparison with reference values obtained either by two trained nurses or by an OMRON HEM-790 IT blood pressure monitor. The procedure underwent for obtaining reference readings follows that of SP10 standard, where one minute gap exists between subsequent nurse readings and oscillometric recordings [50]. Blood pressure values measured using intra-arterial methods would provide the best reference [3], but this is difficult to perform and unavailable for this study. In this

study, either nurse readings or readings from a commercial off-the-shelf blood pressure monitor are used as the reference blood pressure to compare our estimates to. As such, verification of estimates of this study must also take into account the potential discrepancies that exist in these readings as well.

Another limitation is the time delay between the acquisition of oscillometric blood pressure recordings and the reference readings. After a subject's recording, a reference blood pressure measurement is taken after waiting one full minute. However, blood pressure is known to fluctuate over time [6] and thus, the delay between these two events create a discrepancy between blood pressure values. Due to the known fluctuations, the subject's blood pressure could be different when the two measurements take place, producing a reference that is not representative of the subject's blood pressure at the time of the oscillometric recording. The reason for this delay is to follow current implemented safety standards put in place by SP-10 standards for recording blood pressure [51]. Ideally, the reference reading and the oscillometric recording should occur at the same time to account for this variability, but this is not possible for the safety of the subject.

1.7 Thesis Overview

The structure of this thesis is organized as follows: Chapter 2 surveys the current art in this field. Existing algorithms for oscillometric blood pressure estimation are explained. Existing work that studies breathing in blood pressure will also be reviewed to provide the proper fundamentals for the rest of the thesis. Chapter 3 details and compares the implementations of the algorithms for oscillometric blood pressure estimation. Chapter 4 presents the results of these algorithms implemented on a data set of 85 subjects. This chapter will also select a recommended algorithm for oscillometric blood pressure estimation based on this study. Chapter 5 presents the study on breathing in oscillometric blood pressure. Work on how to extract a breathing signal, its influence on blood pressure estimation, suppression of its affects and application to RSA will be provided here. Chapter 5 will show results and discussion for the work on breathing in oscillometry. Chapter 6 will end with a conclusion that summarizes the contributions of this thesis and presents potential future work in this field.

Chapter 2 – Prior Art

2.1 Oscillometric Blood Pressure Estimation

Many different algorithms for estimating blood pressure from the oscillometry have been published [4], [9], [17], [18], [21], [22]. These publications primarily focus on the sub-algorithms that compose of the entire algorithm, such as envelope extraction methods, artifact removal schemes or algorithms to extract SBP and DBP [16], [19], [20], [23]-[34]. Existing literature provides novel methods and algorithms, but in general, the overall procedure for blood pressure estimation from oscillometric recordings can summarized into the following procedure (repeated from Chapter 1):

1. Extract an oscillometric waveform (OMW) from the deflation curve
2. Choose an oscillometric pulse index (OPI)
3. Perform envelope cleaning
4. Find the SBP and DBP points on the envelope
5. Locate the corresponding actual SBP and DBP points from the deflation curve

These 5 steps are general, but provide an outline of the algorithm. Each step of this algorithm relies on a method or sub-algorithm which is discussed next. The goal of this chapter is to explain the current methodologies and algorithms that researchers have developed for oscillometric blood pressure estimation. Implementation of the algorithms will be performed in Chapter 3.

2.2 OMW Extraction

Recording the blood pressure signal by the oscillometric method involves wrapping a cuff around a subject's bicep or wrist and inflating the cuff to a pressure above SBP, then deflating it to a pressure below DBP. Standard cuffs deflate as linearly as possible, at a recommended rate between 2-3 mmHg per second [56]. A pressure transducer is used to measure the pressure inside the cuff. As the cuff deflates, the pressure transducer records a signal, known as the deflation curve, shown in Figure 2.1. Embedded on this curve is all the information regarding SBP and DBP data and it is the focus of all oscillometric algorithms.

Two main components comprise the deflation curve; the pressure from the deflating cuff and the pressure pulsations induced in the artery from the gradual deflation. The objective of this step is to extract these pressure pulsations, also known as oscillometric pulses [4], [9]. Over the duration of the recording, these pulses form a signal known as the OMW [36], but may also be referred to in some literature as the oscillogram [11], oscillometric pulse profile [18], oscillatory pressure curve [20], oscillometric signal [24], or simply as oscillation amplitudes [27]. The term OMW will be used here.

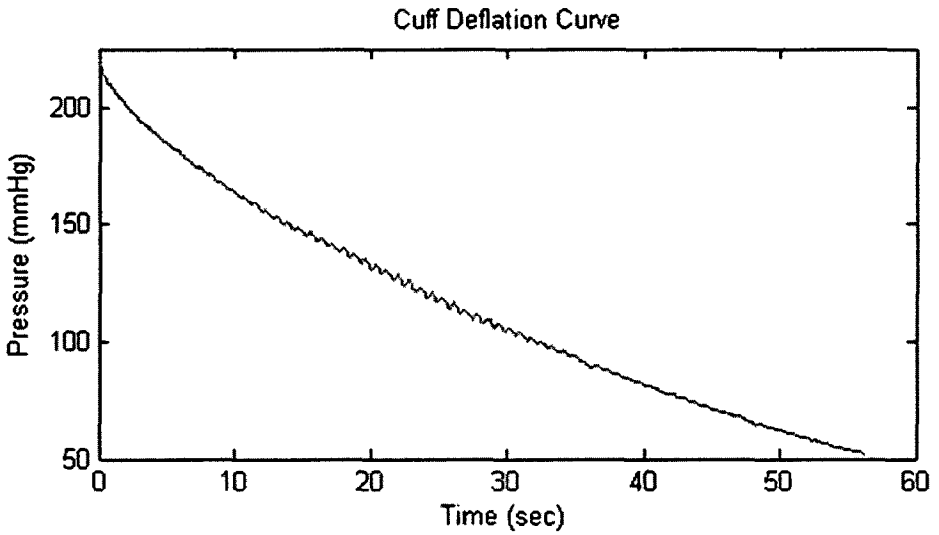

Figure 2.1. Typical cuff deflation curve

Methods to recover the OMW from the deflation curve consist of filtering [9], [16]-[18] and detrending [19], [20]. Filtering, either by band pass [16], [17] or high pass [9], [18], removes the frequency components that belong to the deflating cuff pressure (and sometimes, measurement noise) but keeps everything else, most importantly the frequency components that belong to the subject's pressure pulses. By setting a lower cutoff of the filter such that the deflation is eliminated, the remaining signal components are let in, which comprise the desired OMW. Existing literature usually sets the low cutoff of the high pass or band pass filter somewhere between 0.3 - 1 Hz [16]-[18]. Both band pass and high pass filters can be used for this application but typically, band pass filtering is used so that high frequency noise components that exist in the recording are eliminated as well. A plot of the OMW recovered by this method is shown in Figure 2.2 (a).

Obtaining the OMW may also be performed by detrending [19], [20]. In this method, a line of best fit represents the decreasing cuff pressure and then is subtracted from the deflation curve. Fitting the line requires locating the beginning of each individual pulse on the deflation curve. Points are then joined together on the deflation curve to produce a trend line that estimates of the decreasing cuff pressure [19], [20]. The end of one pulse is also the start of the next pulse so if these are all successfully found, joining them produces a trend line which connects all the pulses. Proper identification of the beginning and end of a pulse is of critical importance in this method so that the trend line is estimated properly. Interpolation is used in [19]. The main difference between detrending and filtering is that if the decreasing cuff pressure is properly estimated by detrending, then each pulse of the produced OMW should start at zero and at no point in the OMW should ever be negative. An example of the OMW extracted by this method is shown in Figure 2.2 (b). Typically, if detrending is used, a low pass filter is also implemented to reduce measurement noise in the deflation curve [19]. As shown in Figure 2.2, a normal OMW exhibits a characteristic envelope that starts off low in amplitude, increases to a maximum and then decreases back to low amplitude again.

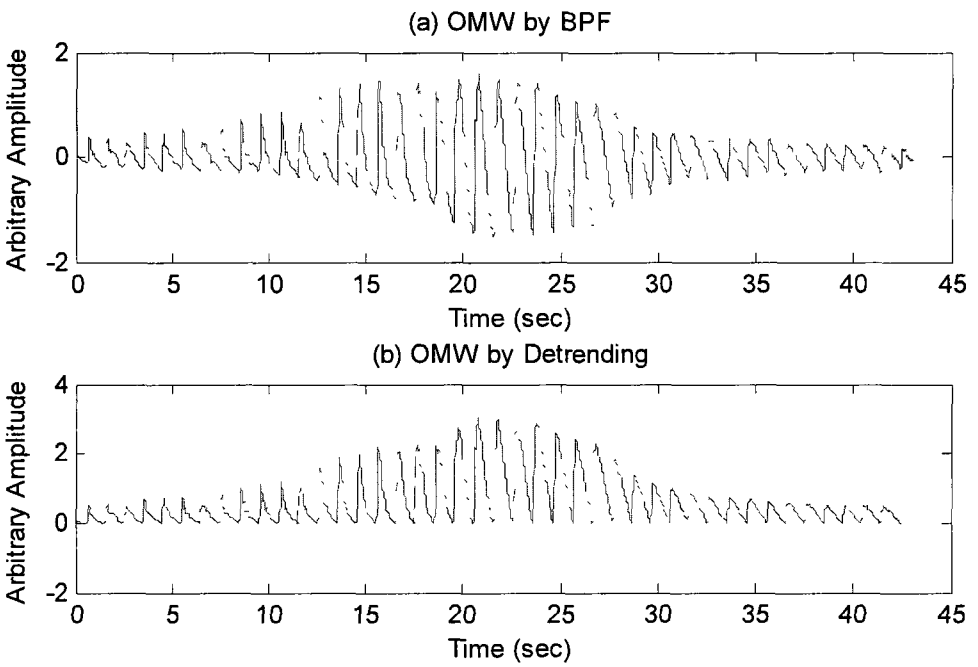

Figure 2.2. OMW extracted by (a) filtering and (b) detrending.

2.3 Peak Detection

An important step in the processing is peak detection in the OMW. Each heart beat corresponds to a pulse in the blood pressure signal and locating the maximum point of each pulse is important for blood pressure estimation. The peaks of each pulse are used to form an envelope for which points which correspond to SBP and DBP are located. Peaks are normally defined as the highest points on an amplitude varying waveform. The extracted OMW, as shown in Figure 2.2, are highly amplitude varying waveforms, exhibiting many local maxima and minima points. Locating each local maximum is a key step in blood pressure estimation. Peak detection is also a large area of interest in ECG analysis for which R-peak locations are desired. Algorithms for peak detection used here are based on existing ECG methods. The considered methods include using amplitude threshold methods combined with the Hilbert transform [52] or adaptive amplitude thresholds [53], slope based methods that use differentiation [54], or zero crossing methods [55].

Use of the Hilbert transform is similar to existing signal processing methods which apply it to envelope detection [52]. Amplitude threshold methods work with a predetermined threshold. The maximum value of a group of points which exceed this threshold is taken as a peak. Thresholds are usually held constant over the duration of the entire signal, but only algorithms whose threshold are adjustable are considered here because unlike the ECG signal, the amplitudes of the peaks in the OMW are not expected to be constant [53]. Algorithms which rely on differentiation are based on the assumption that the slope of the ECG signal is most positive right before a peak occurs and most negative right after a peak occurs. A peak is detected if 3 consecutive points on the differentiated signal are above the positive slope threshold and then in the next 10 points, 2 consecutive points are below the negative slope threshold [54]. The zero crossing method filters the signal, then subtracts out its mean and finds where it crosses zero. Each downward zero crossing should follow an upward zero crossing and vice versa. In between two consecutive crossings should lay a peak. The maximum value in the group of points which lay between the upward and downward zero crossing is the identified peak [55].

2.4 Oscillometric Pulse Index (OPI)

The OPI is a defined quantity that forms a locus, or envelope, where points which correspond to SBP and DBP are located. After the OMW is extracted, the OPI can be found by one of three methods. Methods in current literature compute the OPI as either the height of each pulse from baseline-to-peak, peak-to-peak or as the area under each pulse, which can be found by integration [4], [19], [21], [22]. Peak-to-peak and area values can be estimated after peaks are identified. The definition of baseline-to-peak values is vague because to the best of the author's knowledge, no strict definition of a baseline is ever provided. Here, it is assumed that the baseline is zero for the duration of the recording.

These three approaches produce three different envelopes, but no literature exists that actually quantifies the performance of each. No reasoning is even provided for why a certain OPI is chosen over another. The absence of this comparison provides further motivation for the work done here.

2.5 Envelope Cleaning

Much like other signals, the OMW can be corrupted by noise and interference, some of which are from natural physiological processes and some of which are caused by external factors. Common to all engineering signals, measurement noise is one such interference that exists after the recording takes place. This noise is usually reduced by low pass (or band pass) filtering the cuff deflation curve in step 1 [9], [16], [17], [19], [26]. This measurement noise is dealt with by the envelope cleaning algorithms, but the most important concern here is to reduce interferences that are uniquely present in blood pressure or cardiac signals. These include movement or possible interference from other physiological processes. Here, methods will be discussed which reduce these disturbances so that algorithms in step 4 of the procedure may be applied to estimate SBP and DBP. Since the envelopes formed by the OPI should follow a distinct characteristic, the role of envelope cleaning is to re-shape a corrupted envelope, regardless of what the source of the irregularities may be.

Algorithms specifically designed to target one type of disturbance also exist. For example, motion artifact is a common interference that usually causes large spikes in the OMW [57]. Complicated algorithms based on an external sensor, such as an accelerometer, and adaptive filtering work especially well for the elimination of motion artifacts [57], but they add complexity and only target this specific disturbance. In this work, the focus of envelope cleaning is on less intensive, general purpose methods that clean the envelope. However, a new technique for reducing the effect of breathing, a known interference in oscillometric recordings, is developed in this thesis. For the estimation of blood pressure, envelope cleaning methods which are not limited to one specific type of disturbance are implemented. A potential drawback of these methods is that if the envelope has been distorted too much, it may be impossible to correctly clean the envelope or the cleaned envelope may still be unsatisfactory.

Two simple filtering methods have been proposed to help get rid of artifacts and interference: median filtering and moving average filtering. Median filtering is adopted to remove spurious data points [23]. Median filters replace each sample by the median value of it and its neighboring samples. A fixed window length is first required for this filter. Then, for each sample, only the points in the window are considered. That is, for sample x_n, with fixed window size $2*N + 1$, the median filter proceeds by:

$$x_n = median([x_{n-N}, x_{n-N+1}, \dots, x_n, \dots, x_{n+N-1}, x_{n+N}]) \tag{2.1}$$

Moving average filters also work by considering a window for each point, except instead of replacing a point with the median point of the window, the mean of all the points in the window is used. These are a type of non-causal finite impulse response (FIR) filter that take the average or mean of the samples in the window. An example of a moving average filter that takes the un-weighted mean of the window may be expressed as:

$$x_n = mean([x_{n-N}, x_{n-N+1}, \dots, x_n, \dots, x_{n+N-1}, x_{n+N}]) \tag{2.2}$$

Mathematically, this can be expressed as:

$$x_n = \frac{1}{2 \cdot N + 1}(x_{n-N} + x_{n-N+1} + \dots + x_n + \dots + x_{n+N-1} + x_{n+N}) \tag{2.3}$$

This is an equation of a filter composed of all zeros and no poles, making it FIR. The moving average filter can also be thought of as a LPF with a cutoff dependent on the window size. It generally works well for reducing random noise in the time domain but is poor in its ability to distinguish between different frequency bands. Windows lengths that have been previously used in moving average filtering for this purpose can depend on the size of the width of the pulses [24] or are a fixed length nine-point window for a 128 Hz sampled system [25].

Fuzzy logic has also been used to help clean envelopes as well [26], [27]. This rule based approach is adopted to assess the quality of each individual pulse. Each pulse is assigned a weight as a result of its determined quality. If the quality of the pulse is ruled to be poor or low, then the pulse is weighted with a low value. Otherwise, if the pulse is ruled to be clean, then the pulse is weighted normally. The weights of the pulse provide information that is used further along in the algorithm and represents the degree to which the pulse can be trusted. The properties of each pulse, such as height, width, slope, angle and relation to neighboring pulses are taken as inputs for this fuzzy logic decision making.

Another known technique to clean the envelope is curve fitting. This method has been used by itself in [28], [29] and has also been combined with fuzzy logic as well [30]. Curve fitting is the process of constructing a line or curve through the points of interest that has the best fit. The curve is defined by a mathematical function with variables that are adjusted. Best fit is in terms of least squared error between the points of interest and the curve produced after fitting. Current literature fits the envelope by a Lorentzian function [28] or a Gaussian function [30]. The Lorentzian function is fit by developed algorithms that minimize error in a weighted least-squares sense [28]. Gaussian functions have also been used to fit data using the Gauss-Marquardt algorithm. Best fit is achieved by minimizing the squared error [30].

The final method is to detect oscillometric pulses that are artifactual and replace them with a clean, estimated pulse. Determination of whether a pulse is artifactual or not can be done by comparing the pulse in question to its neighbors. If the pulse falls outside an accepted threshold level that is determined by the previous pulses, then it is replaced by a newly

generated pulse. This level can be determined by the time intervals between pulses [9] or the relative amplitude of the pulse [10]. In [11], a prediction algorithm is developed that, based on the amplitude of previous pulses, sets an upper and lower limit for what the amplitude of the next pulse should fall in between. If it is decided that the pulse is artifactual and needs to be replaced, then the replacement pulse may be found by averaging the neighboring pulses [9], [10] or by some prediction algorithm [11]. Any outliers that may exist should be fixed by this method, but the level of artifactual reduction will depend on the criteria in which pulses are identified to be corrupted.

2.6 Algorithms for Blood Pressure Estimation

Information regarding a subject's blood pressure is embedded on the cleaned envelope formed by the OPI. Blood pressure is estimated by applying algorithms that determine points on the envelope that correspond to the SBP and DBP. Four known algorithms, which may be divided into two different approaches: height based and slope based, were analyzed. Height based algorithms include the most popular MAA [9], [16]-[18], [21], [22], [24], [25], and the lesser known LAA [31]. Slope based approaches include the well-known MMSA [21], [22], [32], [33], and SCA [34]. The SCA is a yet to be published algorithm. Height based algorithms depend on locating the mean arterial pressure (MAP) first. This will be addressed first before the four algorithms are discussed.

2.6.1 MAP Estimation

MAP is defined as average arterial blood pressure of an individual. For intra-arterial blood pressure measurements, it is estimated as the average of the total arterial pressure during one cardiac cycle [17]. As opposed to the SBP and DBP, this quantity is not commonly returned by blood pressure monitors but empirical methods do exist to approximate the MAP. From the SBP and DBP, the MAP may be calculated by [16]:

$$MAP = DBP + \frac{1}{3} \cdot (SBP - DBP) \tag{2.4}$$

In oscillometric measurements, the widely accepted method to estimate the MAP is by finding the maximum point on the OPI. This method was established when a high correlation was found between the point of maximal oscillations in the cuff for an OMW and their actual

MAP [9]. In certain cases, the MAP has also been taken as 95% of the maximum point on the diastolic side [17]. An actual pressure value in mmHg can then be estimated by locating this point on the deflating cuff curve. When looking at the OMW, the point which corresponds to the SBP typically lies to the left of the MAP and the points which corresponds to the DBP lies to the right of the MAP. Thus, when considering the OMW plotted against time, such as the ones in Figure 2.2, it is said that the MAP divides the OMW into two regions: the systolic region and the diastolic region. The left side is the systolic region, containing the point that corresponds to SBP and the right side is the diastolic region, containing the point that corresponds to DBP. The names systolic region and diastolic region do not hold much physical meaning, except to indicate the location where the points for SBP and DBP may lie.

All the processing performed up to this point affects the position where the MAP is located and thus affects SBP and DBP estimation in height based algorithms as well. Systolic and diastolic values are estimated at the end of the entire procedure, but some criterion to evaluate the individual algorithms at each step of the procedure is required as well. One method to do this is by comparing the MAP value obtained by finding the maximum point on the processed OMW and comparing it with the MAP calculated empirically from the reference recordings. This will be used in the procedure to evaluate certain steps of the algorithm.

2.6.2 Maximum Amplitude Algorithm

The MAA is the most popular oscillometric algorithm for determining blood pressure [24]. As shown in Figure 2.3, this algorithm operates by first finding the point on the envelope corresponding to the mean arterial (MAP) [17]. The right side of the maximum point of the envelope is the diastolic side and the left side is the systolic side. In Figure 2.3, this point corresponds to amplitude A. Predetermined systolic and diastolic characteristic ratios, r_s and r_d, are then used to find the points that correspond to SBP and DBP. The systolic ratio can reportedly range from 0.45 to 0.73 and the diastolic ratio may range from range from 0.69 to 0.83 [16]. These ratios seem to differ between devices as well. Some have also adopted dynamic ratios that change depending on the subject's MAP [18]. Regardless of what ratio is

chosen, the point corresponding to SBP can be found by multiplying the height of the MAP point with the systolic ratio, $A \cdot r_s$. The resulting amplitude can then be located on the systolic side of the envelope to produce the SBP point. The same can be done for the point corresponding to the DBP, by multiplying the height of the MAP with the diastolic ratio, $A \cdot r_d$ and locating the point on the diastolic side of the envelope.

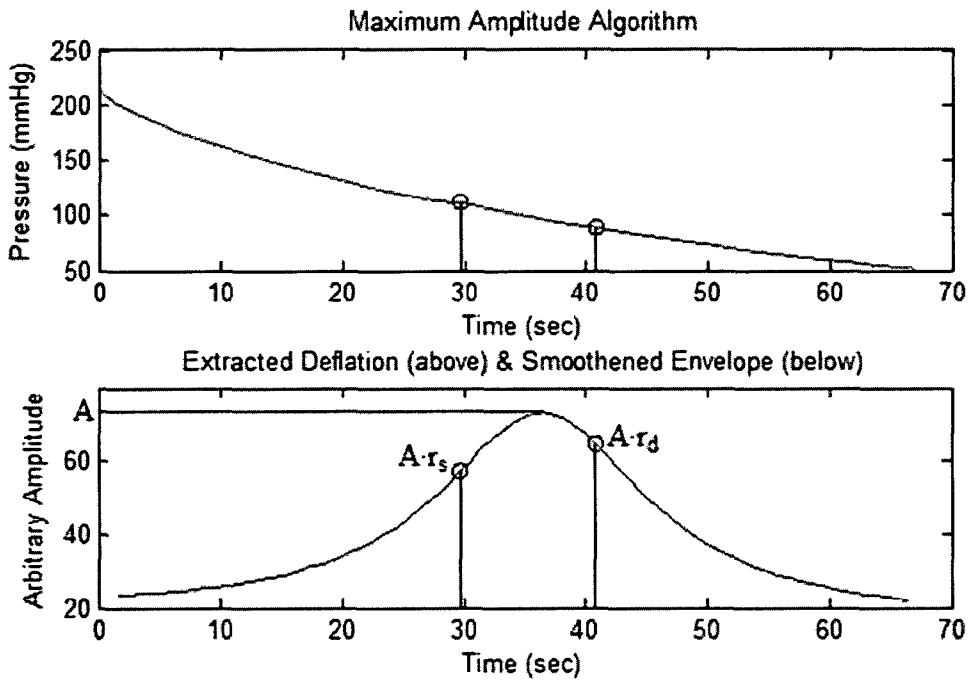

Figure 2.3. MAA implementation.

2.6.3 Linear Approximation Algorithm

Similar to the MAA, the LAA also operates by using the heights of the envelope and also require predefined systolic and diastolic characteristic ratios [31]. This algorithm works by approximating the envelope with a pair of linear lines of best fit based on the peaks of all the oscillometric pulses. A pair of lines is first approximated, one for peaks 1, 2 and another for peaks 3 to N, where N is the total number of peaks. Next, another pair of lines is approximated, one for peaks 1 to 3 and another for peaks 4 to N. This procedure continues until a pair of lines for peaks 1 to N – 2 and peaks N – 1 and N is found. For each pair of lines, it is assumed that the one produced by the first set of the peaks should have positive slope and represent the systolic side, whereas the one produced by the second set of peaks

should have a negative slope and represent the diastolic side. If some artifacts or interference causes any approximated line to have the opposite slope, then it and its paired line are removed from analysis. Each iteration should then produce a valid pair of lines that have an intersection point. Intersection points from all the produced pairs of lines are compared and the highest intersection point is taken as the initial MAP.

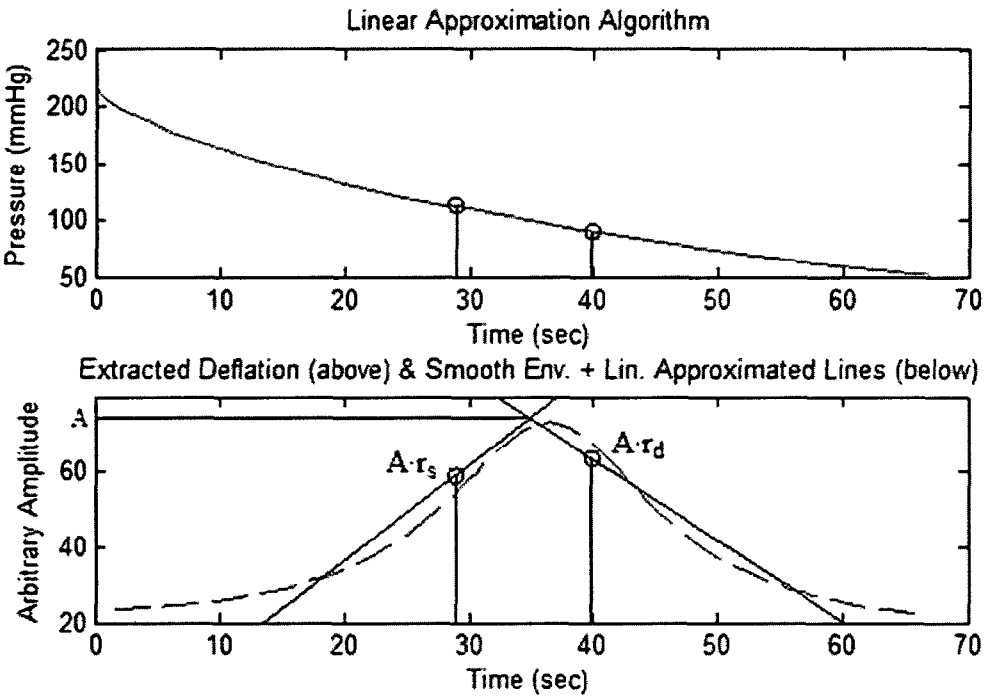

Figure 2.4. LAA implementation.

To eliminate any artifacts or interference, the procedure is performed again, but this time only with peaks that are greater in amplitude than half the initial MAP point. All remaining points after this elimination are then again fitted for pairs of linear lines of best fit. The same procedure as before is performed, except N now represents a lesser number of peaks than before. After each iteration, a pair of lines should be produced, each with a corresponding intersection point. The highest intersection point is taken as the final MAP and the pair of lines that produce this intersection is used to locate SBP and DBP. The line on the left with positive slope is the final systolic line and the line of the right with negative slope is the final diastolic line. The amplitude of the MAP point is multiplied by the corresponding systolic or diastolic characteristic ratio to produce points that are located on the final systolic and diastolic lines, respectively. These points are the final systolic and diastolic points. Figure 2.4

shows the implementation of this algorithm with the final pair of lines of best fit illustrated. The amplitude corresponding to the MAP is A and the systolic and diastolic ratios are r_s and r_d. By using linear approximations, this algorithm provides another layer of artifact reduction. The LAA was developed by Medero in a 1996 US patent [31] and has not been found in any other known literature.

2.6.4 Points of Maximum/Minimum Slope Algorithm

Unlike the previous two algorithms, the MMSA considers the slope of the envelope rather than the heights [21], [22], [32], [33]. Here, the systolic point is found as the point on the envelope where the slope of the envelope is at its maximum and the diastolic point is where the slope of the envelope is at its minimum. As shown in Figure 2.5, these two points can be found by taking the derivative of the signal. Since the derivative represents the slope of the line tangent to each point on the signal, the point where slope is maximum also correspond to the maximum of the derivative signal and the point where slope is minimum also corresponds to the minimum of the derivative signal. Overall, the MMSA is arguably the second most well-known algorithm, just behind the MAA [4].

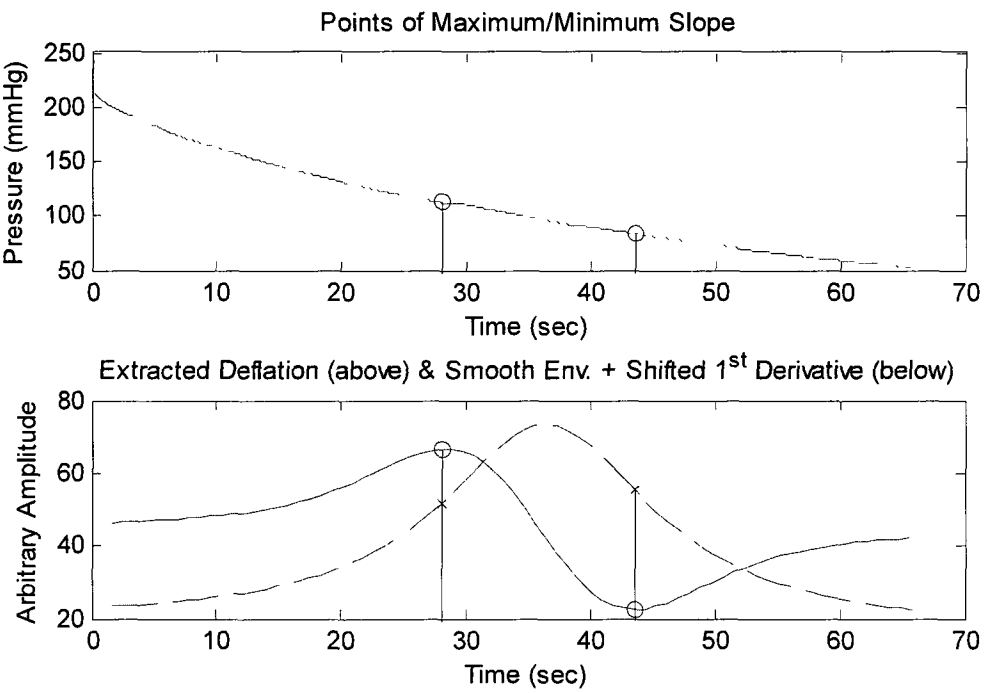

Figure 2.5. MMSA implementation.

2.6.5 Slope Change Algorithm

The SCA finds the points on the envelope where the slope changes, or the inflection points. Although no published literature regarding this algorithm exists, [34] argues that it is based on the physiology of blood pressure. It is hypothesized that the envelope may be split into 4 distinct regions, based on slope. The location of the intersection of these regions are taken as the systolic, MAP and diastolic points. The four regions S1 to S4 are:

- S1: From the beginning of the reading to the systolic point where no blood flow passes under the cuff but oscillations are present because the radial artery pulsations are transmitted to the proximal side of the cuff.
- S2: From the systolic point to the MAP where blood flow is no longer occluded and starts flowing into the arm.
- S3: From the MAP point to the diastolic point where blood flow is turbulent and the artery under the cuff is free from occlusion.
- S4: From the diastolic point to the end of the procedure where the radial artery is no longer occluded.

This algorithm differs from the previous slope based algorithm in that it looks for inflection points on the envelope, which is when the derivative of the signal is equal to zero, rather than the maximum and minimum points. The algorithm is illustrated in Figure 2.6.

2.7 Determining SBP and DBP Pressure Values

Actual systolic and diastolic pressure values must be extracted after their corresponding points are located on the envelope. This can be performed by mapping the points determined to be SBP and DBP on the envelope back to the cuff deflation curve. The cuff deflation curve shows the deflating cuff pressure in mmHg. Points on the envelope where the SBP and DBP are determined correspond to a certain time stamp. This time stamp is then located on the cuff deflation curve, where a pressure value in mmHg can be extracted.

2.8 Respiration in Blood Pressure

Algorithms for extracting SBP and DBP from oscillometric measurements form the basis of any work on blood pressure. They provide a foundation for which blood pressure can be

estimated so that studies in other areas of oscillometry may progress. In these algorithms, envelope cleaning algorithms are used to rid the OMW of any unwanted disturbances. Although they do a good job at that, there are also some cases where the disturbance warrants special attention. This is the reason breathing in blood pressure is studied here. Breathing, at various levels has a large influence on SBP and DBP estimation [8], [9]. In some cases, breathing can be large enough that estimated SBP and DBP values may not be truly representative of the subject's actual blood pressure even after any envelope cleaning algorithms. This section will review the known effects of breathing on blood pressure estimation and the established work on reducing these effects. It is important to note that the current literature primarily uses intra-arterial blood pressure signals to investigate breathing, and not oscillometry.

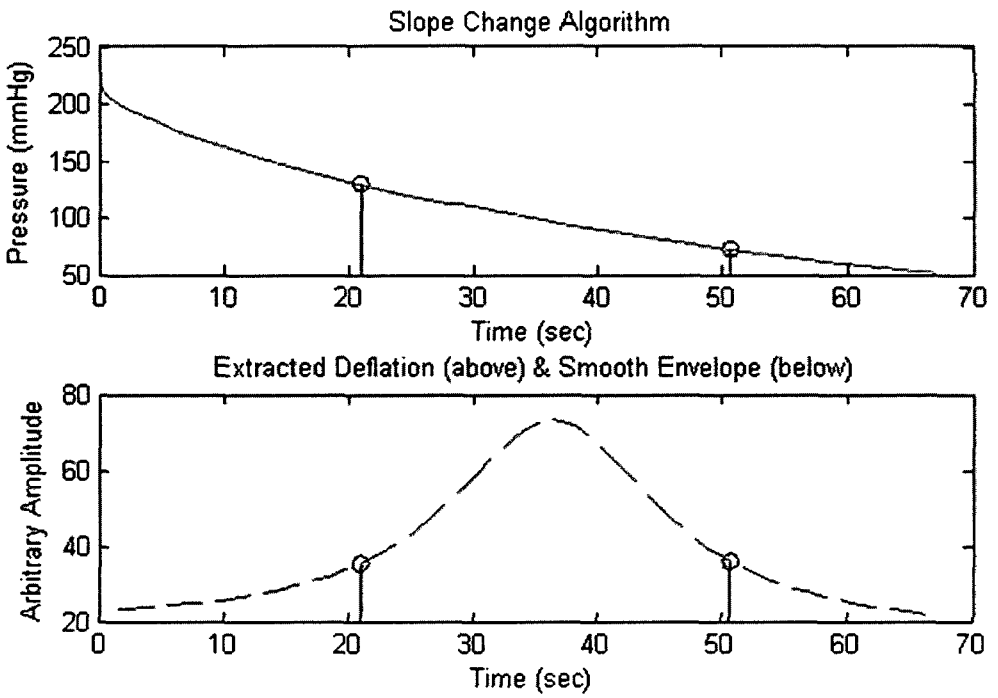

Figure 2.6. SCA implementation.

2.9 Effects of Respiration

In 1733, Stephen Hales was the first to discover that respiratory activity modifies heart rate and blood pressure oscillations [8]. Since then, a number of works have advanced the study of respiration effects in blood pressure signals. It has been discovered that the effects of respiration influence blood pressure through amplitude (AM), frequency modulation (FM)

and additive effects [58], [59]. Deep, pronounced breathing has been found to cause large fluctuations in SBP of up to 15 to 20 mmHg. Breathing at a normal depth can even cause SBP fluctuations of up to 3 to 6 mmHg [9]. This fluctuation is quite large and is the motivation for why breathing is specifically targeted for suppression.

AM and additive effects account for the large fluctuations in the amplitude of the signal [60]. An explanation of these effects requires an understanding of the physical interaction between the lungs and the heart. As respiration occurs, gas is transferred in and out of the lungs, flowing from an area of higher pressure to lower pressure [2]. During the inspiration phase, the diaphragm and intercostals muscles expand the thoracic cavity, which houses the lungs, heart and rib cage. Here, the pressure inside the thoracic cavity, intra-thoracic pressure, decreases below the atmospheric pressure which allows air to move into the lungs. During the exhalation phase, the opposite behavior occurs, where the muscles relax and a rise in intra-thoracic pressure causes air to move out of the lungs.

Cardiac output is the volume of blood pumped into the arteries from the heart per minute. This volume of blood is directly related to blood pressure. Cardiac output is related to blood pressure through stroke volume, which is directly related to cardiac output and blood pressure. Stroke volume is the total volume of blood pumped out of the heart per heartbeat. As cardiac output increases, more blood is pumped out of the heart per minute, resulting in an increase in blood pressure. Blood pressure can even be modeled simply as the cardiac output multiplied by the resistance to blood flow by the blood vessels [61]. The interaction between the cardiac output and intra-thoracic pressure is known to result in the amplitude changes in blood pressure.

During inspiration, cardiac output is known to increase. The thorax expands as intra-thoracic pressure reduces, allowing more room for the heart to fill a larger capacity with blood. Thus, cardiac output increases, which produces a rise in blood pressure. During exhalation, intra-thoracic pressure is high and the thorax contracts. As a result, the heart is compressed and the capacity of the heart to fill with blood is reduced. Cardiac output is decreased and blood pressure is reduced in this stage [61], [62]. This change in cardiac output as a result of respiration is known to cause the large fluctuations in blood pressure readings.

FM is evidenced in the changes in the pulse-to-pulse intervals, or heart rate, of the subject. This shortening and lengthening of heart periods with respect to respiration is a phenomenon known as RSA [63]. Heart rate and HRV is controlled by the autonomic nervous system (ANS). The ANS is a part of the nervous system that acts as an involuntary control system for certain functions such as heart rate and blood pressure [64]. Two motor neurons, the vagal and sympathetic are primarily dominant in controlling heart rate through innervating the cardiac sinoatrial (SA) node of the heart. When active, the vagal motor neuron slows down heart rate (increase the period between pulse-to-pulse intervals) and the sympathetic vagal motor neuron increases heart rate. The excitation of these two neurons depends on respiration phase.

Increases and decreases in CO_2 concentration, with respect to the inspiration and expiration phases of respiration, excite and inhibit these two neurons. During inspiration, the vagal neuron is inhibited and the sympathetic neuron is excited, leading to a higher heart rate. The opposite occurs during expiration where the vagal neuron is excited and the sympathetic neuron is inhibited, leading to a lower heart rate. This cyclic behavior is known as RSA and produces the frequency modulation effects which are observed in the pulse-to-pulse intervals in blood pressure. [64]

Variations in the amplitude and pulse to pulse intervals of blood pressure seem to be influenced by both the depth and frequency of the respiration. These two different manifestations of respiration in blood pressure also appear to have a strong relationship with each other. An example of their effects can be seen in Figure 2.7. A portion of an oscillometric recording is shown here with the pulse peaks identified so that the AM and FM effects may be observed. Higher respiration rates resulted in lower fluctuations in both effects. It has also been discovered that, with the use of ECG R-R intervals, the amplitude changes always precede changes in heart rate. This suggests a tight link in the baroreflex, the mechanism which controls the level of blood pressure [63], [64].

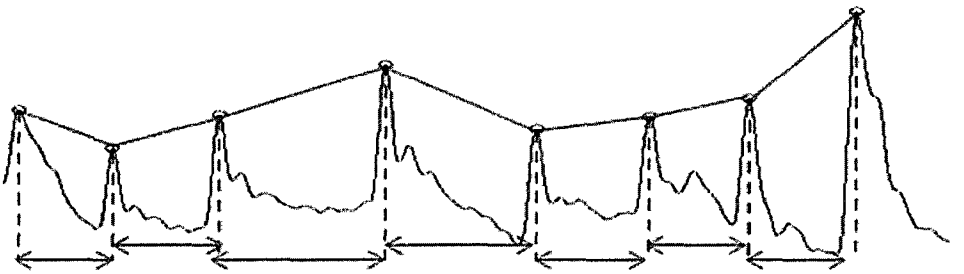

Figure 2.7. AM and FM effects of breathing on blood pressure.

2.10 Blood Pressure Variability

Blood pressure is known to vary with time and this has been shown to lead to an unacceptable level of measurement uncertainty according to SP10 standards [48], [49]. Respiration is a known contributor to this variability. This has been previously studied through frequency domain spectral investigations of blood pressure and heart rate [6]. From this analysis, three specific blood pressure and heart rate rhythmic oscillations have been identified. They are classified based on the different frequencies they reside at, very low frequency (VLF), low frequency (LF) and high frequency (HF). These three components along with their causes and location in the frequency domain are of area of interest to many. Due to the tight link between the cardiovasculatory and the respiratory system, one of the three spectral components, the HF component, has been identified to be induced by respiration [65]. Although the exact ranges differ between studies, their general locations are still similar. The respiration caused HF range used here will follow [66]: 0.15 to 0.5 Hz. This frequency range also corresponds to the rate of respiration. These limits provide boundaries for which the presence of respiration in a signal can be found. Presence of respiration spectrally in the variation of blood pressure and heart rate also provide support for the AM and FM effects discussed in the previous section.

2.11 Breathing Signal Extraction

Before any suppression of breathing can occur, it has to first be detected in the signal. Extracting breathing provides an estimate of how much it is interfering with the important, information bearing part of the signal. Many algorithms to extract breathing from the intra-arterial blood pressure signal have been developed that take advantage of its well-known

additive, AM and FM effects. The simplest of these algorithms puts the blood pressure envelope and pulse-to-pulse intervals into additive, AM and FM estimators to extract the respiratory signals [38]. Extraction from the additive estimator involves applying a bandpass filter around the breathing frequency to simply obtain the signal. AM estimators use a combination the Hilbert transform and filtering to detect the envelope of the signal. Detection of an envelope is performed by the Hilbert transform, which is then filtered to extract only the breathing component. Finally, the FM estimator from this technique simply uses the R-R intervals along with a filter as well. All filters used here are tuned to the frequency of breathing [38].

Other algorithms for extracting breathing from arterial blood pressure also exist. Amplitude demodulation using the Teager energy operator and adaptive eigenvector decomposition has also been used. The algorithm cancels out the cardiac component in the intra-arterial blood pressure signal to produce an estimate of only the respiratory component [39]. Independent component analysis has also been applied to this subject and used to extract the additive effect of breathing. All the harmonics of breathing are estimated, which include portions that overlap with the spectrum of the cardiac component [67]. One final surveyed algorithm estimates breathing by calculating the area under the dicrotic notch of the pulse wave. Arterial pulses normally consist of a large peak, followed by a dip, then a brief rise and finally a gradual decline until the end of the pulse. The dicrotic notch is the dip in each pulse that precedes a small bump after the peak value of the pulse. The peak of the pulse is caused by the blood flow from the heart to the arm, whereas the bump that arises after it results from the reverse flow of blood from the arm to the heart. Area estimates of the dicrotic notch are found to be related to breathing, which gives forth this algorithm for breathing extraction [68].

Breathing may also be derived from ECG analysis as well [41]. Similar to blood pressure, ECG signals also exhibit AM and FM effects due to breathing. These effects have also been exploited to provide valid estimates of respiration. Another signal known as the pulse wave transit time (PTT) has also been used to derive breathing [69]. PTT can be extracted by measuring delay in time for the arterial pulse to travel from the heart to a reference point. In this work, this is found as the delay in time between the ECG R-peaks and the pulse peaks of

the blood pressure signal. Breathing heavily modulates the PTT which can be used to extract another respiration signal [69]. Methods to extract breathing signals from ECG and PTT are mentioned because they will be used later in the study to provide reference signals.

2.12 Adaptive Filtering

Some current methods to reduce or extract breathing from intra-arterial blood pressure or ECG signals employ adaptive filtering. As such, the adaptive filters that will be used are reviewed here. Traditionally, suppressing narrowband interference is performed by applying a fixed notch filter tuned to the frequency of the interference. The precise location of this interference must be known beforehand and is fixed. However, in some situations, the frequency of the signal changes with time and its frequency components may be unknown. Adaptive filters can be used in this situation to overcome these problems. These filters differ from regular frequency domain filtering techniques in that the transfer function self-adjusts according to an optimization algorithm. Thus, they can be used to overcome the difficulties that traditional filters have with these problems [70].

Optimization is based on the well-known least mean squares (LMS) algorithm. This is a linear adaptive filtering algorithm that forms a feedback loop consisting of two basic processes, a filtering process and an adaptive process. Filtering involves computing the output of a transversal filter and then comparing this output with a desired response to estimate an error. Coefficients are updated through an iterative process that progresses sample by sample. Updates of the coefficients proceed to minimize the square of the estimated error. This error should ideally reduce as each sample is inputted until the coefficients converge to a point where error cannot be reduced any further by the algorithm. At this point, the filter coefficients should be stable and remain at approximately these values for the duration of processing of the remaining samples. Adaptation here is also based on a step-size parameter, which acts as a scaling factor. This controls the amount of adjustment after each coefficient update. A step-size that is too small can result in a slower convergence and a step-size that is too large can result in unstable behavior due to adjustments that are too large. For optimal convergence, the step-size parameter should be chosen to satisfy

conditions which relate to the Eigen-structure of the input correlation matrix. Further detail of adaptive algorithms may be found in [70].

Two adaptive filtering schemes used in this work are the adaptive noise canceller (ANC) and adaptive line enhancer (ALE) scheme. Both of these schemes rely on the LMS algorithm for convergence and are used for suppressing the effects of breathing from oscillometric recordings. Although they are used for the same purpose, two filtering schemes are presented because they are applied to two separate situations.

2.12.1 Adaptive Noise Canceller

The ANC scheme is based on suppressing a narrowband interference using a reference noise signal that must be provided [70]. Two inputs are required in this scheme, a primary input and a reference input. The primary input contains the information bearing signal along with some narrowband corrupting interference signal. A correlated version of this signal is supplied to the reference input of the ANC. The ANC behaves like an adaptive notch filter at the angular frequency of the signal provided by the reference. Figure 2.8 shows the block diagram of the ANC.

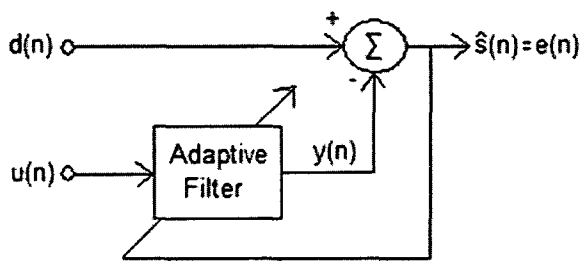

Figure 2.8. Scheme for the adaptive noise canceller (ANC)

The goal of the algorithm is to filter the reference signal in such a way that is becomes an accurate estimate of the interfering signal contained in the primary input. Let the primary signal be represented by:

$$d(n) = s(n) + v(n) \tag{2.5}$$

In this equation, *s(n)* is the information bearing part of the signal and *v(n)* is the additive narrowband interference part of the signal. The reference input provides a signal *u(n)* that is correlated to the interference part of the signal, *v(n)*, but uncorrelated to the information part,

s(n). Using the LMS algorithm, the reference input *u(n)* is adapted to match *v(n)* as closely as possible. An intermediate output, *y(n)*, is taken as the estimate of *v(n)* such that:

$$y(n) \approx v(n) \tag{2.6}$$

Ideally, then at the summing junction, the output of the system, which is also the error signal, should be the input signal with the noise subtracted out:

$$\begin{aligned} \hat{s}(n) &= e(n) \\ \hat{s}(n) &= d(n) - y(n) \\ \hat{s}(n) &= s(n) + v(n) - y(n) \\ \hat{s}(n) &\approx s(n) \end{aligned} \tag{2.7}$$

Tap-update equations that govern the operation of the adaptive filter to produce the output, *y(n)*, are as follows:

$$\begin{aligned} y(n) &= \sum_{i=0}^{M-1} \hat{w}_i \cdot u(n-i) \\ e(n) &= d(n) - y(n) \\ \hat{w}_i(n+1) &= \hat{w}_i(n) + \mu \cdot u(n-i) \cdot e(n) \end{aligned} \tag{2.8}$$

Here, M is the total number of tap weights in the filter and μ is the step size parameter. Step size can be taken as any value between:

$$0 < \mu < \frac{2}{l_{max}} \tag{2.9}$$

The value l_{max} is the largest eigenvalue of the input autocorrelation matrix. The error signal, *e(n)*, also serves as the output of this filtering scheme. Filtering is performed by a finite impulse response (FIR) type of filter. Tap-update equations proceed by minimizing the total output power of the system.

2.12.2 Adaptive Line Enhancer

In the case where no reference signal is available, the ALE scheme is used [71]. This filter is capable of detecting and filtering a narrowband spectral peak in broadband noise, without requiring a secondary input. The block diagram of the ALE is shown in Figure 2.9.

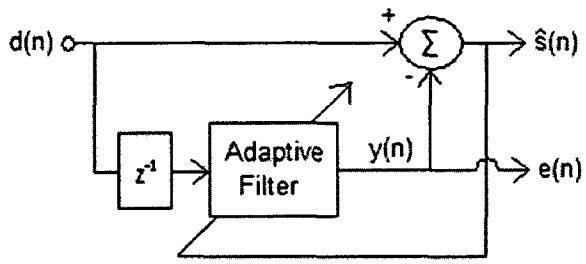

Figure 2.9. Scheme for the adaptive line enhancer (ALE)

In this scheme, the input is split in two signals, where one goes through a delay of one sample. This filter exploits the coherent nature of the signal to separate the narrowband and broadband components. By delaying the input signal by one sample, the broadband noise components will have a weaker correlation than the strongly correlated narrowband component. The adaptive filter then forms a transfer function equivalent to the correlated, narrowband component. A one sample delay is used here, but the delay can be chosen as any value. Adaptation proceeds by forming a transfer function equivalent to a sharp narrowband filter centered at the frequency of the detected narrowband component. Weights of the filter are adjusted such that the narrowband component in the input signal is cancelled out at the summing junction. Again, here the input signal may be represented as in (2.4). At the output of the adaptive filter, *y(n)* is adjusted such that:

$$y(n) \approx v(n) \tag{2.10}$$

Then at the summing junction:

$$\begin{aligned} \hat{s}(n) &= d(n) - y(n) \\ \hat{s}(n) &= s(n) + v(n) - y(n) \\ \hat{s}(n) &\approx s(n) \end{aligned} \tag{2.11}$$

Tap-updates for this adaptive filter operate by minimizing the mean square error of the output power. Minimizing the output power depends on the transfer function of the system. A second order notch IIR filter is used in this scheme:

$$H(z) = \frac{W(z)}{W(\alpha \cdot z)} \tag{2.12}$$

Here, $W = (w_1, w_2)^T$ is the weight vector which may be written as:

$$W(z) = 1 - w_1 \cdot z^{-1} - w_2 \cdot z^{-1} \tag{2.13}$$

$$W(z) = 1 - \alpha \cdot w_1 \cdot z^{-1} - \alpha \cdot w_2 \cdot z^{-1}$$

The parameter α is the debiasing parameter, which represents the magnitude of the pole. In order for proper operation of the filter, this value should be as close to 1 as possible, without actually reaching it. Zeros in the filter are located on the unit circle, with a magnitude of 1. Roots of the transfer function correspond to the angular frequency of the notch filter. For every specified α, there exists a vector W that minimizes the output power. Adaption of coefficients to reach this minimum is performed by the stochastic Gauss-Newton method [68]. The tap-update equations are given by:

$$\begin{aligned} \mathrm{W(n)} &= \mathrm{W(n-1)} + \mathrm{K(n)} \cdot \hat{s}(n) \\ \mathrm{K(n)} &= \frac{\mathrm{P(n-1)} \cdot \psi(\mathrm{n})}{\lambda(\mathrm{t}) + \psi^{\mathrm{T}}(\mathrm{t}) \cdot \mathrm{P(t-1)} \cdot \psi(\mathrm{t})} \\ \mathrm{P(t)} &= \left[\mathrm{P(t-1)} - \frac{\mathrm{P(t-1)} \cdot \psi(\mathrm{t}) \cdot \psi^{\mathrm{T}}(\mathrm{t}) \cdot \mathrm{P(t-1)}}{\lambda(\mathrm{t}) + \psi^{\mathrm{T}}(\mathrm{t}) \cdot \mathrm{P(t-1)} \cdot \lambda(\mathrm{t})} \right] / \lambda(\mathrm{t}) \\ \ddot{e}(\mathrm{t}) &= \lambda_0 \cdot \lambda(\mathrm{t-1}) + (1 - \lambda_0) \end{aligned} \tag{2.14}$$

The variable $\psi(t)$ represents the gradient, which is taken as the output of the ALE scheme, $s(n)$. Matrix P may be initialized as the identity matrix and λ_0 is set to 0.95. The variable λ is equivalent to a forgetting factor.

2.13 Suppression of Breathing Effects

Current literature supports the usage of the ANC scheme for suppressing the effects of breathing in cardiac signals. This has been used for baroreflex sensitivity estimation [40] and in impedance cardiography [72]. Impedance cardiography is a method to detect the properties of blood flow in the thorax. Breathing affects this signal in a similar way that it affects blood pressure as well. The LMS based ANC scheme reduces the interference that breathing causes so that, for example, proper stroke volume can be calculated. The scheme used here does not require any control of the subject's breathing, but does require a breathing signal for the second input of the ANC. Breathing is obtained from a sensor that detects airflow at the nostrils but because there is a delay between the breathing detected here and at the thorax, a manual delay must be introduced. A sample rate of 500 Hz was used in this

analysis. The filter was designed with a tap length of 200 and a manual delay of 70 samples. Stabilization was reached in approximately 500 samples, with a step size of 0.0044 chosen.

Baroreflex sensitivity estimates the response in the heart rate caused by changing blood pressure. In this application, systograms and tachograms are used to estimate this value, but are corrupted with breathing as well [40]. Systograms are derived from the arterial blood pressure signal by detecting the maximum value of blood pressure between R-peaks of the ECG. ECG is used to provide R-R intervals that comprise the tachogram. Breathing is measured by a temperature sensor (thermistor) placed near the nostrils and used as the reference for the ANC. Adaptive schemes for both systograms and tachograms were developed with the same characteristics and respiration was removed only under controlled breathing. All filtering is performed at a sampling rate of 200 Hz. The order of the filter was chosen to be 30, but the order within a range of 10-40 was acceptable, and a forgetting factor of $0.1 \cdot \mu_{max}$ was used. As a result of the adaptive filtering, it was found that the distorting effects of breathing on baroreflex sensitivity was reduced, enabling a more accurate estimation.

The ANC scheme is quite versatile; it may be used for extracting breathing signals as well reducing its effects [39], [67]. Operation of all these filters is also based on the assumption that breathing is a narrowband signal [40], or else the adaptive schemes will fail. Adaptive filtering schemes based on the above methods for oscillometric recordings are developed in this thesis and will be presented in Chapter 4. Suppression of breathing effects relies on the existing methods for reducing breathing effects as well bring forth some new techniques. No existing techniques for the suppression of breathing in oscillometric recordings have been found.

Suppression of FM breathing effects on the pulse-to-pulse intervals of the OMW will also be investigated. This will be performed using the same adaptive filtering techniques. It is well known that FM effects exist, which means that breathing modulates the pulse-to-pulse intervals of the OMW, resulting in changes to the heart rate [64]. How these effects may influence blood pressure estimation though is unknown and never been studied before. FM

effects, however, are expected to play a role in the estimation of HRV. HRV is a known marker of the health of a subject and are also influenced by respiration. Estimation of HRV with these effects suppressed will be attempted as well.

2.14 RSA Estimation

Typically, estimation of RSA is carried out during controlled breathing. However, for a number of practical applications, controlled breathing conditions cannot be achieved. In this case, the best way to compare RSA between patients is to normalize RSA amplitude. The same physiological mechanisms are responsible for the RSA and the variance in the R-R intervals or HRV. There are a number of specific parameters included in the description of HRV but HF components of HRV and RSA amplitude are most correlated.

Estimation of RSA may be performed by calculating the longest R-R interval during expiration and subtracting from it the shortest R-R interval during inspiration [73]. This is a useful quantity because studies have shown that RSA has strong correlation with chronic diseases like obesity, diabetes and hypertension, among other things [15]. Characterization of RSA is affected by respiration patterns. In order to compare RSA among subjects, it should be normalized so these effects are accounted for. Normalization is performed to account for the physiological differences between different individuals. RSA is known to depend on the variance in R-R intervals, or HRV, [74] and the power of the HF component of R-R intervals [75]. As such, the ECG or arterial blood pressure signal, along with respiration, is usually used for normalization to account for these differing factors between different subjects. Afterwards, the normalized RSA can be used as a physiological indicator of the state of a subject's state of health. Usually, this normalization is performed with the power spectra of R-R intervals [75].

RSA is measured with the use of a respiration signal and ECG or arterial blood pressure signal present. It has not been investigated using an oscillometric blood pressure recording before. Now that detection and extraction of respiration through oscillometry is studied, implementing RSA estimation is attempted.

2.15 Measurement Terminology

Current work in blood pressure estimation is performed by researchers from several research fields including engineering, medicine and physiology. The work in this thesis provides an engineering approach. In order to avoid confusion regarding terminology, we define next some commonly used measurement terms [76].

Signal: A time-varying or spatial-varying information bearing quantity. It may be represented as a physical quantity or digitally as well.
Measurement: Process of estimating some physical information or magnitude of a subject, such as length, relative to a unit of measurement.
Sampling: Conversion of a continuous signal into a discrete signal, a set of finite values at a point in time or space.
Recording: Process of capturing physical information to a format stored digitally. A physical quantity blood pressure may be measured by invasive means and this measurement can be sampled to produce a recording of the signal stored in a computer.
Waveform: Graphical representation of a varying quantity over time.
Reading: The indication of a graduated instrument. Nurses who use the auscultatory method produce blood pressure readings by noting the level of mercury on a sphygmomanometer.
Estimate: A calculated approximation of the value of a physical quantity.
Calculation: Process of transforming one or more inputs into one or more results by mathematical means.
Accuracy: The degree of closeness of a measurement or estimate is to its true value.
Error: The difference between a computed estimate or measured value and its true value.
Pulse: The arterial palpation of a heartbeat.
Processed Signal: A signal obtained from one or more signals which have been processed by some mathematical algorithm.
Filtered Signal: A signal obtained from another signal which has been processed by a filter.
Filter: Process that removes some unwanted features or components from the input.

2.16 Estimation Tools

The work done in this thesis spans a variety of sub-topics in oscillometric blood pressure and requires the evaluation of different sub-algorithms. Although the end goal is to improve blood pressure estimation, there are many sub-algorithms where the estimates of SBP and DBP are unavailable. Evaluation of these sub-algorithms requires an understanding of different estimation tools to properly interpret the results. These tools will be defined in this section.

For algorithms used in the estimation of blood pressure, mean absolute error (MAE) and standard deviation (STD) are used. MAE is calculated by taking the mean of the absolute error. STD is calculated as the square root of the variance of the error. Error is determined by finding the difference between estimated blood pressure and reference blood pressure readings and is shown in units of mmHg. The reference blood pressure is usually taken as a nurse auscultatory reading or by a reading by a trusted device. Error is a vector with a number of values, determined by the number of subjects in the data set. MAE and STD are used over other conventional metrics (such as mean square error) because they are the more common tools for evaluation of performance of blood pressure algorithms [9], [16], [21], [27].

In order to verify the methods used to extract a breathing signal from blood pressure, several statistical tools are also used. Correlation coefficient compares one signal to another and examines how similar they are to one another. This quantity measures the strength of linear dependence between two signals. The closer it is to 1, the more similar the two signals are. Signal-plus-noise-to-noise ratio (SNNR) is used to measure how much a signal has been corrupted by noise. This quantity is calculated by finding the ratio of power of the signal with the corrupting noise to the power of the noise alone. This is a useful tool to evaluate the degree of influence breathing may have on blood pressure estimation.

Fluctuation in blood pressure estimates is also important to evaluate, especially in the case of breathing. It is defined as the amount of variation or change in blood pressure. Fluctuation has been previously estimated using frequency analysis tools [65], [66], but due to the short length of OMW recordings, these techniques will not be applied here. The short length and

non-stationary nature of the OMW make locating the breathing component difficult using conventional frequency analysis tools. Instead, fluctuation will be estimated by a method similar to the one in [9], which was applied to arterial blood pressure. Here, fluctuation is calculated by finding the difference between highest estimated blood pressure value and lowest estimated blood pressure value over a fixed period of time over multiple oscillometric recordings. To evaluate fluctuation over a group of subjects, the fluctuation is first calculated individually for each subject, and then the mean is taken for the group.

Statistical t-tests are also used to assess whether the means of two groups are statistically different from each other. This analysis is appropriate for comparing the means of two groups. Because the t-test is able the judge the mean of two groups relative to their distribution as well, this provides a useful tool to assess whether improvement in any of the abovementioned metrics is evident. For example, we may observe that after some processing, an estimate is lower in error than before the processing was applied. In order to ensure that these results are indeed statistically significant, a t-test is able to statistically show that the two sets of results are indeed different from each other there is indeed improvement. Paired t-tests will be used in the breathing suppression part to confirm whether there is a statistically significant difference between SNNR values before and after suppression.

Chapter 3 – Oscillometric SBP and DBP Estimation

3.1 Oscillometric Algorithm Implementation

Algorithms for SBP and DBP estimation from oscillometric measurements were implemented and assessed in a procedure shown in Figure 3.1. The algorithms here were implemented on a data set of subjects provided by Biosign Technologies Inc. All algorithms for the five step blood pressure estimation algorithm discussed in Section 2.1 were tested on this data set except for two envelope cleaning algorithms: fuzzy logic and the method of identifying and replacing corrupted pulses. These two methods both rely on a rule based approach to detect corrupt pulses. All other algorithms described in Section 2.1 are implemented step by step and compared. In order to properly assess these algorithms, performance metrics are defined in each stage. These metrics are shown in Figure 3.1 as well and will be discussed in detail later. All algorithms here were developed using MathWorks MATLAB®.

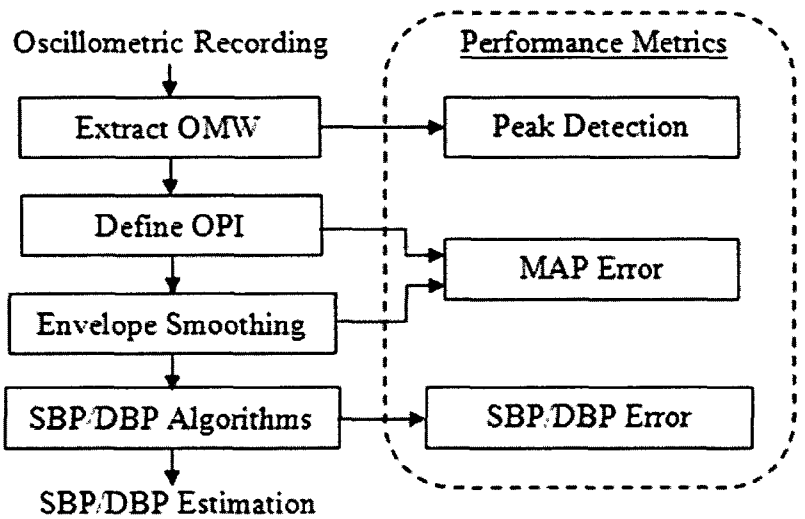

Figure 3.1. Assessment of oscillometric algorithms.

3.2 Data Acquisition

A data set of oscillometric measurements were provided by Biosign Technologies Inc for this study. These oscillometric measurements were recorded using a digital blood pressure monitor (UFIT® TEN-10) from Biosign Technologies Inc. This is a wrist worn device that plugs into a personal computer through USB interface and samples at a rate of 100 Hz. After

the recording, the deflating cuff pressure CP and the discrete derivative of the pulse pressure PP are acquired on the personal computer. Through processing the CP and PP signal, the OMW and deflation curve may be computed.

This data set consists of multiple oscillometric measurements recorded from 85 subjects. Each of the 85 subjects underwent the recording procedure outlined in Figure 3.2. This procedure is designed according to SP10 standard, which is established to provide safe practices for automated sphygmomanometer performance evaluation [50]. This procedure consists of an oscillometric blood pressure recording, followed by readings of SBP and DBP by two trained nurse after a one minute pause. This is then followed by another one minute pause. The procedure is repeated again four more times to produce a total of five recording trials with ten reference blood pressure readings from two trained nurses. In this procedure, the subject is sat comfortably and upright in a chair where the UFIT device is strapped to the left wrist of the subject, which is raised to heart level. Another cuff is placed on the upper left arm also at heart level. Oscillometric measurements are recorded by the UFIT, while nurse readings are performed by auscultation using the cuff on the left upper arm. This procedure is repeated for all subjects, except for one who only underwent four recording trials instead of five, producing a total of 484 measurements. Each subject's age and gender are also recorded, along with their first name for identification purposes. Although the subjects are assumed to be healthy, many waveforms returned appeared to contain unknown disturbances or possible artifacts. Blood pressure estimation algorithms are implemented on this dataset and assessed using the nurse readings as the reference.

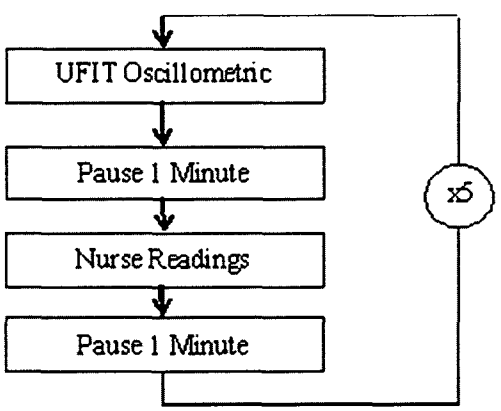

Figure 3.2. Flowchart of Biosign recording procedure

The two nurse readings are averaged to provide one SBP and one DBP reading for the reference. The data set provided contains relatively stable nurse readings, in that the maximum difference between the two nurses is no more than 2 mmHg. This again satisfies SP10 standard, which requires the mean difference to be no more than 5 mmHg [50]. In this case, averaging is an appropriate method to provide a single reference point that will be used to evaluate the performance of algorithms. Ages of the subject in this data set range from 12 to 80 years old. The distribution of the ages is shown in the histogram in Figure 3.3. Of these 85 subjects, 37 were female and 48 were male. Nurse readings of SBP ranged from 78 to 147 mmHg and DBP ranged from 42 to 99 mmHg across all subjects.

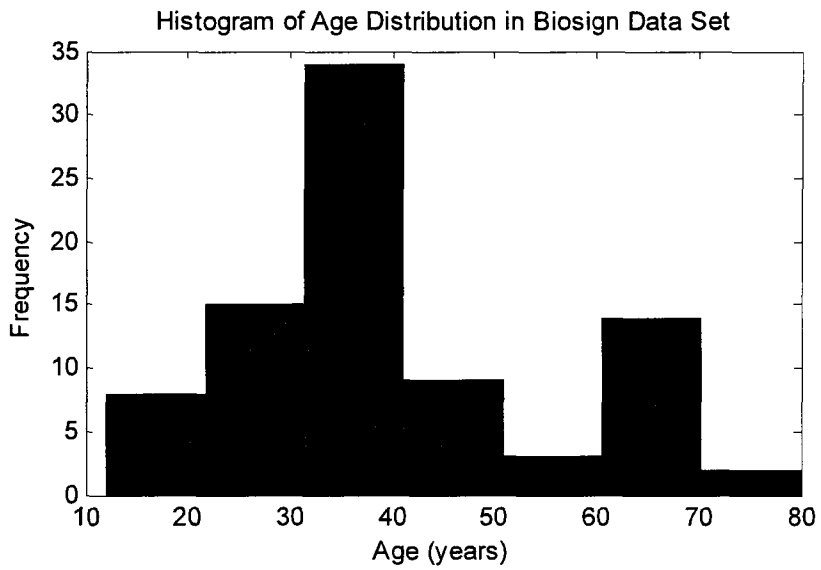

Figure 3.3. Distribution of ages in Biosign data set.

3.3 UFIT Signals

From each oscillometric recording, the UFIT produces a PP and CP signal instead of a deflation curve. This is the reason why the deflation curve and OMW must be reconstructed first from the PP and CP signals. The CP signal is the pressure signal in the cuff after passing through a low pass filter and the PP curve is the amplified discrete derivative of the pressure signal, which is defined by the following equation, where n is the sample number and $Def(x)$ is the deflation curve:

$$PP(n) = Def(n) - Def(n-1) \tag{3.1}$$

In this case, OMW extraction involves reconstructing the curve from the PP and CP signals. These two signals are a result of the signal acquisition method that is specific to the UFIT. Recovering the deflation curve and OMW will be discussed first.

3.3.1 Delay

A typical CP signal provided by Biosign is shown in Figure 3.4 (a) with a zoomed in segment shown in Figure 3.4 (b). This plot differs from the deflation curve shown in Figure 1.3 in that it has been filtered by an analog low pass filter and also digitized. Figure 3.5 shows a plot of the PP signals. Although these signals come from the same source and have the same duration, it was discovered that the CP signal seemed to exhibit a delay in comparison to the PP signal. This delay was determined by computing the cross correlation of the PP signal with the discrete derivative of the CP signal.

Since the CP signal is digitized, the signal must be filtered before taking its discrete derivative. Passing the signal through a 10^{th} order finite impulse response (FIR) low pass filter (LPF) with a cutoff at 10 Hz produced a smooth signal. The discrete derivative of this signal is then computed, which now has a similar shape to the PP signal. The two are then compared by cross correlation.

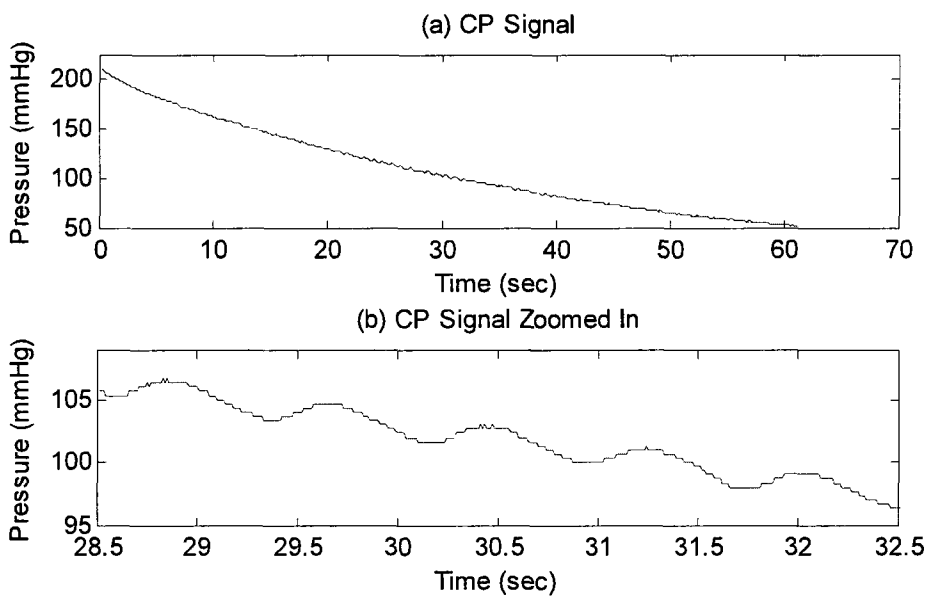

Figure 3.4. (a) Plot of the CP signal returned by the UFIT. (b) Zoomed in segment of the CP signal from the plot (a).

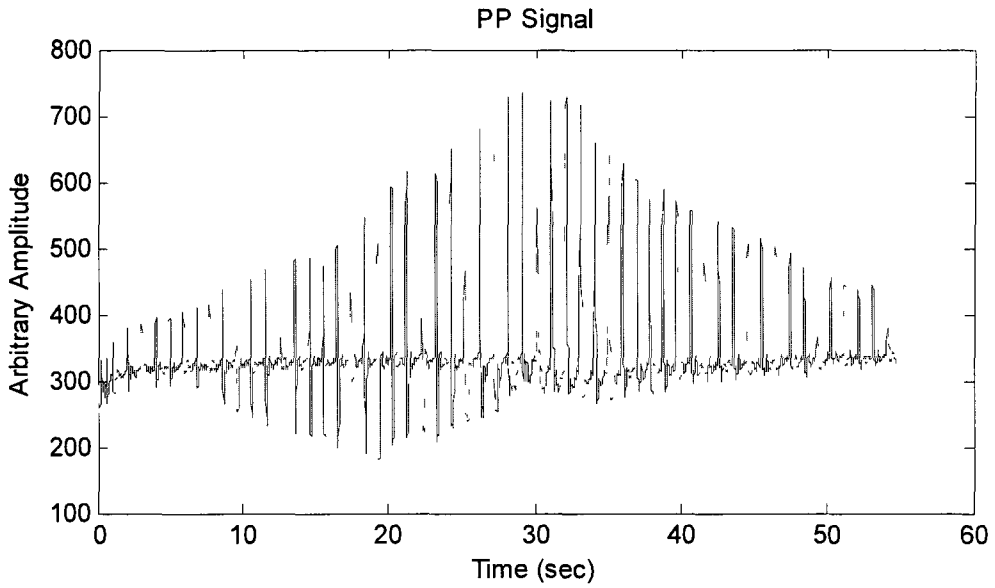

Figure 3.5. Plot of the PP curve returned by the UFIT.

Cross correlation was computed for all subjects and the maximum was never found to be at zero, indicating that a shift between the two signals was always present. The two signals are most similar when the signals are shifted, but the value of this shift differed among recordings. As a result, a part of this algorithm uses cross correlation to measure the delay and correspondingly trim the beginning of the CP signal to compensate for the delay.

3.3.2 PP Signal Amplification and Addition

The PP signal was also modified by multiplication and addition during its acquisition both by some unknown values. This leads to difficulties in recovering the original signal. By multiplying the discrete derivative of a signal with some gain, the signal recovered by integration will have the same shape as the original, but a larger magnitude. This effect will not affect the actual estimation of blood pressure because the algorithms rely on relative values of the amplitudes. However, adding some constant to the signal, or shifting the discrete derivative, will bias the slope information and change the shape of the signal when recovering it by integration. These effects may be observed in Figure 3.5, where it is seen that the entire signal is positive meaning the original signal should have an entirely upward trend, which is contradictory to what is expected. Deflation curves are decreasing curves,

with a downward trend, meaning that the derivative should contain some negative values as well.

In order to account for these effects, the CP signal is used to help provide a reference. A recursive process is implemented for the procedure of retrieving the deflation curve, as shown in the block diagram in Figure 3.6. First, the PP signal is subtracted by an initial guess of the additive constant, x, and then integrated by taking the cumulative sum and initializing the integration at 0. The initial guess of x must be chosen such that integration produces a signal with a negative trend. Second, this signal is put through a LPF with a cut-off frequency of 5 Hz so that the signal can be compared with the CP signal. Third, the integrated signal is scaled such that the start and end points lie within between the start and end points of the CP signal. The integrated signal should be decreasing, but unless the initial value x is chosen correctly, it may decrease at a faster or slower rate than the CP curve. Fourth, the new scaled signal and the CP signals are both fitted with a fourth order polynomial function and compared. If the initial estimate, x is correct, then the curve fitted to the CP signal should be very close to the curve fitted to the signal derived from the PP signal. This procedure is performed recursively for a range of values where the additive constant is expected to lie within. This range was simply experimentally determined such that any value that was outside of this range would produce a curve that either does not have a downward trend or has too much of a downward trend. After fitting to a polynomial, the two curves are compared by taking the difference and finding the mean square error. The x value in the range that produces the minimum mean square error is taken as the additive constant.

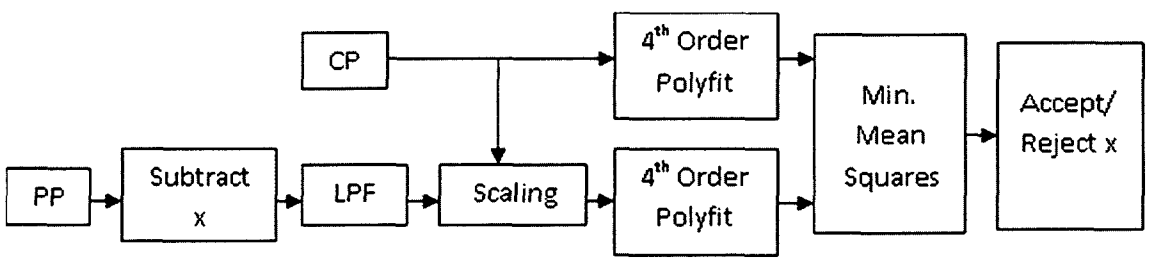

Figure 3.6. Block diagram of procedure to find the additive constant

3.4 OMW Extraction

Once the delay and amplification constants are determined, the deflation curve may be reconstructed by taking the integral of the PP signal. The delay is adjusted by trimming the CP signal and the additive constant is compensated for by shifting the PP curve. Integration is performed by calculating the cumulative sum of the PP signal, initialized with some starting value. The drawback of this method is that if there is error present in the starting value, then this error will accumulate throughout the integration. An accurate initialization of the integral is required so that the error does not grow with the summation. This initial value can be found from the CP signal. In order to reduce error as the integration carries through, the integration is re-initialized at different points. That is, instead of using just one initial value at the beginning, the integration is re-initialized at a few points. Initialization points are found by passing the CP signal through an FIR LPF with a cutoff at 0.3 Hz. The location where the CP signal intersects with the filtered signal is taken as the initialization points. When the LPF of the CP signal intersects the CP signal, these points are most likely to be points on the CP curve that are also on the original cuff deflation curve.

After initialization points are found, the cumulative sum of the PP signal is computed to recover the deflation curve. Due to the amplification effects, the deflation curve produced from the PP and CP signals will lead to extracted OMW signals with arbitrary amplitude. Once the deflation curve is recovered by integration, OMW extraction is then performed by the methods explained in Chapter 2, section 2.3. Both methods, filtering and detrending are performed and shown in Figure 3.7. Filtering is performed by a band pass filter with cutoff 0.1 Hz to 20 Hz. Since the PP signal produced by the UFIT to extract the OMW already passed through a LPF, a high pass filter was also found to be sufficient. The OMW extracted by this method is shown in Figure 3.7 (a). Detrending was performed by locating the pulses on the deflation curve using the zero crossing method. Because the deflation curve is a decreasing curve and has no flat, horizontal baseline, it was first flattened by a high pass filter so that peaks could be found. Correspondingly, the troughs were found as the minimum value in between each two peaks. After the minimum points were found, they are located on the deflation curve and connected by a piecewise linear function to produce a baseline. This

baseline is used in detrending to produce an OMW. Figure 3.7 (b) shows the OMW extracted by this method.

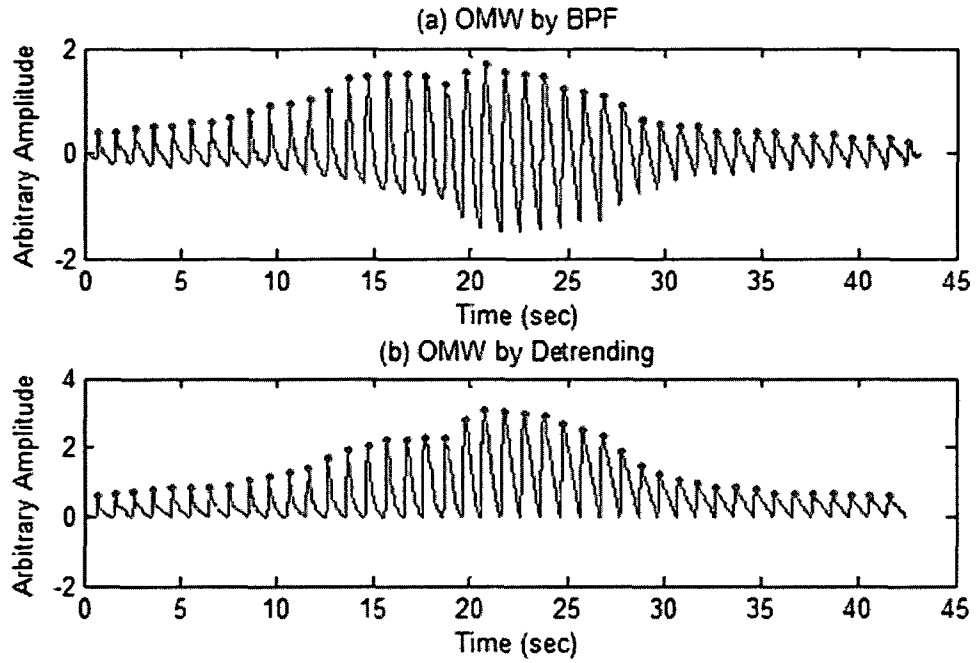

Figure 3.7. (a) OMW extracted using a BPF (b) OMW extracted by detrending.

The deflation curve consists of the pressure pulsations produced by the artery superimposed on the deflation of the cuff wrapped around the subject's arm. For accurate blood pressure estimation, the deflation of the cuff must be extracted as well. Here, the line of best fit constructed in the detrending method will be taken as the deflation of the cuff. This signal is important because it will is used to map systolic and diastolic points determined by algorithms applied to the OMW to actual blood pressure estimates.

3.5 Peak Detection

Before the remaining processing continues, peak detection algorithms must be settled on. Four different methods for peak detection were discussed in chapter 2. These algorithms were implemented and evaluated on 30 chosen recordings from the data set whose peaks were easy to identify manually. Manual identification of a pulse was performed by comparing their well-known characteristics. The shape should follow that reported in [77], where each pulse is first caused by a contraction of the left ventricle in the heart. This produces a displacement of blood volume, which produces a maximum point at the rounded

top of the waveform, as labeled in Figure 3.8 for one pulse. Afterwards, the aortic valve closes and the pressure pulse decreases. The dicrotic notch, also labeled in Figure 3.8, represents this stage in the cardiac cycle. Following the dicrotic notch, the reflected flow of blood from the arm back to the heart is shown in Figure 3.8 by a smaller, secondary peak in the waveform. The pressure pulse then continues decreasing until the minimum point in the cycle where the pulse repeats itself again for each heartbeat. The timing of these pulses should also occur relatively evenly spaced out, with some natural variation in heart rate known as HRV. A zoomed in portion of a pulse from the oscillometric method is shown in Figure 3.8. In oscillometric waveforms, due to the deflation of the cuff, the peaks of the OMW form an envelope which increases to a maximum amplitude (MAP) and then decreases. Only pulses which satisfied these criteria totally were chosen to evaluate the peak detection algorithms. Sometimes, measurements produce pulses that do not obey to the defined characteristics of a normal pulse and are unexpectedly shaped. The cause of these pulses is not known and due to the fact that no trained medical observer was present, they were not considered when evaluating the peak detection algorithms.

A subset of 30 chosen signals from the entire 484 data set was used to evaluate performance of peak detection algorithms. The OMW for these subjects contained pulses which varied individually in height and width. Each pulse still exhibited the same shape as described above and could be visually identified. Four existing methods for ECG peak detection, with some adjustments to compensate for the shape of oscillometric waveforms, are implemented and tested. These four methods, as mentioned from above consist of the Hilbert transforms [52], adaptive amplitude thresholds [53], slope thresholds [54], and zero crossings [55]. Another important quantity, which is used for finding the line of best fit in detrending, is the minimum value, or troughs, of each pulse. After the peak detection algorithms are evaluated and one is settled on, troughs are taken simply as the minimum point between each two detected peaks.

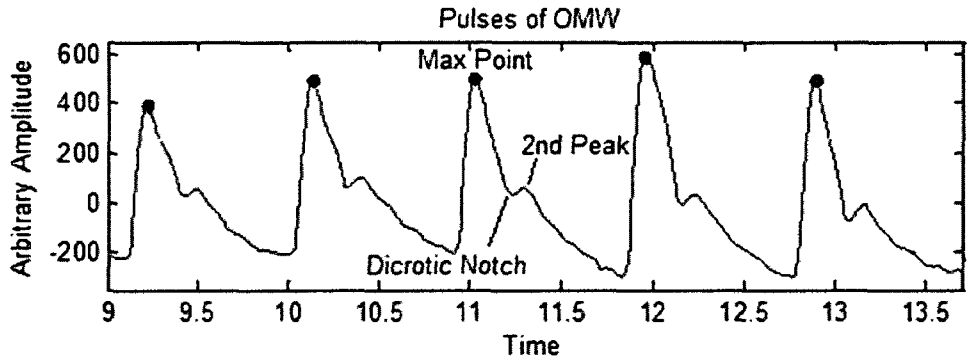

Figure 3.8. Manually identified pulse peaks.

In the first peak detection algorithm, the Hilbert transform is applied on the derivative signal. The derivative signal is recommended for use here [52]. The Hilbert transform is then applied to find the peaks, which is then re-located on the original signal. The discrete time Hilbert transform $\hat{u}(n)$ of the signal $u(n)$ can be found by convoluting the input signal by $-1/(\pi n)$. The definition is given in [78] as:

$$\hat{u}(n) = \frac{1}{N}\sum_{k=0}^{N-1} f(k) \cdot [1 - (-1)^{k-n}] \cdot \cot[(k-n) \cdot \frac{\pi}{N}] \tag{3.1}$$

This is equivalent to introducing a -90° phase shift and produces the imaginary part of the analytic function for which an analytic signal may be constructed:

$$z(n) = u(n) + j\hat{u}(n) \tag{3.2}$$

From this, the envelope of $u(n)$ may be obtained by the magnitude of $z(n)$ [52], [78]:

$$e(n) = |z(n)| = \sqrt{u^2(n) + \hat{u}^2(n)} \tag{3.3}$$

Adaptive amplitude threshold methods are borrowed from photoplethysmography [53]. This algorithm is based on finding a group of points that exceed the amplitude of some threshold and then the maximum in this group of points is detected as the peak. Here, the amplitude threshold is adaptive. To find the first peak, the threshold is initially set at some value multiplied by the maximum point in the signal. This was set to 0.2 times the maximum of the signal. After the first peak is detected, the threshold is determined by drawing a line with decreasing slope as shown in the zoomed in version of the oscillometric waveform in Figure 3.9. The threshold line has an adaptive slope, where the slope of each threshold is defined by:

$$Slope(n) = Slope(n-1) + s_r \frac{(v_{n-1} + STD_{OMW})}{F_s} \tag{3.4}$$

Here, *Slope(n)* is the slope of the n^{th} threshold line, s_r is the slope change rate (set to 0.6 in accordance to [53]), v_{n-1} is the previous peak amplitude STD_{OMW} is the standard deviation of the OMW envelope amplitudes and F_s is the sampling rate, 100 Hz.

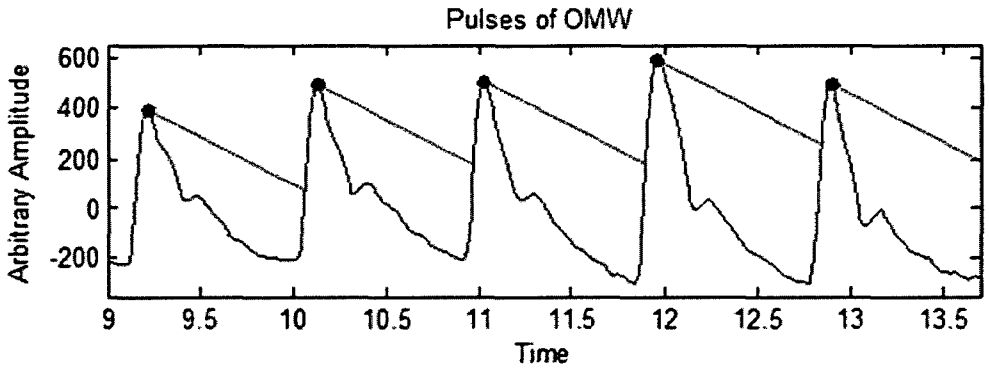

Figure 3.9. Adaptive amplitude thresholds.

A threshold based method is adopted in the slope based method. Again, the first derivative of the recovered OMW signal is taken because it is hypothesized that this signal is less susceptible to artifacts [54]. It is also assumed that peaks should occur right after the maximum slope and just before the minimum slope of each pulse. Once the first derivative is found, a set of rules based on two slope thresholds are applied. These two thresholds are A_{pos} and A_{neg}, the positive slope threshold and the negative slope threshold respectively. When three consecutive samples are greater than A_{pos} and then two consecutive samples out of the next 10 samples are less than A_{neg}, the maximum and minimum slopes are found. The peak should then be detected on the original signal as the maximum between these two inflection points.

Peaks can also be found by applying the method of zero crossings. Here, the signal is first filtered and then upward and downward zero crossings are found. The filter used here differs from [55] in that it will be slightly adaptive to the subject. A two-step recursion is performed where a third order IIR Butterworth bandpass filter with fixed cutoffs at 0.25 Hz and 2.5 Hz is used in the first iteration. The filter is fed both in the forward and reverse directions. This centers the signal on zero and eliminates the high and low frequency components of the signal. Zero crossings are then detected and the peaks are found as the maximum values in

between each upward crossing and downward crossing. The second iteration uses these detected peaks to build a bandpass filter which is centered on the frequency of the heart rate with cutoffs at twice the standard deviation on each side. That is, the cutoffs are now at $HR - 2 \cdot STD_{HR}$ and $HR + 2 \cdot STD_{HR}$, where HR is heart rate and STD_{HR} is the standard deviation of heart rate. The heart rate is taken as the inverse of the mean of the peak intervals from the first iteration and the standard deviation is calculated as the standard deviation of the peak intervals. Finally, zero crossings are once again found, for which the final peaks are detected as the maximum value in between each upward and downward crossing.

3.6 OPI

Three definitions of the OPI (baseline-to-peak, peak-to-peak and area) are applied to the OMW extracted by filtering, while only two definitions of the OPI (peak-to-peak and area) are applied to the OMW extracted by detrending. The OMW extracted by detrending has a zero baseline as shown in Figure 3.7 (b). The OPI defined from baseline to peak and from peak to peak will produce the same results for the OMW extracted by detrending. Figure 3.10 shows the three different OPI calculations on a single pulse for an OMW extracted by a HPF.

Simpson's rule was used as the numerical approximation for the definite integral. Area of the discrete signal *f(n)* is then found by the following calculation:

$$\int_a^b f(n)dn \approx \frac{b-a}{6}[f(a) + 4f\left(\frac{a+b}{2}\right) + f(b)] \tag{3.5}$$

Here, the area is calculated for each pulse to produce an OPI. The start and end of each pulse on the OMW is taken as the troughs. Evaluation of the extraction methods and OPI definitions is the goal here. Five signals are available at this point, three defined OPI values from the filtered OMW and two defined OPI values from the detrended OMW.

3.7 Envelope Cleaning

Once the OPI is identified, an envelope is formed which can soon be used for estimating SBP and DBP values. Before this estimation though, envelope cleaning methods are required.

This produces a curve that allows for applying algorithms for SBP and DBP estimation. Methods for this step include median filtering, moving average filtering and curve fitting. These algorithms will be implemented and the resultant envelopes will be assessed individually.

Envelope cleaning methods are necessary so that algorithms that locate SBP and DBP points on the envelope may proceed. For example, Figure 3.11 presents the waveform before cleaning where the OPI used is the baseline-to-peak on an OMW extracted by filtering. High frequency fluctuations are evident on the envelope. These fluctuations have a great effect on the algorithms for estimating blood pressure. For instance, when the derivative of the envelope is found for the slope based algorithms, the fluctuations between each peak will heavily influence SBP and DBP estimation. For the SCA, if the OMW is not smooth, inflection points caused by the high frequency fluctuations will be taken as the SBP and DBP instead of the inflection points caused by the overall trend of the OMW envelope. Amplitude based methods will also be effected. These fluctuations are the reason for the fact that one amplitude value may correspond to more than one point on the envelope. Envelope cleaning is implemented to reduce in the number of points that one amplitude value may correspond to.

Median filtering is a nonlinear filter which is often applied to image processing because of its strong ability to preserve edges and remove impulse noise. In blood pressure, median filtering has shown to work well in removing spurious points caused by possible motion artifacts [23]. Moving average filters are employed like in [24], [25]. The order of these two filters will be the same as in corresponding literature: a 3 point median filter is used as in [23] and 9 point moving average filter is used as in [25].

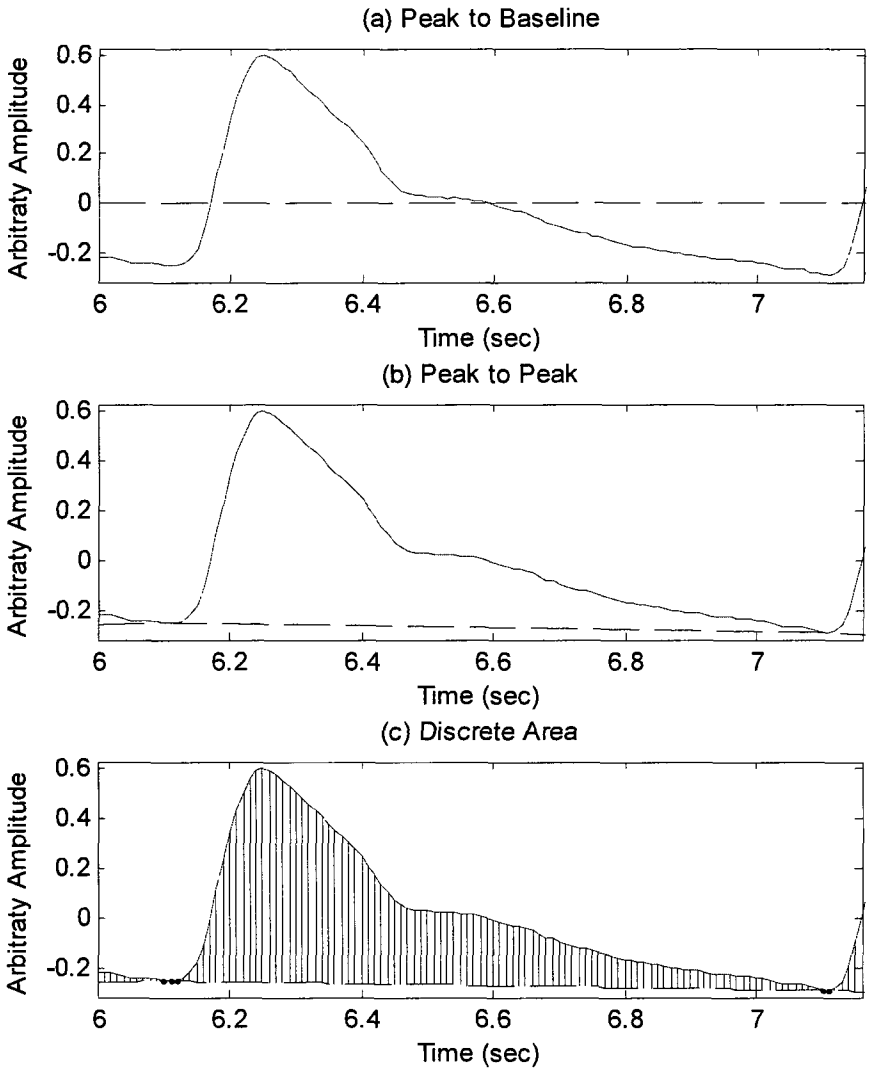

Figure 3.10. OPI extracted by (a) Baseline to peak, (b) Peak to peak, (c) Area

Curve fitting is the final technique considered to clean the envelope. Fitting is performed by constructing either a Gaussian or Cauchy-Lorentzian function that best fits the given data. These functions are defined by a set of input parameters, such as mean, variance and amplitude. The set of inputs that minimize the sum of squares between the fitted curve and the data is known as the least squares best fit. Given a data set $Y = [y_1, \ldots, y_M]$ that depends on $X = [x_1, \ldots, x_M]$, it is desired to replace Y with cleaned data $\hat{Y} = [\hat{y}_1, \ldots, \hat{y}_M]$. The function is defined by $f(x)$ such that $\hat{Y} = [\hat{y}_1 = f(x_1), \ldots, \hat{y}_M = f(x_M)]$, which depends on N parameters $f(x; a_1, \ldots, a_N)$:

$$\hat{y}_1 = f(x_1; a_1, a_2, \ldots, a_N)$$
$$\hat{y}_M = f(x_M; a_1, a_2, \ldots, a_N) \tag{3.1}$$

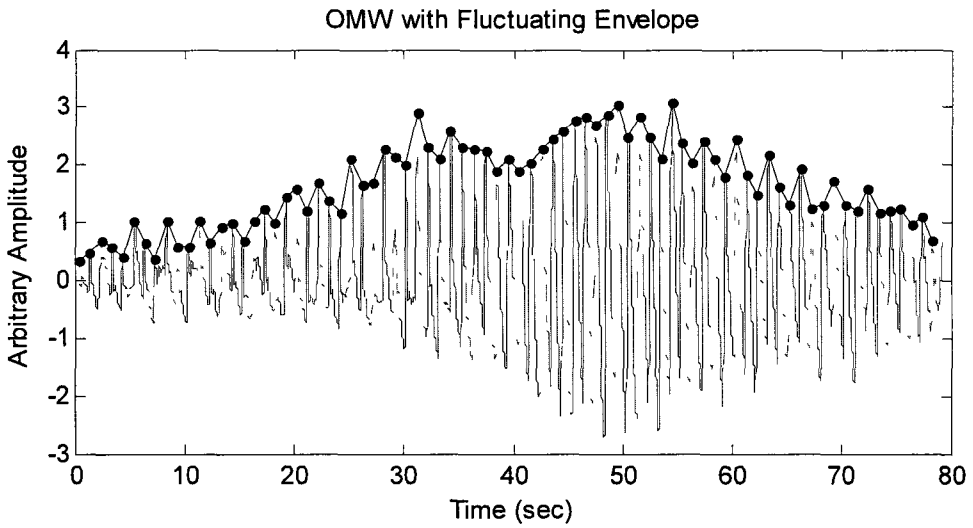

Figure 3.11. OMW prior to cleaning.

It is desired to solve these set of equations to obtain a_1, a_2, ... a_N which minimizes the difference between Y and $\hat{Y}$ in terms of the least square error:

$$R^2 = \sum_{i=1}^{M} [y_i - \hat{y}_i]^2$$
$$R^2 = \sum_{i=1}^{M} [y_i - f(x_i; a_1, a_2, \ldots, a_N)]^2 \tag{3.2}$$

To obtain the least square error, the variables a_1, a_2, ... a_N can be found by setting the partial derivatives to zero and solving:

$$\frac{\partial R^2}{\partial a_1} = 0$$
$$\frac{\partial R^2}{\partial a_M} = 0 \tag{3.3}$$

Existing literature uses symmetric Gaussian and Lorentzian functions to fit the envelope [28]-[30]. However, the OMW envelope is not always symmetric so, in this work, asymmetric functions are also proposed and implemented. These will account for the obvious differences between the systolic and diastolic side of the envelope. Firstly, the Gaussian

function will be considered where μ represents the mean, σ represents standard deviation and A represents amplitude:

$$f(x) = A \cdot exp\left\{\frac{-(x-\mu)^2}{2 \cdot \sigma^2}\right\} \tag{3.4}$$

This function is symmetric, which may be undesired. An asymmetric version of this function can be constructed with different standard deviation and amplitude to the left and right side of its mean:

$$f(x) = \begin{cases} A_1 \cdot exp\left\{\frac{-(x-\mu)^2}{2 \cdot {\sigma_1}^2}\right\}, & x < \mu \\ A_2 \cdot exp\left\{\frac{-(x-\mu)^2}{2 \cdot {\sigma_2}^2}\right\}, & x > \mu \end{cases} \tag{3.5}$$

To the left side of the mean, μ, this function has a standard deviation and amplitude, σ_1 and A_1. To the right side of the mean, this function has a standard deviation and amplitude, σ_2 and A_2. This gives the function asymmetric properties, as two different distributions are used to construct the function. At the point where $x = \mu$, the two functions should be equal to each other and A_1 can be expressed in terms of A_2 as:

$$A_1 \cdot exp\left\{\frac{-(\mu-\mu)^2}{2 \cdot {\sigma_1}^2}\right\} = A_2 \cdot exp\left\{\frac{-(\mu-\mu)^2}{2 \cdot {\sigma_2}^2}\right\} \tag{3.6}$$

$$A_1 = A_2$$

On both sides of the mean, the function exhibits the same distribution as the Gaussian function, but with different standard deviation. Amplitudes are also found to be the same. Another function, which exhibits properties of an asymmetrical Gaussian function, is also implemented which is built by summing two Gaussian functions. This function has been implemented for OMW in [29] and is expressed here:

$$f(x) = A_1 \cdot exp\left\{\frac{-(x-\mu_1)^2}{2 \cdot {\sigma_1}^2}\right\} + A_2 \cdot exp\left\{\frac{-(x-\mu_2)^2}{2 \cdot {\sigma_2}^2}\right\} \tag{3.7}$$

This is simply two Gaussian functions with different mean, standard deviation and amplitude summed together.

Second, the Lorentzian function is implemented [30]. This function may be represented by the following equation where again, A is amplitude, μ is mean and σ is standard deviation:

$$f(x) = A \cdot \left\{ \frac{1}{\sigma^2 + (x - \mu)^2} \right\} \tag{3.8}$$

Like the Gaussian, this function is also symmetric about its mean. An asymmetric representation of this function may be expressed by:

$$f(x) = \begin{cases} A_1 \cdot \left\{ \frac{1}{\sigma_1{}^2 + (x - \mu)^2} \right\}, & x < \mu \\ A_2 \cdot \left\{ \frac{1}{\sigma_2{}^2 + (x - \mu)^2} \right\}, & x > \mu \end{cases} \tag{3.9}$$

At the point where $x = \mu$, the amplitude A_1 can also again be expressed in terms of A_2:

$$\begin{gathered} A_1 \cdot \left\{ \frac{1}{\sigma_1{}^2 + (\mu - \mu)^2} \right\} = A_2 \cdot \left\{ \frac{1}{\sigma_2{}^2 + (\mu - \mu)^2} \right\} \\ A_1 \cdot \left\{ \frac{1}{\sigma_1^2} \right\} = A_2 \cdot \left\{ \frac{1}{\sigma_2^2} \right\} \\ A_1 = A_2 \cdot \left\{ \frac{\sigma_1^2}{\sigma_2^2} \right\} \end{gathered} \tag{3.10}$$

This function will exhibit Lorentzian distribution on both sides of the mean, but with different standard deviation and amplitude. Also, like the Gaussian implementation, two Lorentzian functions can also be summed up. This function has not previously been used for curve fitting an OMW, but it combines the idea of using a Lorentzian function presented in [30] with the idea of summing up two functions like the one used for Gaussian distributions in [29]. Two Lorentzian functions, with different mean, amplitude and standard deviation, are summed up as follows:

$$f(x) = A_1 \cdot \left\{ \frac{1}{\sigma_1{}^2 + (x - \mu)^2} \right\} + A_2 \cdot \left\{ \frac{1}{\sigma_2{}^2 + (x - \mu)^2} \right\} \tag{3.11}$$

All four of these functions are implemented and evaluated. Minimization to produce the least square error is performed in MATLAB by Levenberg-Marquardt optimization. The initial parameters used for mean, amplitude and standard deviation are found by applying a LPF to the signal to be fitted. Then, the location of the maximum point and its amplitude are found, which are taken as the initial guesses for the amplitude and mean. On both sides of the

maximum point, the point which corresponds to half the maximum is found and its width is taken as the initial standard deviation. These initializations are estimated to try and reduce the amount of time needed for the optimization to converge.

3.8 Algorithms for Blood Pressure Estimation

After the OPI is cleaned, algorithms for blood pressure estimation may be applied to produce an estimate of SBP and DBP. These algorithms are applied as described in Chapter 2. One important step not mentioned in any of the literature survey but used in this work is the use of interpolation on the envelope. The envelope is derived from each heartbeat, so it can be considered as a signal which is sampled at a rate equivalent to the subject's heart rate. Typically, heart rate can range between 60 to 120 beats per minute (or 1 Hz to 2 Hz), depending on the age of the individual [79]. Also, the heart rate is not always regularly timed and actually contains known HRV as well [6]. This poses a problem because if blood pressure can only be estimated at the location of these pulses, the period in between the maximum of the pulses is lost.

In the procedure for recording oscillometric blood pressure, a cuff is deflated and the pressure pulsations in the artery are recorded. These pulsations are used to determine SBP and DBP. However, it is still possible that the pulse which corresponds to SBP or DBP may not actually be induced at the right time. For example, consider a typical deflation rate of 2.5 mmHg per second, which is the mean of typical deflation rates which range between 2-3 mmHg discussed earlier [56]. At a rate heart rate of 60 beats per minute or 1 beat per second, there is an average drop of 2.5 mmHg between each identified pulse. This means that blood pressure values can be identified at no closer than 2.5 mmHg apart. Assuming that deflation is linear and no HRV is present, then in this example, the timing of the heart beats may result in a pulse induced at 121.5 mmHg and another at 118.75 mmHg. However, if the subjects true SBP is 120 mmHg for this recording, then algorithm will not detect it because of the timing of heart beats and the deflation rate. No pulse was actually induced at this pressure, which is why interpolation is used to help overcome a scenario such as this. If the actual non linear deflation rate of the cuff and the HRV are considered as well, which both can lengthen

the time period between two heart beats, the pressure between two pulses could potentially be even larger. Estimation of blood pressure is less accurate when interpolation is not used.

In order to compensate for this loss in accuracy, interpolation between peaks is performed. Since the data points in the envelope have already been fitted to a defined function, interpolation can be performed easily to produce a clean curve. The new sampling rate is chosen to be 100 Hz, the same sampling frequency of the original data. As a result, the envelope is interpolated such that a fixed difference of 0.1 seconds exists between each timestamp. Interpolation is important so that SBP and DBP may now be found at points in between detected the peaks. Algorithms are then applied to locate the points on the envelope which correspond to SBP and DBP.

Implementations of the algorithms for blood pressure estimation are illustrated in Figure 2.3 to Figure 2.6. These figures show both the cleaned envelope and the cuff deflation, which is used to find the actual pressure values in mmHg. These four algorithms all operate differently and as a result produce different estimates of SBP and DBP.

For MAA and LAA, the two height based algorithms, systolic and diastolic ratios must be defined prior. Some works have defined characteristics ratio which work best for them, but here, these ratios will be found by least squares optimization. Suppose the function $s_i(r_s)$ returns the SBP for a given subject, i, with input systolic ratio r_s, and the function $d_i(r_d)$ does the same but returns the DBP with the input diastolic ratio r_d. The value i is subject number, which ranges from 1 to 85, and the values r_s and r_d are ratios, which range from 0 to 100. For a given ratio, the least squared error in blood pressure across all subjects may be expressed as:

$$\begin{aligned} Err_{SBP} &= \sum_{i=1}^{85} [SBP_i - s_i(r_s)]^2 \\ Err_{DBP} &= \sum_{i=1}^{85} [DBP_i - d_i(r_d)]^2 \end{aligned} \tag{3.12}$$

Here, SBP_i and DBP_i represent the nurse readings for subject i. It is then desired to find the ratios r_s and r_d which minimize the produced systolic and diastolic error.

Since the functions $s_i(r_s)$ and $d_i(r_d)$ represent the entire blood pressure estimation algorithms, they are quite complicated and a mathematical function is difficult to derive. Instead of performing the least squares optimization analytically, the ratios which produce the minimum least squared error are found by evaluating the error empirically for a predefined set of ratios. The errors are found by using the defined systolic and diastolic ratios for all 85 subjects. Using a set of ratios results in a set of errors which can be taken as points to which a polynomial function can be fitted too. Fitting a polynomial allows for the points in between to be interpolated and then a minimum value can be estimated. This minimum point then corresponds to the minimum least squared error so that the appropriate ratios can be determined. Both the MAA and LAA go through this procedure so that systolic and diastolic ratios can be determined.

3.9 SBP and DBP Computation

The implemented algorithms all locate different points according to how the algorithms operate as described in Section 2.6. The time stamps on the envelope that are found to be the SBP and DBP points are located are then found on the cuff deflation so that SBP and DBP can be estimated. Figure 2.3 to Figure 2.6 show the operation of these algorithms in finding SBP and DBP. The deflation curve is also shown in these figures, which illustrates how the final SBP and DBP values are obtained.

3.10 Performance Metrics

In order to assess algorithm performance, metrics are defined. These are used to evaluate the performance of the different peak detection algorithms, OPI definitions, envelope cleaning methods and SBP/DBP estimation algorithms. Evaluation of methods for OMW extraction is assessed together with the OPI definitions. For peak detection, performance is graded based on Type II errors, also known as false negatives. Some subjects were selected whose pulses are identified manually. Since no trained observer was present to identify these pulses, only obvious pulses were selected. Due to this restriction, evaluation of the robustness of each algorithm depended primarily on how the algorithm performed in terms of identifying false negatives. False negatives occur when pulses which are manually identified are not identified by the algorithm. Since manual peak detection identifies only the obvious pulses, then the

peak detection algorithm should always be able to identify these peaks as well. Peaks that are not obvious and difficult to identify as fitting the model of a typical blood pressure pulse are not considered. If false peaks are detected however, their effects will be compensated for when envelope cleaning algorithms are employed.

Evaluation of the OPI definitions, envelope cleaning methods and SBP/DBP estimation algorithms rely on comparison with reference blood pressure readings. MAP will first be used to assess the OPI and envelope cleaning algorithms. At this point, estimated SBP and DBP values are not available, so MAP is used because it can be easily estimated and compared to a reference reading. Estimation of MAP from the OMW is found as the cuff pressure which makes the amplitude of the envelope maximum. Reference MAP readings can be computed by using equation (2.4) where SBP and DBP are the nurse measurements. To assess performance, MAE and STD are used to compare the differences between the estimated and reference MAP values in units of mmHg. Algorithms to locate SBP and DBP points on the envelope are evaluated by comparing the estimated blood pressure to the nurse readings. This is the final step of the algorithm shown in Figure 1.1, where the outputs are estimated blood pressure values. Again, the MAE and STD are used as metrics to compare the estimated values obtained by the algorithms with the reference values obtained by the two nurses.

Chapter 4 – Results for Oscillometric Algorithms

Using the data set of 85 subjects provided by Biosign, the algorithms for oscillometric blood pressure estimation described in Chapter 3 are implemented and results are assessed.

4.1 Peak Detection

Algorithms that are used for peak detection are tested with 30 selected subjects whose OMW appeared to be composed of differently sized pulses. The OMW of these subjects were extracted and then peaks were manually identified. Peak detection algorithms were evaluated using these peaks. From these 30 subjects, a total of 2032 peaks were identified. Table 4.1 shows the results of the four peak detection algorithms in identifying these peaks. The numbers here represent the percentage of the total number of peaks identified.

	Peak Detection Algorithms			
	Hilbert Transform	**Amplitude Threshold**	**Slope Threshold**	**Zero Crossing**
Identified	2032	1973	1995	2032
Percent of peaks detected	100.0%	97.1%	98.2%	100.0%

Table 4.1. Results of the peak detection algorithms.

From these results, it is clear that the Hilbert transform and zero crossing methods outperform the amplitude and slope thresholds methods. Amplitude and slope threshold based methods are respectively able to identify 96.6% and 97.7% of peaks. The other two methods, however, are able to identify all peaks and thus are more suitable for this application. This can be attributed to the fact that the envelope of the OMW is known to start at low amplitudes, increase to a maximum point and then decrease back down to low amplitudes again. This behavior is very different than that of ECG and arterial blood pressure signals. ECG and arterial pressure signal amplitudes may vary over time, which is what the thresholds established in these algorithms attempt to compensate. Amplitudes of an OMW envelope vary over time as well, but the envelope itself also exhibits a trend where it increases to a maximum point and then decreases back down. This envelope is unique to the OMW and results in the much larger amplitude swings than in ECG and arterial blood pressure. Threshold based algorithms that were created for ECG and arterial signals may have a difficult time adjusting to the OMW envelope. An initial threshold must also first be

set and this threshold must adapt to the shape of the envelope and take into account the variations in the OMW. This complicates matters when compared to the ECG or arterial blood pressure signal.

Zero crossing methods and Hilbert transforms are more robust, in that different OMW amplitudes do not affect their performance. Between these two, the zero crossing method was settled on for the remainder of the analysis. This is because performing Hilbert transforms on the derivative signal, then relocating the peaks on the original signal is a more computationally intensive process than the zero crossing method, which consists of filtering and finding zeros. Zero crossings are preferred because they also provide an estimate of heart rate when tuning the frequency of the band pass filter, which is used for other parts of the study.

4.2 OMW Extraction & Oscillometric Pulse Index

Extraction of the OMW by filtering and detrending, along with the three definitions of OPI are assessed. As mentioned in Section 3.9, the MAP is used to for assessment by comparing the estimated MAP from the algorithms to the MAP derived from the nurse reference readings. Three definitions of OPI are considered for the OMW extracted by filtering, whereas two definitions of OPI are considered for the OMW extracted by detrending because the peak to baseline and peak to peak OPI yield the same results. MAE and STD between the estimated MAP by these methods and the calculated MAP using equation (2.4) are shown in Table 4.2.

OMW Extraction Method:	Filtering			Detrending	
OPI Defined:	P2B	P2P	Area	P2B/P2P	Area
MAE (mmHg)	16.70	9.70	7.54	10.03	7.55
STD (mmHg)	11.56	12.42	9.48	12.39	9.51

Table 4.2. MAE and STD comparing estimated MAP for different OPI definitions and two OMW extraction methods.

From the results here, the method which produces the smallest MAE and STD is the OPI calculated by taking the area under each pulse defined for the OMW extracted by filtering, although the area calculated OPI defined for the OMW extracted by detrending follows behind it very closely. In both cases, area values defined as the OPI perform the best. This can be explained by the fact that area values contain more information. Peak-to-baseline and

peak-to-peak methods contain information only about the height of the pulse which is a one dimensional quantity. Area values are two dimensional and are influenced by the overall shape of the pulse, including its width. On top of that, the peak-to-peak OPI outperforms the peak-to-baseline OPI because it considers the entire pulse amplitude, not just the upper portion of it. Based on these results, information regarding the width and shape of the pulse seem to play an important role in the definition of the OPI.

Table 4.3 also shows that filtering to extract the OMW is better than detrending to extract the OMW however, these differences are very small. This can be attributed to the fact that detrending is similar to high pass filtering. Both of these operations remove low frequency components of the signal, just by different means. The small differences that are shown in the results can be attributed to the band pass filtering operation where high frequency components of the signal are filtered out. Detrending does not reduce the spectral component at these frequencies. For the remainder of this work, the extracted OMW by filtering is used and the OPI chosen is defined by taking the area under each pulse.

4.3 Envelope Cleaning

Algorithms that clean the envelope are compared using estimated MAP values as well. First, the six different algorithms are evaluated on the area defined OPI value, as shown in Table 4.3. Errors, along with the original data, are shown in terms of MAE and STD again. The methods here are median and moving average (MA) filtering, and curve fitting by summing two Lorentzian or two Gaussian functions and curve fitting by defined asymmetrical Lorentzian or asymmetrical Gaussian functions.

	Cleaning Algorithm						
	Original	**Median Filter**	**MA Filter**	**Sum Two Lorentz**	**Sum Two Gaussian**	**Asymm. Lorentz**	**Asymm. Gauss**
MAE (mmHg)	7.54	6.65	6.31	5.32	5.28	6.11	6.69
STD (mmHg)	9.48	8.67	8.62	7.57	7.52	8.27	9.03

Table 4.3. Estimated MAE and STD in comparison to MAP after cleaning.

From the results, all cleaning algorithms show improvement in MAP estimation when compared to the original envelope. Summing two functions and then performing curve fitting produced the best results out of all the methods and even better results than the asymmetric

functions. This can be attributed to the fact that these functions contain more variables. Summing up two functions in equations (3.7) and (3.11) are based on 5 variables: μ, A_1, A_2, σ_1 and σ_2, whereas the asymmetric functions in equations (3.5) and (3.9), are based on 6 variables: μ_1, μ_2, A_1, A_2, σ_1 and σ_2. An additional variable in this case gives the function more versatility in fitting, while maintaining the desired shape set by the functions.

One drawback of curve fitting is that they can be biased if the input envelope is noisy or contains unwanted outliers. This can be suppressed by median or moving average filters. Combining these filters with curve fitting is also investigated to see if better results may be produced. Table 4.4 shows the results of curve fitting after the median filter is applied and Table 4.5 shows the results of curve fitting after the moving average filter is applied.

	Median Filter	
	Sum Lorentz	**Sum Gaussian**
MAE (mmHg)	5.31	5.34
STD(mmHg)	7.45	7.58

Table 4.4. Curve fitting after median filter is applied.

	Moving Average Filter	
	Sum Lorentz	**Sum Gaussian**
MAE (mmHg)	5.21	5.20
STD (mmHg)	7.42	7.44

Table 4.5. Curve fitting after the moving average filter is applied.

Both these filters add a level of noise reduction that improves the estimation of MAP after curve fitting. The moving average filter, which is a realization of a low pass filter, provides the best results. Differences in fitting the function by Gaussian or Lorentzian are minor. This small difference may be attributed to the fact that the two functions are very similar to each other in shape [84]. Both are also already accepted methods for fitting the OMW as well. In this work, the method used for artifact removal and reduction of interference will consist of a two-step procedure, where first the envelope is passed through a moving average filter and then fitted by a sum of two Gaussian functions, since this method performs the best overall.

4.4 Algorithms for Blood Pressure Estimation

MAA ratios were estimated as 0.55 for systolic and 0.45 for diastolic and LAA ratios were estimated as 0.6 for systolic and 0.3 for diastolic. Figure 4.1 shows the curves of the MAE (in solid dots) and STD (in open squares) for the error in MAA from (a) SBP estimation and

(b) DBP estimation. These ratios are found from a set of 40 randomly selected subjects from the 5th trial of Biosign recordings. The ratio which produces the lowest point for the MAE in dots is taken as the final characteristic ratio for the algorithms. Figure 4.2 shows the same curves for the LAA algorithm.

After applying all algorithms onto the Biosign data set, the results in terms of MAE and STD are shown Table 4.6. This table shows the error for each trial, where error is calculated in terms of the nurse SBP and DBP readings. The two height based algorithms seem to perform better than the slope based ones, with MAA performing slightly better throughout the five trials. This could be the reason why the MAA is the far most popular algorithm used today. Of the two slope based algorithms, the MMSA performs the best. Its DBP estimates are comparable to the height based ones, but the SBP estimates still lag behind. The SCA, which is yet to be published, performs the worst out of all.

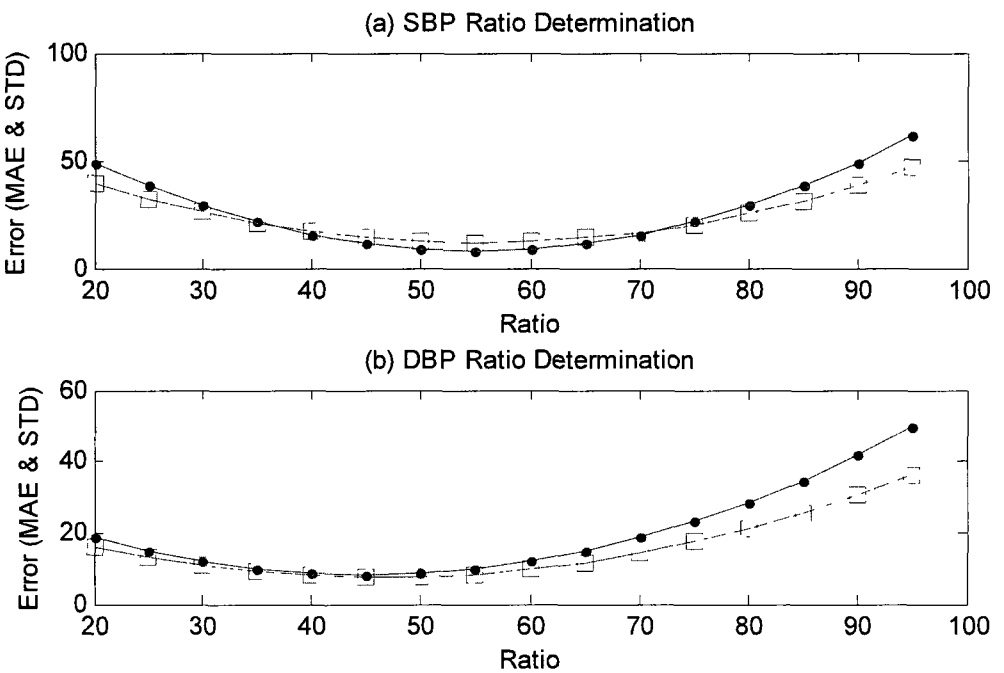

Figure 4.1. MAA ratio determination for (a) systolic and (b) diastolic.

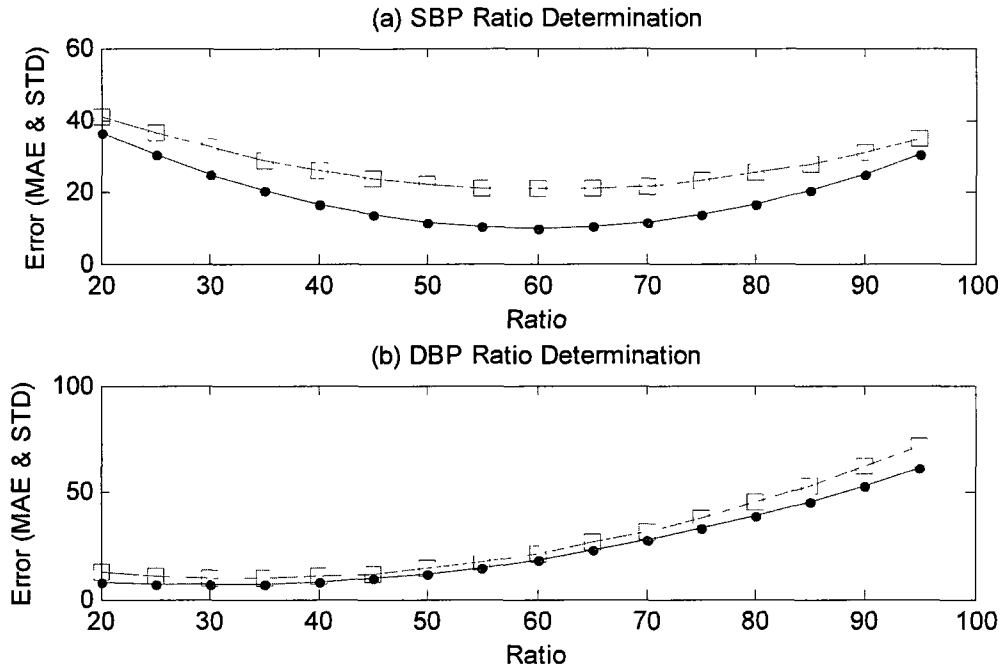

Figure 4.2. LAA ratio determination for (a) systolic and (b) diastolic.

		Trial 1		Trial 2		Trial 3		Trial 4		Trial 5	
		MAE	STD	MAE	STD	MAE	STD	MAE	STD	MAE	STD
MAA	SBP	7.94	7.01	7.07	6.77	7.11	5.43	7.94	6.96	6.40	6.96
	DBP	7.65	7.72	7.05	7.31	6.53	5.96	7.26	7.21	6.84	7.79
LAA	SBP	7.73	7.29	8.14	10.77	7.37	5.79	7.46	6.51	7.09	7.86
	DBP	6.78	5.99	7.98	8.62	6.70	4.92	6.71	5.15	5.96	5.82
MMSA	SBP	9.88	8.41	9.13	8.10	9.87	7.54	9.66	7.17	9.75	7.83
	DBP	7.21	5.76	7.74	9.677	6.75	5.50	6.78	5.53	6.93	5.56
SCA	SBP	15.67	9.26	15.40	8.13	15.88	8.87	15.55	8.43	15.88	8.58
	DBP	7.61	5.66	7.74	9.32	6.97	5.47	7.08	5.55	7.17	5.38

Table 4.6. Estimated MAE and STD in mmHg between estimated SBP and DBP and nurse readings for all algorithms over 5 trials.

Bland-Altman plots are also constructed for the 5th trial of results and shown in Figure 4.3 to Figure 4.6. These plots are constructed for each of the four algorithms. SBP and DBP estimates from each algorithm are compared with the nurse readings and plotted in the four figures. Lines which represent the mean difference between the readings and limits of agreement are also shown in each Bland-Altman plot. The limits of agreement are computed as the mean difference ± 1.96 the standard deviation.

It is also worth mentioning that the algorithms may perform differently for each subject. That is, someone whose nurse reading may vary with their MAA estimation by over 20 mmHg

may still be within 5 mmHg for the MMSA. It is difficult to choose one algorithm over another because they rely on two different fundamental approaches. Moreover, choosing one algorithm over the other may eliminate important physiological features that might otherwise be useful. A potential future work might be to determine which algorithm performs best on which subject and why. However, work here is focused on improving the overall accuracy of the SBP and DBP estimation for all subjects. Oscillometric algorithms here are used to compare SBP and DBP with nurse measurements for each trial. Another way to obtain an accurate blood pressure estimate could be to average the pressure of each subject over their 5 recording trials. Rather than selecting a single value from the 5 trials, taking the average of all pressure estimates produces one SBP and DBP estimate that is more representative of the subject true blood pressure.

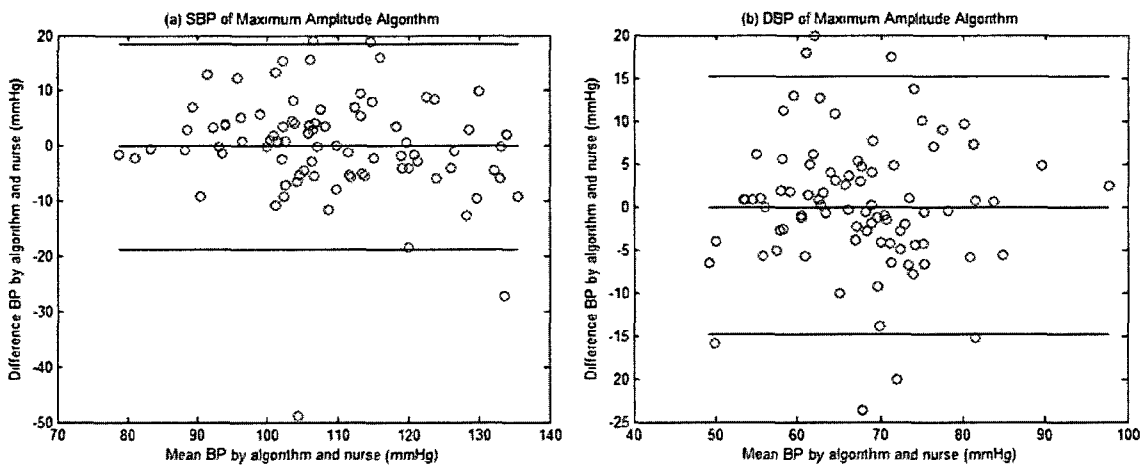

Figure 4.3. Bland-Altman plot of MAA results for (a) SBP and (b) DBP.

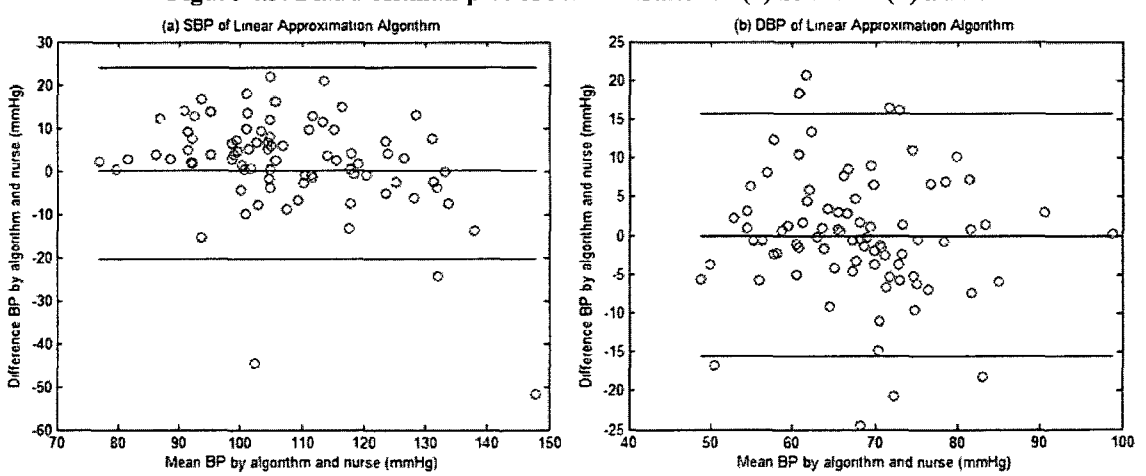

Figure 4.4. Bland-Altman plot for LAA results for (a) SBP and (b) DBP.

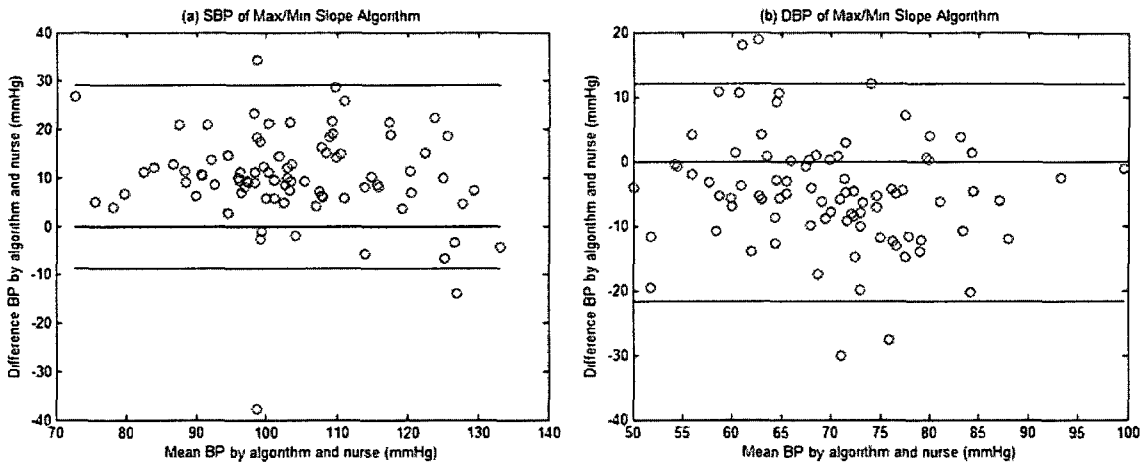

Figure 4.5. Bland-Altman plot for MMSA results for (a) SBP and (b) DBP.

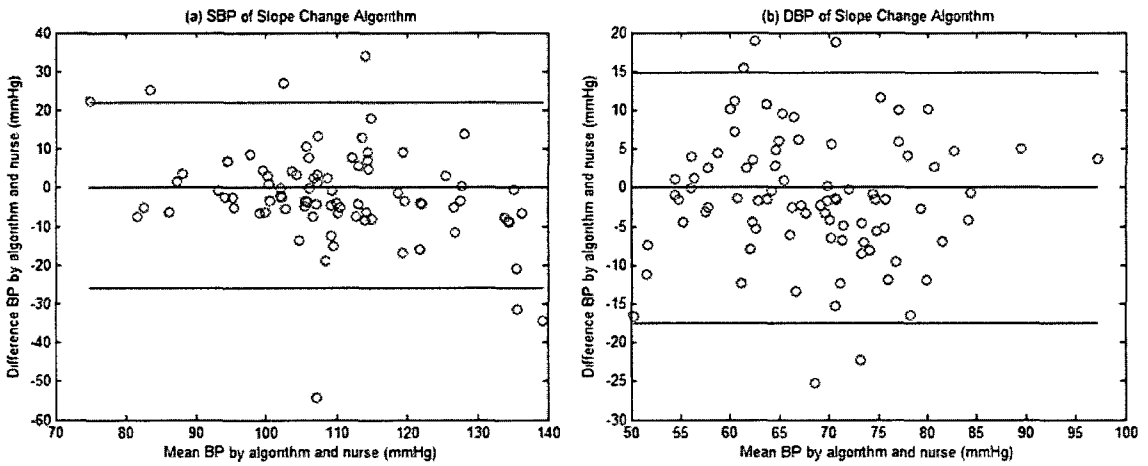

Figure 4.6. Bland-Altman plot for SCA results for (a) SBP and (b) DBP.

4.5 Algorithms Summary

For steps 1-3 of the oscillometric algorithm, (extract an OMW, define the OPI and envelope cleaning), the numerical results are shown in Table 4.2 to Table 4.5. In order to present a concise summary of these results, the tables are reproduced with the results presented qualitatively as MODERATE, GOOD or VERY GOOD in Table 4.7 to Table 4.9. Table 4.7 shows the performance of the different ways to extract an OMW and define the OPI. Respectively, the ratings MODERATE, GOOD and VERY GOOD correspond to MAP estimation improvement of less than 5 mmHg, between 5 to 7 mmHg and greater than 7 mmHg with reference to the nurse readings. Table 4.8 and Table 4.9 show the performance of envelope cleaning methods. For these results, the ratings MODERATE, GOOD and

VERY GOOD correspond to MAP estimation improvement of less than 1 mmHg, between 1 to 2 mmHg and greater than 2 mmHg. These performance ratings are assessed from the same results as in Sections 4.2 and 4.3, using the Biosign data set. The algorithms for SBP and DBP estimation with results presented in Table 4.6 are not summarized this way because all algorithms will be used later on, with the exception of SCA.

OMW Extraction Method:	Filtering			Detrending	
OPI Defined	P2B	P2P	Area	P2B/P2P	Area
Performance	MODERATE	GOOD	VERY GOOD	GOOD	VERY GOOD

Table 4.7. Performance of different OPI definitions and two OMW extraction methods

Cleaning Method	Median Filter	MA Filter	Sum Two Lorentz	Sum Two Gaussian	Asymm. Lorentz	Asymm. Gauss
Performance	MODERATE	GOOD	VERY GOOD	VERY GOOD	GOOD	MODERATE

Table 4.8. Performance of envelope cleaning methods.

Cleaning Method	Median Filter		Moving Average Filter	
	Sum Lorentz	Sum Gaussian	Sum Lorentz	Sum Gaussian
Performance	VERY GOOD	VERY GOOD	VERY GOOD	VERY GOOD

Table 4.9. Performance of envelope cleaning methods that combine two methods.

Chapter 5 – Suppression of Breathing Effects

5.1 Breathing in Oscillometry

One of the largest causes for variation in blood pressure estimation is due to the effects of breathing. These effects will be studied and then targeted for suppression. The goal is to suppress the influence of these effects on the algorithms such that the estimated SBP and DBP are more representative of a subject's actual blood pressure. To do this, breathing must first be detected and extracted from a subject's OMW and then its effects will be suppressed. The approach is shown in Figure 5.1, along with new performance metrics that will be used.

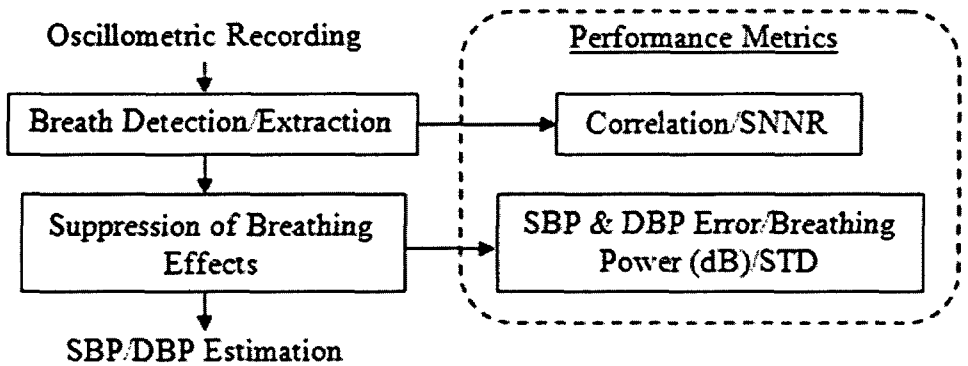

Figure 5.1. Detection and extraction of breathing and suppression of its effects.

Suppression of breathing is performed on the OMW with and without the aid of an ECG signal. ECG is used to aid in the development of algorithms because we were able to reply on existing work on detecting the breathing signal using the ECG. A scheme which does not use ECG and relies only on the blood pressure measurement is also investigated. This approach largely reduces costs and complexity because it does not require additional hardware. This scheme also has a potential to further enhance capabilities of existing oscillometric blood pressure monitors. Breathing suppression algorithms are not intended to replace the envelope cleaning method of the oscillometric algorithms, but complement them.

This thesis discusses a new set-up, which is used to record breathing and ECG signals. Then, the methods to detect, extract and suppress the effects of breathing from the OMW are discussed. A block diagram of this procedure is shown in Figure 5.2 ECG is used to aid in this procedure. From the OMW and ECG, the beat-to-beat intervals, envelopes and PTT are extracted. These signals are then put through a band pass filter with passband of 0.15 – 0.5

Hz. In order to verify these signals are induced by breathing, a device which records a subject's breathing signal is used. If breathing is detected, five breathing signals are extracted. The reason for extracting five signals is to perform research on the quality of extracted breathing signals using these methods. In the case where ECG signal is not present, the method is still applied to the OMW and produces two breathing signals.

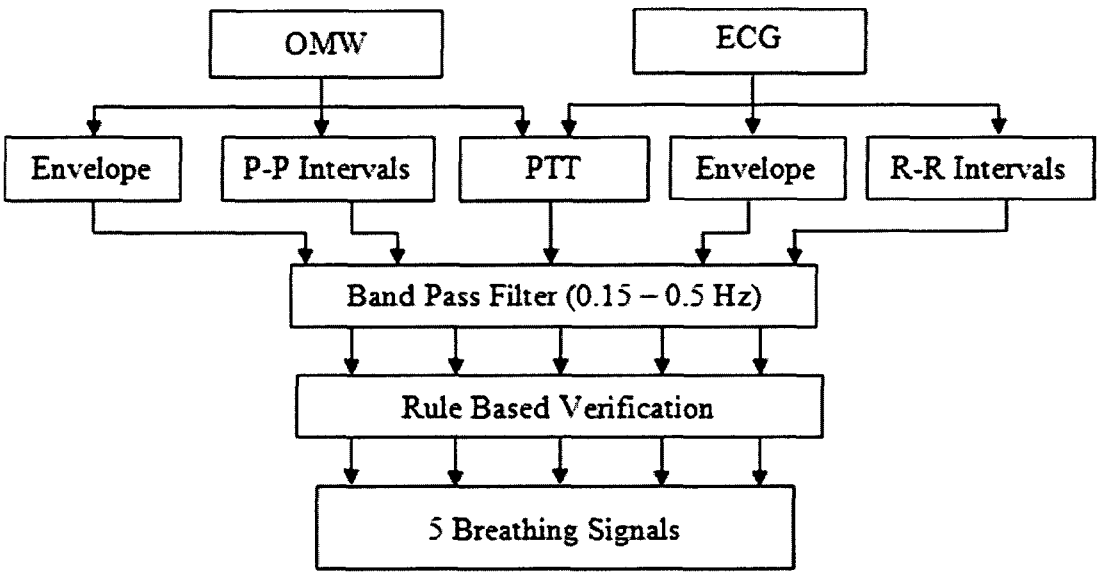

Figure 5.2. Block diagram showing the breathing detection and extraction procedure.

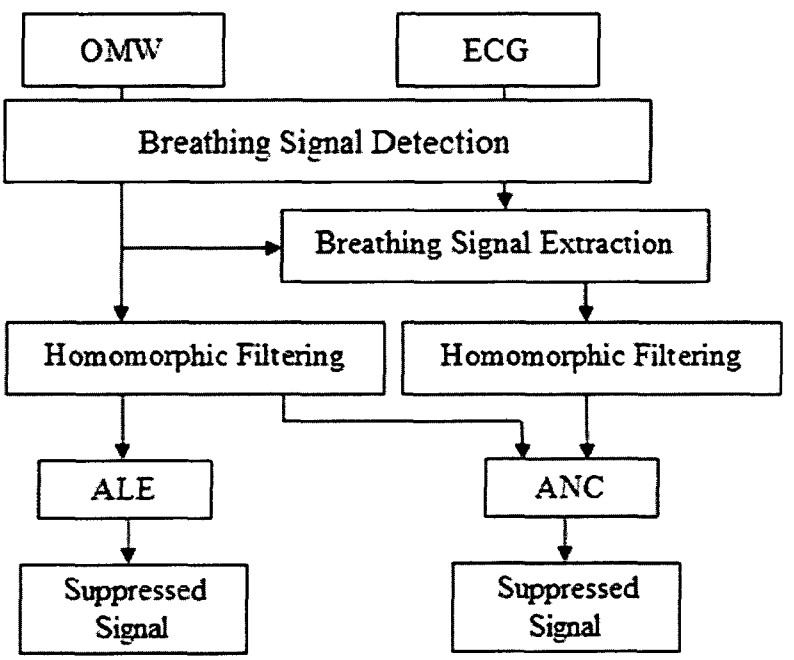

Figure 5.3. Block diagram of the filtering procedure.

If breathing is detected, filtering to suppress its effects is implemented as shown in the block diagram in Figure 5.3. A homomorphic filter is applied first to transform the multiplicative noise into additive. In the case where an ECG signal is present, the breathing signal extraction occurs before homomorphic filtering. Then, adaptive filtering techniques are applied. In the case where the ECG signal is available to use, the ANC scheme is applied. This filtering scheme relies on a reference signal, which is provided by the ECG because it has been known how to extract breathing effects from the ECG signal. In the case where only the OMW is present, the ALE scheme is adopted. This scheme has the distinct advantage that it does not require a reference signal like the ANC scheme does.

It is important to note that the term respiration is used in the literature. However, respiration is generally regarded as a chemical process. Instead, in this thesis, the term breathing is used, because it relates to the ventilation movement of air in the lungs and diaphragm, which is a physical process. Although both chemical and physical processes are responsible for the fluctuations in blood pressure, the term breathing will be used because the physical effects are better known. Some chemical processes which affect blood pressure are still unclear today.

FM effects of breathing have also been studied. These effects have an influence on the beat-to-beat intervals of the ECG and OMW. Beat-to-beat intervals are taken as the time period between each detected heart beat plotted over time as shown in Figure 5.4. For ECG signals, beat-to-beat intervals are more specifically known as the R-R intervals and for the OMW signal they are known pulse-to-pulse intervals. Beat-to-beat intervals are known to vary naturally over time according to the subject's HRV, but as explained in Section 2.9, breathing also has a huge influence on it as well. Breathing results in larger beat-to-beat intervals during exhalation and shorter intervals during inhalation. These effects are evident in Figure 5.4, where the beat-to-beat intervals can be observed fluctuate over time in what appears to be a constant frequency. More details on this procedure will be explained later in the procedure. FM effects are used to extract a breathing signal, but to the best of the author's knowledge, their influence on blood pressure estimation has not been studied before. Methods that will suppress the FM effects will also be discussed.

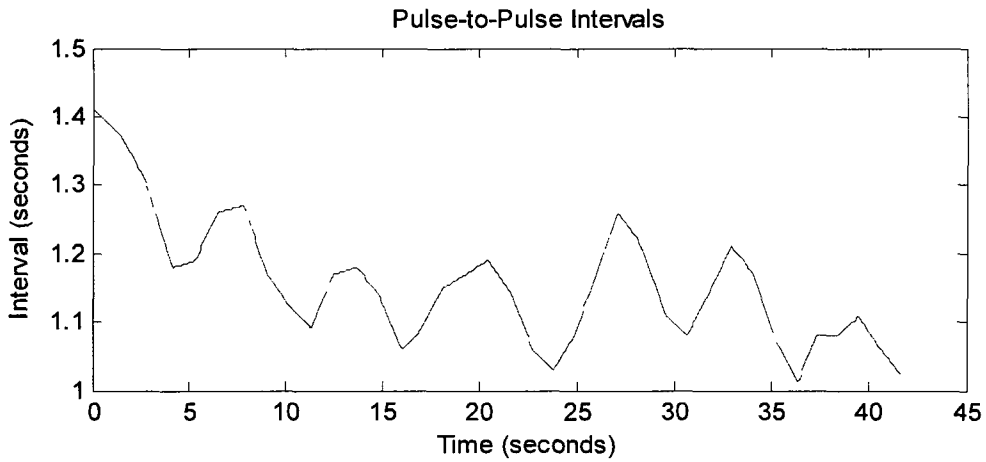

Figure 5.4. Pulse-to-pulse intervals from the OMW.

5.2 Data Acquisition

For the work done here, the goal is to identify breathing and suppress their effects in oscillometric blood pressure measurements. Waveforms from Biosign data set are used as an input to the algorithms. However, this data set contains only oscillometric recordings from the UFIT and does not contain ECG recording whereas ECG is also required for this analysis. ECG is included for two main reasons. First, established work based on extracting breathing signals from ECG signals exists [41]. This provides a solid starting point to develop breathing signal extraction algorithms of oscillometric measurements. Second, the work in this thesis is part of a research team that is also concurrently working on a physiological signal acquisition system that records both ECG and blood pressure [50]. Algorithms developed here to extract breathing signals from the ECG can be transferred over to this system.

We performed an experiment in which the OMW is recorded using Biosign's UFIT along with ECG and breathing data recorded by another device: BioHarness by Zephyr Technology. This is a chest worn device that transmits data wirelessly to a PC. Posture, skin temperature, respiration and ECG signals are all recorded by the device. Respiration and ECG, the two signals that are used here, are reportedly sampled at 18 Hz and 250 Hz, respectively. To record ECG, the BioHarness belt has two pieces of conductive fabric sewn to the inside. However, when ECG was measured, these contact points were not used. Instead, conductive fabric was wrapped around both the wrists of the subject and then

connected by alligator clips to the input terminals of the BioHarness. This was done so that an artifact could be introduced to synchronize the two devices based on the timing of the artifact. Placing the conductive fabric on the wrist was also more convenient for subjects as they are not required to take off their shirts, like in typical chest worn ECG devices. Some experimentation revealed that the BioHarness did not actually sample ECG signals at the reported 250 Hz. By connecting a recently calibrated function generator to the BioHarness, the true sampling period of the device could be determined. It was then determined that the time stamps in all signals returned by the BioHarness needed to be scaled by a factor of 1.075. After this scaling, the signal could be processed along with the signals recorded by the UFIT.

Six healthy subjects (3 male, 3 female), volunteered to have their ECG, respiration and oscillometric blood pressure all simultaneously recorded with the UFIT and BioHarness. This data set, to be known as the respiration data set from here on, is used to validate the algorithms for the detection and extraction of breathing signals. The subjects breathed at their own natural rate and depth, with no outside control, as ECG, OMW and respiration signals were all acquired with the BioHarness belt placed on the chest.

Another data set was collected by performing another experiment with six healthy subjects (3 males and 3 females) with simultaneous ECG and oscillometric blood pressure recordings. This data was collected under a similar procedure used by Biosign, but with ECG also recorded using the BioHarness. The difference between this data set and the previous data to validate the breathing algorithms is that breathing was not recorded and the recording procedure followed that used by Biosign, as recommended by SP10 protocol. Each subject underwent 5 recording trials to produce both an ECG and OMW. In lieu of nurse readings, an Omron HEM-790 IT blood pressure monitor was used to provide reference SBP and DBP readings. The subject's were asked to sit upright and perform deep breathing at their own natural pace. This data set will further be noted as the ANC data set, as it will be used to validate the ANC filtering scheme.

5.3 Detection and Extraction of Breathing

As mentioned in Chapter 2, breathing is known to manifest itself in ECG and arterial blood pressure signals. In these signals, breathing effects can be seen spectrally in the range of 0.15 to 0.5 Hz, which corresponds to the range of normal breathing frequency [66]. In these signals, respiratory components can be observed by finding the Fourier transform or power spectral density of the signal. The duration of these signals is typically a few minutes or more. A disadvantage of oscillometric recordings is that it is shorter, typically lasts less than a minute and non-stationary. Tools like Fourier transforms and power spectral density are not recommended for investigating the existence of breathing in oscillometric recordings. They could be used to detect the presence of breathing but due to the signal being non-stationary and the poor spectral resolution, it is difficult to accurately determine the location of the spectral component. Instead, new methods, based on some existing techniques and some known breathing effects, are implemented for detection and extraction.

When the ECG signal is collected simultaneously along with the oscillometric recording, breathing may be extracted from one of the following signals:

- Beat-to-beat intervals (pulse-to-pulse intervals in the OMW and R-R intervals in the ECG)
- Amplitude envelope of the OMW or ECG
- Pulse transit time (PTT)

Each of these signals relies on proper pulse detection in the OMW and R-peak detection in the ECG. When only the OMW is available, then breathing can be extracted using the pulse-to-pulse intervals and envelope of the OMW. If ECG is present, then the R-R intervals and amplitude envelope of the ECG may also be used. Having ECG present also allows the PTT to be extracted, which provides a fifth breathing signal. These extraction methods are based on known effects, but extracting breathing from them has never been performed with the OMW.

5.3.1 Beat-to-Beat Intervals

Pulse-to-pulse intervals in the OMW or R-R intervals in the ECG provide two excellent ways to extract a breathing signal. Frequency modulation due to breathing imposes oscillatory behavior on the beat-to-beat intervals of the heart, measured as either pulse-to-pulse intervals in the OMW or R-R intervals in the ECG. During inspiration, beat-to-beat intervals shorten and during expiration, they lengthen [44]. These effects have been studied in arterial blood pressure signals [38], [63], but never on the OMW. Pulse-to-pulse intervals and R-R intervals can be processed to return a breathing signal whose amplitude is measured in units of time.

5.3.2 Amplitude Envelopes

Envelopes of the OMW and ECG can also be used to extract breathing signals. Amplitude envelopes of both the OMW and ECG exhibit oscillatory behavior due to the AM effects of breathing [38], [41]. The goal here is to actually reduce these effects in the OMW, but they also assist in identifying the problem. Envelopes of both signals may be extracted after peaks are detected. For the OMW, peaks detected are also be superimposed on the rising and decreasing envelope itself too, so filtering is used to flatten out this signal. Actual magnitudes of both the ECG and OMW are unknown, so the breathing signal extracted here is of unknown amplitude.

5.3.3 Pulse Transit Time

The PTT represents the time delay for the arterial pulse pressure to travel from the heart to a measurement point in the body. Often, this location is taken as the finger [65], but here the PTT is chosen to be measured at the wrist, which is also the location of where the oscillometric reading occurs. When simultaneous ECG and oscillometric recordings are available, the PTT is found as the time delay between the ECG R-peaks and the 50% amplitude of the pulse peaks of the OMW. Current methods that obtain the PTT do not use an OMW. Instead, they rely on the ECG coupled with the arterial blood pressure signal and it has been found that breathing heavily modulate the PTT [69].

5.4 Breathing Signal Filtering

Simply taking the extracted signals from the above mentioned methods does not always immediately return a breathing signal. In some cases, the signal extracted from the above mentioned methods are clear enough to be breathing but in most other cases, the depth of breathing is not sufficient. In order to enhance the fidelity of the extracted breathing signal, filtering is required. After confirming the presence of breathing using the respiration data set, a third order IIR Butterworth band-pass filter is implemented to extract the breathing signal. The filter is fed both in the forward and reverse directions. The passband is chosen as 0.1 to 0.5 Hz, which is based on the location of the HF spectral component of blood pressure. The HF component is a known narrowband part of the envelope and beat-to-beat intervals of the ECG and blood pressure signal that is caused by breathing. It is known to lie by itself between 0.15 to 0.5 Hz [66]. As a result, the band pass filter used here only allows the component caused by breathing to pass through.

5.5 Validation of Breathing

Methods to extract the breathing signal need to be verified. The five extracted signals, even after filtering, need to be validated to be caused by breathing. Verification is performed using ECG, breathing and OMW signals acquired from the six subject respiration data set as described in section 5.2. Breathing signals are known to exhibit certain properties or characteristics. In order to eliminate the possibility of interpreting other periodic disturbances as the breathing signal, a rule-based verification to ensure the extracted signal exhibits these properties is adopted. The first step required for this approach is instantaneous frequency estimation, which will be used to estimate breathing rate.

5.5.1 Instantaneous Breathing Frequency Estimation

Estimation of breathing frequency from the extracted signals helps validate whether a breathing signal was successfully extracted. Instantaneous frequency estimation is performed by using a known zero-crossing method [80] similar to how it was used for peak detection. Zero crossings of the signals extracted in section 5.2 are counted as either an upward or downward trend. An upward zero crossing must follow with a downward crossing and a downward zero crossing must follow with an upward crossing. Two consecutive upward crossings or downward crossings correspond to one full period, or breathe, in the signal. For

each period, the instantaneous frequency is estimated by finding the next zero crossing of the same direction. Taking the inverse of the period produces the instantaneous frequency. Zero crossings are chosen because of the simplicity of the approach and its ability to find the instantaneous frequency in a short length oscillometric recording.

5.5.2 Rule Based Verification

A rule based verification of the extracted signal is adopted to confirm the presence of breathing. These rules are based on properties that breathing signals are known to exhibit. Rules are adopted to ensure that the extracted breathing signal adheres to these properties. The filtered signals are subjected to the following test.

Inter-breath interval (IBI), which is the time period between breathes, is first estimated. If the signal is breathing induced, the IBI is expected to exhibit consistent periodic behavior. The standard deviation of the IBI is expected to be between 0.27-0.76 seconds depending on the demographic [81]. To find IBI, the inverse of the instantaneous frequency in the last section is computed. As IBI is expected to exhibit a low standard deviation, 0.8 seconds is chosen as a threshold to validate the breathing signal. If the standard deviation of the extracted signal exhibits a standard deviation greater than 0.8 seconds, the signal is not considered as breathing signal.

If breathing is present, the extracted breathing signals should also have detectable breathing within a recognized normal breathing rate of humans. That is, all breathing frequency should be within the range of 0.15 to 0.5 Hz [85]. Filtering performed to extract the breathing signal should eliminate all other interferences such that, if present and strong enough, all estimated instantaneous breathing frequencies are within this range.

5.5.3 Validation of Breathing Signal

Breathing signal extraction was confirmed independently on the respiration data set of six subjects whose ECG, OMW and breathing signals were all simultaneously acquired. Breathing signals were extracted from the ECG and OMW, and then compared to the acquired breathing signal from the BioHarness. Comparisons were performed by computing

the error between the extracted breathing signals and the signal from the BioHarness. Correlation between the two signals and estimated breathing frequencies were also compared. Although the BioHarness also returned an estimate of instantaneous frequency, zero crossings were used instead so that the comparisons were not affected by computational differences. The breathing signal returned by the BioHarness was also filtered by an FIR LPF with a cutoff at 1 Hz to remove noise in the signal.

5.6 Breathing Depth

To validate our estimation of the depth of breathing, a controlled experiment is performed in which a known breathing signal is added to the envelope of the OMW. The breathing signal to be added to the envelope is artificial and is taken from a subject who breathed at a controlled rate. The goal of this experiment is to estimate a level at which the breathing effects are large enough to warrant some suppression. Breathing depth was assessed so that the level of breathing that requires suppressing is determined. The depth of breathing is found by taking several subjects who have an OMW that is visually inspected to be quite clear in the sense that breathing and other sources of artifacts or interference are obviously not evident. These subjects were also found to have quite a low error between the estimated blood pressure and nurse measurements.

The artificial breathing signal is first varied for a number of different breathing depths by amplifying it. Each breathing signal is then added to the envelope of the OMW in log domain to simulate the AM effects of breathing. Multiple realizations of the OMW envelope corrupted by breathing at different depths now exist. The level of noise (breathing) to the signal (OMW envelope) can then be estimated by the SNNR. SNNR is used, as opposed to the signal to noise ratio (SNR), because it is more applicable in later situations where the signal power is difficult to estimate without the contaminating noise. Afterwards, each envelope is converted back to the time domain where SBP and DBP are estimated. The goal of this experiment is to find out what level of SNNR do breathing effects lead to blood pressure estimates with an unacceptable amount of error. The unacceptable amount of error will be discussed quantitatively in the results. This depth of breathing establishes a threshold at which adaptive filtering for the suppression of its effects in the OMW is required.

Breathing effects are not added to the pulse-to-pulse intervals of the signal, as it will be shown later on that these effects are negligible when considering SBP and DBP estimation.

5.7 Homomorphic Filtering

Due to the multiplicative nature of breathing, in that its effects are modeled by modulation, homomorphic filtering is performed. This transforms the multiplicative operation that combines a signal and noise into an additive operation, which is easier to deal with. Homomorphic filtering is performed by applying the logarithmic operation [82]. Consider the signal $d(n) = s(n) \cdot v(n)$, where $s(n)$ is the useful information bearing part of the signal and $v(n)$ is some unwanted multiplicative disturbance. To convert the effects of $v(n)$ to additive, the natural logarithm can be taken:

$$d'(n) = \ln[d(n)] \tag{5.1}$$

This signal $d(n)$ can be expressed using $s(n)$ and $v(n)$ such that:

$$\begin{aligned} d'(n) &= \ln[s(n) \cdot v(n)] \\ d'(n) &= \ln[s(n)] + \ln[v(n)] \\ d'(n) &= s'(n) + v'(n) \end{aligned} \tag{5.2}$$

Filtering techniques can now be used to remove or suppress the unwanted $v'(n)$ in the signal, where $Filter\{x(n)\}$ is some filtering operation, to recover $s'(n)$ only:

$$\begin{aligned} f(n) &= Filter\{d'(n)\} \\ f(n) &= s'(n) \end{aligned} \tag{5.3}$$

Then the useful information bearing part of the signal can be recovered by the inverse operation of the natural logarithm, the exponential operation:

$$\begin{aligned} o(n) &= \exp[f(n)] \\ o(n) &= \exp[s'(n)] \\ o(n) &= s(n) \end{aligned} \tag{5.4}$$

Proper recovery of the signal, $s(n)$, and suppression of $v(n)$, depends on a proper filtering operation. Homomorphic filtering allows the use of the ANC and ALE adaptive filtering schemes because it transforms multiplicative noise into a more manageable additive noise.

5.8 Suppression of Effects by Adaptive Filtering

Since the algorithm for blood pressure estimation developed here only deal with the envelope of the OMW, processing of breathing is performed on the envelope rather than the entire waveform. Two adaptive filtering schemes were developed, one for the situation where an ECG signal is available and another for when it is not.

5.8.1 Adaptive Noise Canceller

In the situation for which the ECG and OMW are both recorded, the ANC scheme is adopted. After homomorphic filtering, the multiplicative effects of the filter are converted to additive effects, and then the ANC is implemented to suppress the breathing effects. A reference breathing signal is required for this scheme. This signal can be taken from one of the five mentioned extracted breathing signals in section 5.2. From the scheme shown in Figure 2.8, *d(n)* is the OMW envelope and *u(n)* is the extracted breathing signal. It is important to note that since the primary input to the filter, the OMW envelope, has been passed through the homomorphic filter, the reference input to the filter, the extracted breathing signal, is also passed through the homomorphic filter. This is required because all filtering must be performed in the same domain, which in this case is the log domain.

The adaptive filter implemented here is based on an FIR filter of length 30. The step size parameter is determined by first finding the largest eigenvector of the input autocorrelation matrix, which is constructed using all 85 realizations of the OMW envelope obtained from the 85 subjects. The results of this analysis gave a step size parameter of 0.04.

5.8.2 Adaptive Line Enhancer

For the data set provided by Biosign, where only the OMW is present, the ALE scheme is implemented. Homormorphic filtering is still required because the operation of the filter assumes that the noise to be suppressed is additive in nature. This filter requires an initialization of the coefficients and the debiasing parameter. Initialization of the coefficients was set to the estimated average breathing frequency. The debiasing parameter was set to 0.95.

5.9 FM Effects

Modulation of the heart rate is the result of the FM effects in blood pressure. Pulse locations are altered, but it is unknown whether or not blood pressure estimation is affected. The adaptive filters mentioned above will be applied to the pulse-to-pulse intervals of the OMW as well. Pulse-to-pulse intervals are known to exhibit fluctuations; they are not constant and fluctuate with many factors, one of them being breathing. The method outlined in Figure 5.3 is applied to the pulse-to-pulse intervals instead of the OMW. A new set of pulse-to-pulse intervals are produced, which are corrected for the effects of breathing. These should exhibit less fluctuation and are used to fix the locations of pulses in the envelope of the OMW. Then, the envelope is processed and blood pressure is estimated.

Suppression of the effects of breathing on the pulse-to-pulse intervals will result in a new estimate of HRV as well. Since HRV estimation requires the pulse-to-pulse intervals, it is also heavily influenced by breathing. The applied adaptive filters should produce new estimates, with breathing effects suppressed. Computation of HRV is performed by the simple method of finding the standard deviation between pulse-to-pulse intervals. It is expected that the HRV after filtering should be less than before, but also be less influenced by the effects of breathing and more representative of the natural fluctuation in the heart.

5.10 RSA Estimation

Another marker of a subject's health is RSA. Proper estimation of RSA is dependent on proper detection of beat-to-beat intervals and proper breathing signal extraction. RSA is a mathematical quantity calculated as the maximum R-R interval during expiration, minus the shortest R-R interval during inspiration, thus returning a quantity in milliseconds:

$$RSA = Max(RR_{inspiration}) - Min(RR_{expiration}) \tag{5.5}$$

Traditional devices for RSA monitoring require a respiration signal, so that the inspiration and expiration phase is known, along with an ECG or arterial blood pressure signal, to find R-R intervals. In this work, the pulse-to-pulse intervals given by the OMW will substitute the R-R intervals of the ECG as the algorithms will be implemented on the Biosign data set.

Calculation of RSA does depend on valid breathing signal extraction in order to be able to detect inspiration and expiration cycles.

Breathing used here is the one extracted by the pulse-to-pulse intervals of the OMW rather than the one extracted by the amplitude of the OMW. This is because the pulse-to-pulse intervals of the OMW are not affected by the pre-processing of the PP signal. The unknown amplification process during the signal acquisition of the PP signal leads to extracted OMW signals with potentially inconsistent amplitudes for each subject. Although a majority of these amplification effects were eliminated for OMW extraction, the amount of amplification per subject is still different and this causes discrepancies when comparing extracted breathing signals. Breathing signals extracted from the amplitude of the OMW cannot be compared between subjects because the amplification constant differs. Pulse-to-pulse intervals of OMW are extracted in terms of time (milliseconds) and are unaltered between subjects.

Typically, RSA is estimated after ECG and breathing signals are recorded during controlled breathing. However, controlled breathing conditions cannot be achieved for the Biosign data set used here. In this case, the best way to compare RSA between patients is to normalize RSA to account for the physiological differences between different individuals. Normalization will follow a similar procedure as to in to [75], where ECG and breathing were recorded on subjects without controlled breathing. RSA was normalized by dividing with the power of breathing, or HF component, found spectrally.

5.11 Performance Metrics

After applying the breathing extraction and suppression algorithms, the final goal is to provide improved SBP and DBP estimates. However, before that, the algorithms are evaluated by newly defined performance metrics to ensure that breathing is the phenomenon that is correctly detected and suppressed. Here, the work done on breathing may be split into two types of algorithms: breathing detection and extraction algorithms and breathing suppression algorithms. For the breathing suppression algorithms, performance is assessed based on SBP and DBP estimates. For the breathing detection and extractions algorithms,

new metrics are defined because SBP and DBP estimates are not available during this stage of processing.

Breathing detection and extraction algorithms are verified by comparing the extracted signal with a reference breathing signal produced by the BioHarness device. As mentioned, the respiration data set contains six subjects who breathed at their own natural rate as ECG, oscillometric blood pressure and breathing were all recorded. By comparing the five extracted breathing signals with the breathing signal recorded from the BioHarness, the extracted ones can be verified. Here, the signals are compared by finding the individual MAE and STD between the extracted signals and the reference signal. MAE and STD will also be calculated using the formulas presented in [86] and reproduced here:

$$\mu = \frac{1}{S}\sum_{q=1}^{S}\frac{1}{N_q}\sum_{k=1}^{N_q}\Delta f_q(k) \tag{5.6}$$

$$\sigma^2 = \frac{1}{S}\sum_{q=1}^{S}\frac{1}{N_q-1}\sum_{k=1}^{N_q}\left(\Delta f_q(k) - \frac{1}{N_q}\sum_{k=1}^{N_q}\Delta f_q(k)\right)^2 \tag{5.7}$$

Here, S is the number of subjects, and N_q is the number of instantaneous breathing frequency and Δf_q is the difference between estimated instantaneous breathing frequencies of the extracted breathing signal and the reference breathing signal. These equations essentially calculate the mean error and variance between the instantaneous frequency of the extracted breathing signals and the instantaneous frequency of the reference breathing signal. Correlation and estimated breathing frequency between the extracted breathing signals and the BioHarness will also be shown.

Breathing suppression algorithms rely on estimating breathing depth of the extracted signals. This will be evaluated using SNNR, where breathing is taken as the noise or unwanted component of the signal. SNNR is chosen, as opposed to the more popular signal to noise ratio (SNR), because it is more suitable for this application. SNR relies on finding the power of the information bearing component of the signal, which is unavailable in this case. What is

available is the OMW, which is composed of the information bearing part of the signal (blood pressure information) and the unwanted breathing component. Because the blood pressure information part of the OMW is not 100% known, the SNNR is used and the power of the noise is found from the extracted breathing signal.

Suppression of breathing effects is further evaluated by comparisons to reference SBP and DBP readings. Using the algorithms defined in the previous chapter, improvement in the SBP and DBP is expected by reduced MAE and STD after breathing effects are dealt with. One other performance metric which relies on SBP and DBP values is to estimate the fluctuation of a subject over 5 recordings. In blood pressure, breathing is known to cause fluctuations, which is estimated by the tools explained in Section 2.16. In this data set, each subject has 5 oscillometric measurements, which provide snapshots of a subject's blood pressure in time. For subjects whose OMW are detected to be influenced by breathing in all 5 recording trials, the fluctuations of the SBP and DBP estimates are found. It is expected that the fluctuation before filtering should be larger than after. Estimating fluctuations provides a metric which will show if the suppression of breathing effects affects estimation of blood pressure.

Chapter 6 – Results for Suppression of Breathing Effects

6.1 Breathing Signal Extraction

Once the procedure for breathing signal extraction is applied, 5 potential breathing signals are extracted. Figure 6.1 and Figure 6.2 show an ECG and OMW signal recorded from one subject undergoing uncontrolled breathing with pulses identified. It can be seen from these figures that the envelopes and beat-to-beat intervals exhibit some type of variability. To extract breathing signals, the five signals from Section 5.3 are extracted and this is shown in Figure 6.2. In this figure, the OMW amplitude envelope is flattened by a high pass filter strictly for illustration purposes.

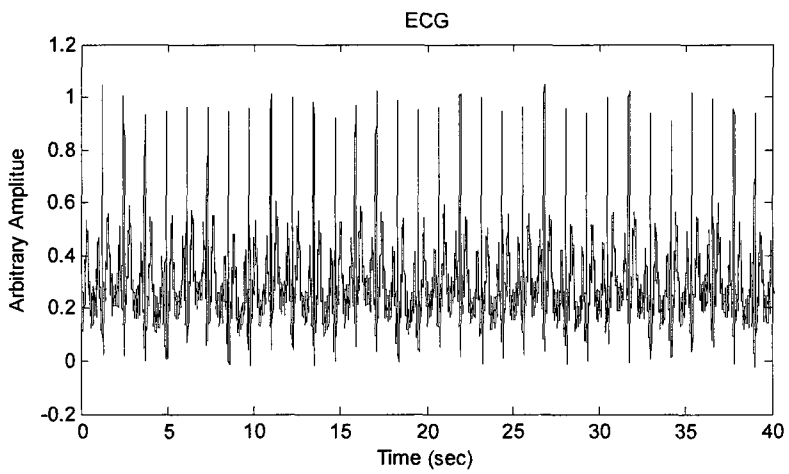

Figure 6.1. Recorded ECG from the BioHarness.

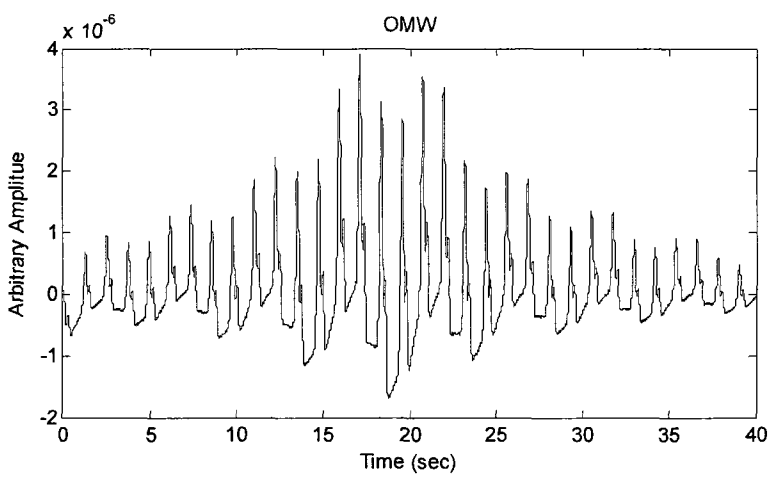

Figure 6.2. Recorded OMW extracted from the UFIT.

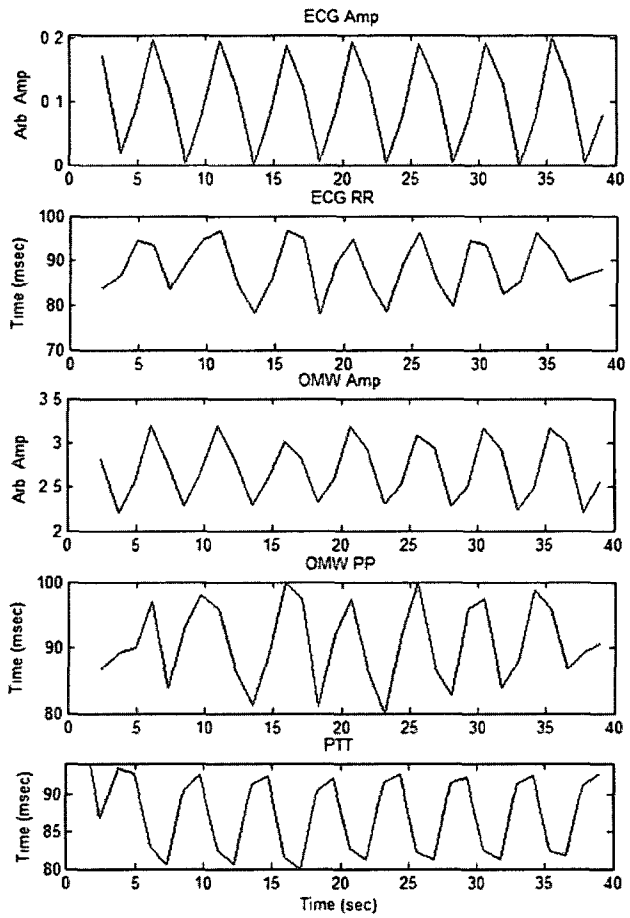

Figure 6.3. Five extracted signals from the ECG and OMW.

Strictly from observation, the extracted signals in Figure 6.3 do show similar behavior. However, these signals are corrupted by some other interferences and it is difficult to truly distinguish a discernable breathing pattern. In order to enhance the fidelity of the extracted signal, the breathing filter described in Section 5.4 is applied, producing 5 candidate breathing signals, shown in Figure 6.4. The breathing signals are then put through the rule based verification of Section 5.5 to ensure that the signal is breathing induced. Figure 6.1 to Figure 6.4 provide an illustration of the algorithm at different steps for extracting breathing from the ECG and OMW signal. Verification of the extracted breathing signals must be performed to ensure that the signals are indeed caused by breathing.

To verify that the five extracted signals after processing are indeed breathing signals, the algorithms were confirmed independently on the respiration data set that each have ECG, OMW and breathing signals simultaneously acquired. Breathing signals were extracted from

the ECG and OMW using the methodology described in Chapter 5 and verified with the breathing signal acquired from the BioHarness. BioHarness detects breathing by the physical expansion and contraction of the belt. The breathing signal returned by the device is in some arbitrary units, but only the shape and breathing frequency are relevant for this verification. In order to maintain consistency, the belt was always placed on the subject's chest, right above the diaphragm.

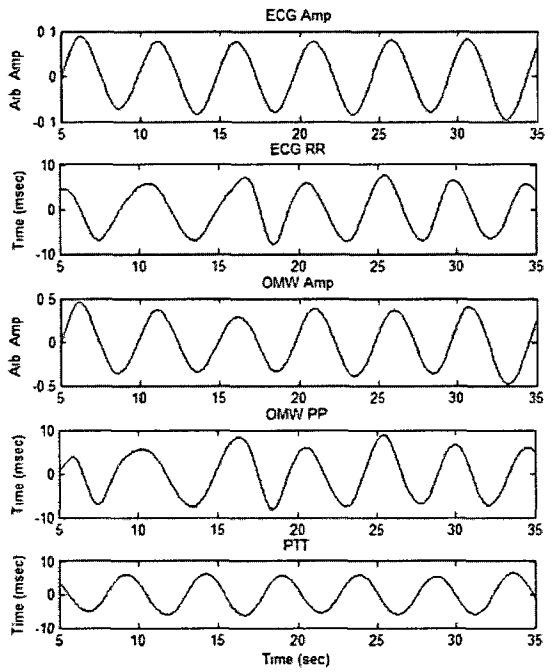

Figure 6.4. Five extracted breathing signals after filtering.

Table 6.1 shows the normalized MAE between the extracted breathing signals and the reference breathing signal from the BioHarness. Amplitudes of the breathing signals from the extracted algorithms and the BioHarness are all scaled before they are compared. To do this the local maxima of the extracted breathing signal of, for example Figure 6.4, are found by the zero crossing method. Then, the corresponding local minima are also found. Taking the a as the mean of the local minima and b as the local maxima, scaling of the signal $x(n)$ is done by the following method:

$$Scaled\ x(n) = \frac{x(n) - a}{b - a} \tag{6.1}$$

As can be seen in Figure 6.4, the extracted breathing signal is sinusoidal in shape due to the filtering procedure.

Normalized MAE is displayed in the table so that the error may be shown as a percentage. Normalized MAE is found by the following formula where *x(i)* is one of the extracted breathing signals, *r(i)* is the reference signal and *n* is the number of samples:

$$NMAE = \frac{\sum_{i=1}^{n}|x(i) - r(i)|}{\sum_{i=1}^{n}|r(i)|} \tag{6.2}$$

From Table 6.1, it can be seen that the errors between the extracted breathing signal and the BioHarness are quite low, which supports the use of the breathing signal extraction algorithm.

	Normalized MAE with BioHarness (Normalized Units)				
Subject	**OMW P-P**	**ECG R-R**	**OMW Env**	**ECG Env**	**PTT**
1	0.12	0.07	0.05	0.05	0.09
2	0.09	0.06	0.14	0.13	0.04
3	0.13	0.12	0.07	0.07	0.08
4	0.07	0.09	0.10	0.08	0.11
5	0.09	0.09	0.12	0.09	0.12
6	0.04	0.03	0.12	0.11	0.12

Table 6.1. Normalized MAE between extracted breathing signal and BioHarness.

	Correlations with BioHarness (Coefficient)				
Subject	**OMW P-P**	**ECG R-R**	**OMW Env**	**ECG Env**	**PTT**
1	0.723	0.854	0.890	0.890	0.755
2	0.781	0.873	0.715	0.715	0.920
3	0.692	0.680	0.853	0.853	0.831
4	0.856	0.838	0.609	0.786	0.750
5	0.817	0.812	0.678	0.678	0.677
6	0.911	0.940	0.643	0.627	0.715

Table 6.2. Correlations between the extracted breathing signals with the BioHarness reference breathing signal.

	Average Breathing Frequency (breathes per minute)							
Subject	**OMW P-P**	**ECG R-R**	**OMW Env**	**ECG Env**	**PTT**	**Mean**	**STD**	**BioHarness**
1	13.6	12.9	14.9	12.5	12.5	13.28	1.01	12.83
2	15.8	15.4	10.3	16.1	16.1	14.74	2.50	14.85
3	11.5	14.8	11.5	12.9	12.9	12.72	1.36	13.69
4	13.8	13.9	11.0	11.7	11.7	12.42	1.34	12.52
5	14.3	14.2	13.6	14.8	14.8	14.34	0.50	13.75
6	14.4	13.5	13.0	10.6	10.6	12.42	1.74	11.89

Table 6.3. Average breathing frequencies.

Results of the breathing signal verification are shown in Table 6.1 to Table 6.3. Cross correlations between the extracted breathing signal and the one obtained using the

BioHarness are shown in Table 6.2. A high correlation between the extracted breathing signals and the reference breathing signals is obtained. The average of the instantaneous breathing frequency was found for the five extracted breathing signals and the BioHarness. Their means and standard deviations are also shown in Table 6.3. Frequencies here are expressed in breaths per minute. STD is also reported to show that the error in estimated breathing frequencies is relatively small for all subjects.

6.2 Algorithms Summary

Using equations 5.6 and 5.7, the instantaneous frequency estimates are summarized by the MAE ± STD in Table 6.4. This table represents the error between instantaneous breathing frequency estimates between extracted breathing signals and the reference breathing signal.

	Resp. Data
OMW P-P	7.75 ± 5.77
ECG R-R	7.55 ± 5.87
OMW Env.	9.33 ± 6.01
ECG Env.	6.70 ± 4.72
PTT	8.73 ± 5.92

Table 6.4. Mean ± STD of error as a percentage between instantaneous frequency estimates for the respirations data set.

The work of [86] also performs a similar study aimed at extracted breathing signals from multi-lead ECG. Extracted breathing signals are verified using the MAE ± STD on real data. Results of Table 6.4 show that the ECG derived breathing signals have maximum error of 1.7 ± 2.0 for simulated data and 9.0 ± 4.4 for real data. In comparison, the results of our study that utilize ECG to extract breathing show maximum error of 3.89 ± 0.77 for simulated data and 7.55 ± 5.87 for real data. The results are in close agreement with each other.

Table 6.5 presents a concise summary of the results for the extracted breathing signals. The table is presented qualitatively as MODERATE, GOOD and VERY GOOD. Respectively, the ratings MODERATE, GOOD and VERY GOOD correspond to MAE ± STD estimation improvement of less than 7 ± 5 percent, between 7 ± 5 to 8 ± 5.9 percent and greater than 8 ± 5.9 mmHg.

	OMW P-P	ECG R-R	OMW Env.	ECG Env.	PTT
Performance	GOOD	GOOD	MODERATE	VERY GOOD	MODERATE

Table 6.5. Performance of different extracted breathing signals.

6.3 Breathing Depth

Once the presence of breathing is validated, the level of breathing at which it negatively affects the estimation of SBP and DBP is assessed. There are cases where breathing effects can be detected and extracted from a subject, but the depth of breathing may not warrant any action. For this reason, the level at which breathing negatively affects the estimation needs to be determined.

For a few subjects whose OMW were deemed to be influenced very little by breathing and whose estimated blood pressure was close to the nurse recordings, breathing was added to the signal and the SBP and DBP error were determined. These subjects were taken from the Biosign data set and deemed to be influenced very little by breathing in that their OMW was relatively clean, immediately after extraction and no clear breathing signal was evident after extraction methods were applied. The envelope of the subject's OMW was extracted and converted to the log domain. Then a breathing signal, which was extracted from a subject at controlled breathing, was added. This breathing signal was extracted from the envelope of the OMW and then added to the clean signal at varying depths. Both signals were converted to the log domain, then added and converted back.

Figure 6.4 shows a plot of the absolute error at different levels of breathing. The error in estimated SBP is shown in the line plotted with triangles and the error in the estimated DBP is shown in the line plotted with squares. The dashed, straight lines in the bottom represent the estimated SBP and DBP of the ideal, clean OMW. These are the minimum possible errors that can be obtained for this subject. Depth of breathing here is expressed in terms of the SNNR, where the signal is defined as the clean OMW and the noise is the breathing signal added. As SNNR increases, the depth of the breathing added is smaller and the error approaches closer and closer to the dashed lines. As SNNR decreases, the depth of breathing added is large and the error grows. At lower SNNR values, where breathing effects are

significant, the error also increases up to a certain level, where the SBP and DBP error appear to flatten out. This can be attributed to the effects of the moving average filter and curve fitting techniques, which limit the amount of error that the breathing can induce. For this subject, it can also be observed that the error in SBP is less sensitive to the added breathing effects than the error in DBP.

Only four subjects from the Biosign data set were deemed to have OMW recorded clean enough for this experiment. The threshold at which the effects of breathing were deemed to negatively affect the estimation of blood pressure was defined to be the point on the x-axis of the subject in Figure 6.5 when the absolute error of either SBP or DBP was double relative to the error of the clean signal. For the plot of the subject in Figure 6.5, the error in DBP is doubled at an SNNR around 19.44 dB and the error in the SBP is doubled at an SNNR around 14.45 dB. Table 6.6 shows the thresholds found for all four subjects.

From this table, the level of breathing at which suppression of its effects is required is when the SNNR is less than to be 14.45 dB, the minimum threshold. Breathing affects both SBP and DBP estimation, so all SNNR values are considered for determining this depth of breathing. SNNR is used here, as opposed to the more common signal to noise ratio (SNR), because the signal obtained here contains breathing effects present. SNNR is found by calculating the power of the OMW signal and dividing it with the power of the breathing signal extracted from it.

6.4 Suppression of Breathing Effects

The ANC scheme was applied to the ANC data set. The adaptive filter used has an order of 30 and step size 0.04. The results are tabulated in Table 6.7 and Table 6.8. These tables show the MAE and mean STD of blood pressure after the ANC filter is applied with all 5 extracted breathing signals used as references. The tables also show the results of the ALE for comparison in the last column. The total MAE across all algorithms is shown in the last row. Results are limited due to the small sample size, but improvements are observed. Table 6.7 shows the MAE results and Table 6.8 shows the STD. All filtered results perform better than the non-filtered results. Results here are shown only for three algorithms: MAA, LAA and

MMSA. SCA performed the worst out of the four algorithms, as shown in Table 4.6, is not included

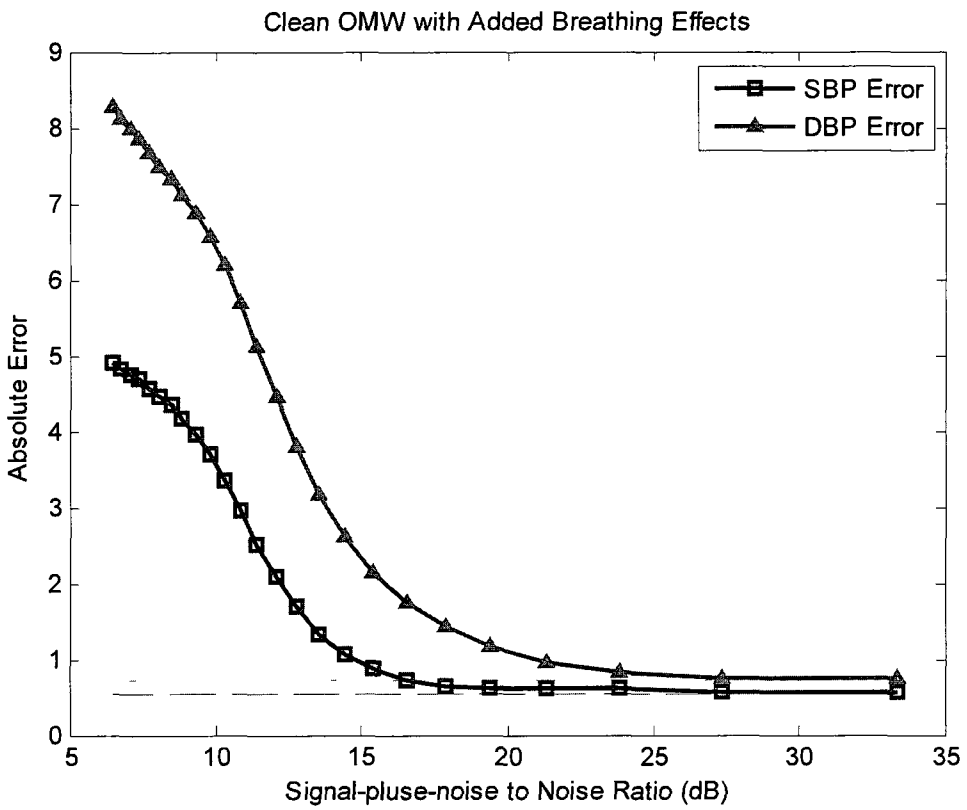

Figure 6.5. Error in SBP and DBP with varying amplitude of the breathing signal that modulated the clean OMW.

	SNNR (dB)			
SBP	14.45	19.92	17.16	18.07
DBP	19.44	18.11	18.48	16.93

Table 6.6. SNNR thresholds for four different subjects

			Filtered					
			ANC					ALE
		No Filter	OMW Env	OMW P-P	ECG Env	ECG R-R	PTT	
MAA	**SBP**	12.39	7.43	9.46	7.27	6.99	7.55	9.35
	DBP	7.38	5.11	4.83	5.78	4.51	6.01	7.15
LAA	**SBP**	10.49	7.29	9.01	7.16	6.92	7.39	8.92
	DBP	11.39	8.89	8.45	9.92	7.96	10.28	11.04
MMSA	**SBP**	11.33	10.64	7.42	10.75	6.96	10.51	11.04
	DBP	12.31	10.22	11.65	7.86	11.5	11.74	11.58

Table 6.7. MAE of SBP and DBP estimates in mmHg for subjects with ECG.

			Filtered					
			ANC					ALE
		No Filter	OMW Env	OMW P-P	ECG Env	ECG R-R	PTT	
MAA	SBP	5.01	5.18	4.83	4.54	4.51	4.81	4.75
	DBP	4.03	3.42	3.49	3.66	2.14	3.41	3.98
LAA	SBP	5.61	5.80	5.41	5.08	5.05	5.39	5.32
	DBP	5.42	4.60	4.69	4.92	2.88	4.59	5.35
MMSA	SBP	5.23	4.59	4.82	4.62	3.06	4.79	4.85
	DBP	3.74	3.84	3.63	2.87	3.26	3.71	3.54

Table 6.8. STD of SBP and DBP estimates in mmHg across all 5 trials for subjects with ECG.

Overall, the ANC schemes outperform the ALE scheme when considering MAE and mean of the STD. In considering the 5 extracted breathing signals, it can be seen from the total error of both tables that estimates obtained using the R-R intervals of ECG for breathing signal extraction perform the best. The reason can be attributed to the fact that the breathing extracted from this source is most similar to the actual breathing pattern. ECG amplitude envelopes also outperform OMW envelopes when used as a reference. In addition, the OMW envelope contains LF and VLF components, whose frequency components are very close to breathing. ECG envelopes are not known to contain such perturbations.

Also, in order to obtain the OMW from the PP and CP signal, more processing is required than it is to obtain the ECG signal. The processing involved to obtain the OMW from the recordings provided by the UFIT can contribute some error when also trying to extract a breathing signal. In this case, another advantage is given to using ECG, where the processing to retrieve this signal is much simpler. As a result of these factors, blood pressure estimation is improved more when the breathing is extracted from the ECG than when the breathing extracted from the OMW for the ANC scheme.

The ANC data set of six subjects used show good results for both adaptive filtering schemes but a larger assessment of the adaptive filter is needed. The Biosign data set of 85 subjects can provide us a larger assessment. These recordings only contain an OMW so the ALE was the chosen adaptive filter to suppress breathing effects. Adaptation took on average a time of 200 samples, or 2 seconds for this data obtained at a sample rate of 100 Hz. MAE and STD improvement for SBP is shown in Table 6.9 (A) and for DBP is shown in Table 6.9 (B).

(A) Systolic		Trial 1		Trial 2		Trial 3		Trial 4		Trial 5	
		No Filt	Filt	No Filt	Filt	No Filt	Filt	No Filt	Filt	No Filt	Filt
MAA	MAE	7.84	6.49	7.05	6.24	7.52	6.37	7.48	5.94	7.11	5.85
	Diff		1.35		0.81		1.15		1.54		1.27
	STD	7.50	5.78	7.06	4.46	6.02	4.18	6.74	4.64	7.87	5.56
	Diff		1.72		2.60		1.83		2.10		2.31
LAA	MAE	7.88	6.98	6.93	6.44	7.64	6.55	7.14	6.13	8.03	6.16
	Diff		0.90		0.49		1.09		1.01		1.86
	STD	7.61	5.31	7.00	4.67	6.50	4.87	6.72	4.61	9.01	5.90
	Diff		2.30		2.33		1.63		2.12		3.11
MMSA	MAE	10.45	9.29	9.99	8.78	10.47	9.81	9.92	9.10	10.01	9.41
	Diff		1.16		1.21		0.66		0.82		0.60
	STD	9.17	8.18	8.22	7.35	8.28	7.59	7.59	6.90	8.84	8.08
	Diff		0.99		0.88		0.69		0.69		0.76

(B) Diastolic		Trial 1		Trial 2		Trial 3		Trial 4		Trial 5	
		No Filt	Filt	No Filt	Filt	No Filt	Filt	No Filt	Filt	No Filt	Filt
MAA	MAE	6.40	6.24	7.50	6.19	6.41	5.75	6.56	6.12	6.44	5.83
	Diff		0.16		1.30		0.66		0.45		0.61
	STD	5.93	5.17	12.05	4.74	4.60	4.55	5.22	4.44	5.54	5.16
	Diff		0.77		7.32		0.05		0.77		0.38
LAA	MAE	7.84	6.36	8.73	6.33	8.14	6.48	7.04	6.17	7.91	6.22
	Diff		1.48		2.41		1.67		0.86		1.68
	STD	7.32	5.88	10.30	5.07	9.34	4.90	7.26	4.70	8.48	6.02
	Diff		1.45		5.22		4.44		2.56		2.46
MMSA	MAE	8.13	7.94	6.84	6.55	6.59	6.58	6.38	6.28	6.95	6.91
	Diff		0.19		0.30		0.01		0.10		0.05
	STD	5.98	5.96	5.39	5.33	5.49	5.28	5.57	5.39	5.69	5.47
	Diff		0.02		0.05		0.21		0.17		0.22

Table 6.9. MAE and STD in mmHg of the Biosign data set before and after filtering for suppression of breathing effects is applied for (a) SBP and (b) DBP.

Error in blood pressure estimation is determined by comparing the estimated values from our algorithms to the reference nurse readings. Table 6.9 shows the MAE and STD of subjects who were detected as breathing deeply. In total, this amounted to 253 recordings (46, 49, 58, 46 and 54 from trials 1 to 5 respectively). In all cases, the differences between MAE and STD before and after filtering show positive values which represent improvement in blood pressure estimation and support the use of adaptive filtering for the suppression of breathing effects.

In order to verify that the effects of breathing were indeed reduced, SNNR was also computed for the breathing signal before and after filtering on the Biosign data set. Before filtering, the SNNR of the extracted breathing signal extracted from the OMW envelope was first calculated. Then, after filtering, the same method to extract breathing was applied to the OMW envelope and the SNNR was once again calculated. Table 6.10 shows the SNNR estimates before and after where the procedure in Section 5.3 is used to extract the breathing signal. SNNR found after filtering is much higher than before since the breathing effects have been suppressed. Table 6.10 also shows the improvement in SNNR that the filter produces and also the p-value from a t-test comparing the SNNR before and after. The p-values all are very low, which supports the use of adaptive filtering to suppress breathing.

	SNNR (dB)			
	Initial	**Filter**	**Improve**	**p-value**
Trial 1	56.203	74.252	18.049	< 0.001
Trial 2	56.514	64.542	18.083	< 0.001
Trial 3	56.408	73.735	17.327	< 0.001
Trial 4	56.948	73.871	16.922	< 0.001
Trial 5	56.454	73.756	17.302	< 0.001

Table 6.10. SNNR computed before and after adaptive filtering.

To further investigate the effect of breathing suppression, fluctuations in blood pressure estimates was analyzed for 24 subjects from the Biosign data set who were detected as being affected by breathing across all 5 oscillometric recording trials. Fluctuation in blood pressure is estimated by finding the difference between the highest estimated blood pressure value and the lowest estimated blood pressure value for each subject's 5 recordings. SBP and DBP both exhibit their own fluctuations in blood pressure. The difference between the highest and lowest estimated blood pressure over 5 trials shows the largest swing in blood pressure, which is the same metric used in other studies [9].

In order to confirm a reduction in the fluctuation over five recording trials, the differences are calculated before and after filtering. The fluctuation should be lower after the adaptive filter is applied than before. Table 6.11 shows the mean of fluctuation values across all 24 subjects before and after the ALE filter is applied. This is representative of the overall fluctuation across all subjects who are detected as breathing deeply. Considering the decrease in fluctuation, positive results in terms of breathing suppression is shown. For all cases, improvement due to the suppression of breathing effects by adaptive filtering is evident.

Table 16 shows that after suppression, both SBP and DBP exhibit less fluctuation, which may be the evidence that the estimates are converging closer to the average blood pressure.

		Fluctuation (mmHg)	
		Before	ALE
MAA	SBP	14.38	8.96
	DBP	10.94	6.69
LAA	SBP	16.89	10.06
	DBP	9.76	6.54
MMSA	SBP	19.54	11.62
	DBP	13.60	12.24

Table 6.11. Fluctuations in SBP and DBP estimates across all 5 trials.

A visual inspection of the suppression effects was also performed. Figure 6.6 shows a plot of a subject's OMW envelope before and after breathing is suppressed. The envelope before suppression is plotted with dashed thin lines and the envelope after the adaptive filtering is plotted with solid, thick lines for both the ANC and ALE scheme. The ANC scheme used the breathing signal extracted from the R-R intervals of the ECG. Figure 6.7 shows further visual evidence of the breathing suppression. The frequency spectrum of the OMW envelope for the ALE scheme is plotted before and after filtering. The arrow in this figure points to the frequency component identified to be breathing induced. After suppression, the breathing component is visibly reduced in the spectrum. Frequency domain analysis is used here, but is generally not recommended because the recording duration of an oscillometric recording is rather short and also unstationary. However the plot shown here is a special case for a subject whose recording exceeds a minute in length.

6.5 FM Effects

Suppression of the FM effects was also attempted on the data set provided by Biosign. This was performed by extracting the pulse-to-pulse intervals of the OMW and then applying the ALE. Figure 5.4 shows an example pulse-to-pulse interval extracted from the OMW. From existing literature, the presence of breathing is known to influence the pulse-to-pulse intervals of blood pressure [64]. With the OMW, these breathing effects are known to be present in the pulse-to-pulse intervals, as verified with the BioHarness in Table 6.1 to Table 6.3. Here, the breathing signal is extracted from the pulse-to-pulse intervals by the previously explained methods of section 5.4 and is shown in Figure 6.8, confirming the existence of breathing.

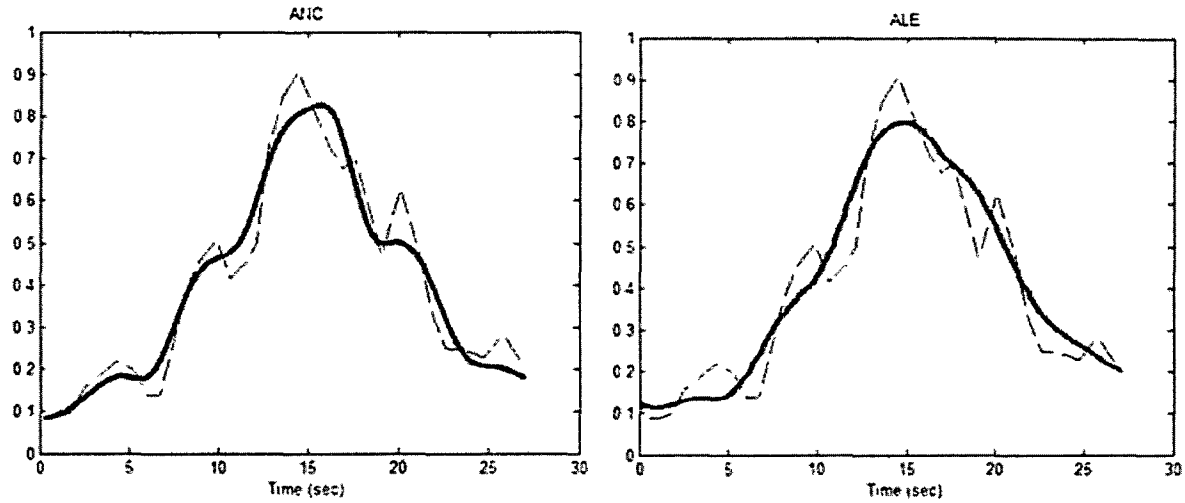

Figure 6.6. OMW envelope before and after breathing for both ANC and ALE schemes.

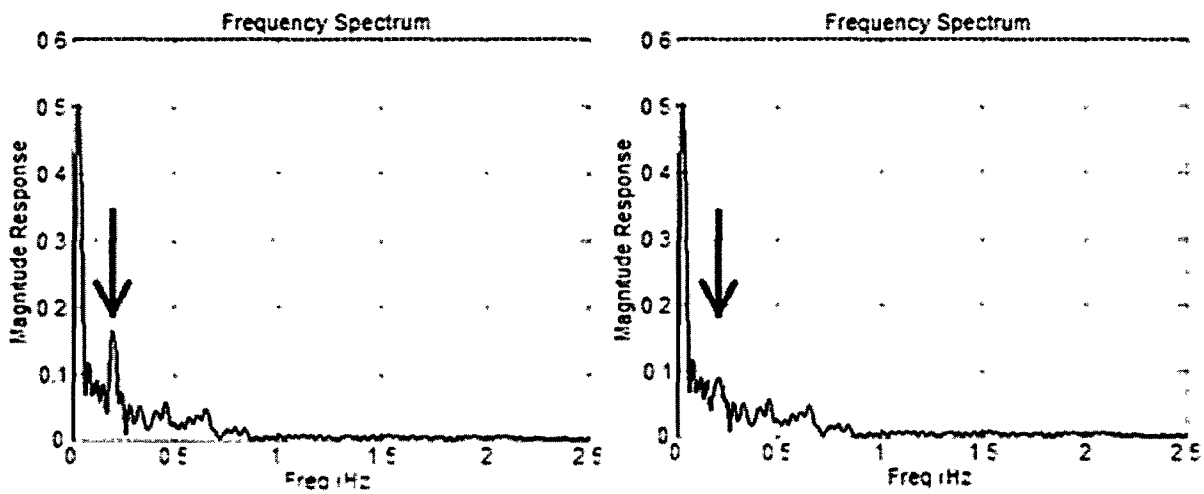

Figure 6.7. Spectrum of OMW envelope before (left) and after (right) ANC suppression scheme is applied.

Adaptive filtering, along with a homomorphic filter, was applied to the signal in the same manner that is applied to the envelope, except this time the pulse-to-pulse intervals are filtered instead of the envelope. First, the pulse-to-pulse interval of the OMW are extracted, as shown in Figure 5.4. The pulse-to-pulse interval signal shows the duration in time between peaks of the OMW. A breathing signal may be extracted from this, as shown in Figure 6.8. Then, the ALE scheme is applied on the pulse-to-pulse intervals to produce the signal shown in Figure 6.9. These new pulse-to-pulse intervals exhibit a lot less fluctuation

than before filtering. A downward trend is seen in the intervals both before and after filtering, which may be due to the VLF or LF components of blood pressure.

After the ALE is applied, the OMW envelope is reconstructed with new pulse locations determined by the filtered pulse-to-pulse intervals. Then, the SBP and DBP are estimated from this envelope. This procedure effectively alters the locations of the peaks of the OMW, but not the actual amplitudes. Estimated blood pressure after filtering the FM effects was found to produce absolutely no change in error. This can be attributed to the level of FM effects as compared to the AM effects. Variations in the pulse-to-pulse intervals attributed to breathing are insignificant when compared to the duration of the intervals itself. Unlike the envelope itself, these intervals do not affect the actual estimation of SBP and DBP. However, these intervals are useful in providing evidence of the effects of breathing in the OMW.

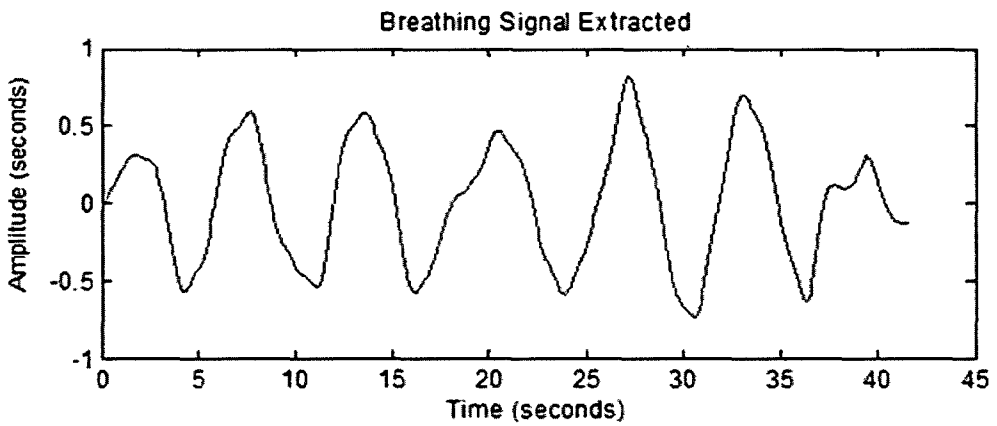

Figure 6.8. Breathing signal extracted.

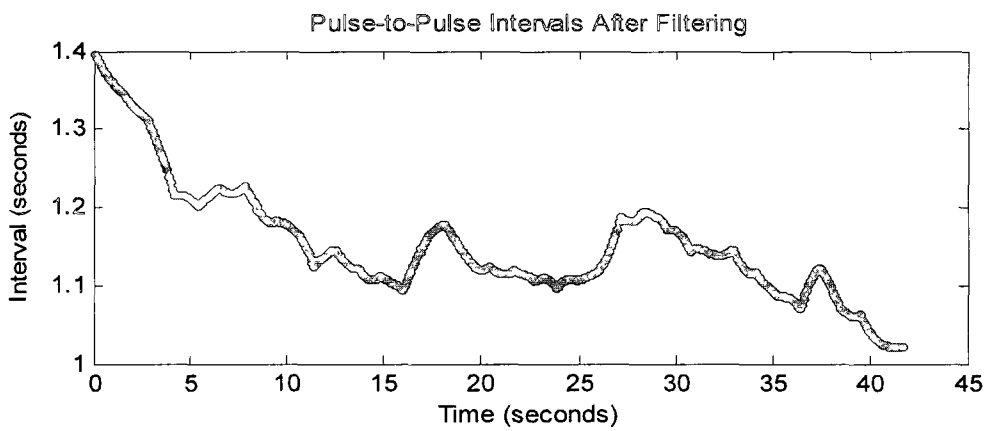

Figure 6.9. Pulse-to-pulse intervals after filtering.

Filtered pulse-to-pulse intervals do lead to new estimates of HRV. For the Biosign data set, the HRV was calculated by finding the standard deviation of the pulse-to-pulse intervals for

all subjects across 5 trials. Table 6.12 shows the mean estimated HRV for all subjects, per trial, before and after filtering. The new HRV estimates are all smaller than the original HRV estimates and the p-value, obtained after performing a paired two-tailed t-test, also shows strong significant difference between the two means.

Trial	Original HRV (milliseconds)	Filtered HRV (milliseconds)	P-Value
1	6.16	4.69	< 0.001
2	5.36	4.19	< 0.001
3	4.68	3.56	< 0.001
4	4.94	3.86	< 0.001
5	4.96	3.85	< 0.001

Table 6.12. HRV values calculated from the pulse-to-pulse intervals before and after filtering.

6.6 RSA Estimation

With the breathing signal properly extracted, using the formula from (5.5), RSA was estimated from the breathing signal extracted from the OMW. The correlations between the estimated RSA with HRV and breathing amplitudes were computed. HRV was found by the standard deviation of the pulse-to-pulse intervals and the breathing amplitude was found as the mean peak to peak amplitude of the breathing signal extracted from the pulse-to-pulse interval method using the OMW. An example is shown in Figure 6.10. Both RSA and breathing amplitude are plotted in units of milliseconds (ms). The slope and the y-intercept of the line here are found as 0.279 and 1.039, respectively.

Results of these correlations are tabulated in Table 6.13 for all subjects in the data set provided by Biosign. High correlations can be observed for all subjects across all 5 trials. Current literature show RSA exhibits a correlation with HRV and breathing amplitude [74] with a correlation coefficient of about 0.81 and 0.87, respectively. Both HRV and mean breathing amplitude exhibited a correlation with RSA similar to this level. This agrees with the linear relationship reported in existing literature and shows that it can also be obtained from breathing signals extracted from the OMW.

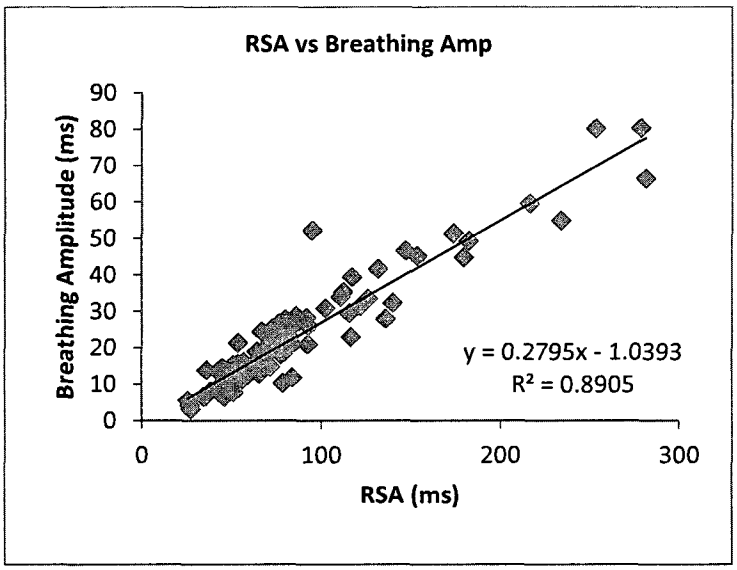

Figure 6.10. Scatter plot of RSA vs. breathing amplitude

	Correlations of RSA	
Trial	**with HRV**	**with Breathing Amp**
1	0.926	0.920
2	0.848	0.792
3	0.905	0.854
4	0.848	0.903
5	0.898	0.943

Table 6.13. RSA correlations with HRV and breathing amplitude.

RSA estimation needs to be normalized between subjects so that it can be compared. A technique similar to [75] is used here, but instead of using the power of the HF component, the amplitude extracted breathing signal is used. Since the actual power spectrum is difficult to find in the OMW, breathing amplitude is estimated from the breathing signal. Normalization is performed by dividing the extracted RSA with the breathing amplitude. This produces an estimate of RSA that is normalized with breathing. After normalization, the RSA may be compared between subjects segmented into different age groups. It is known that RSA decreases with age, so it is expected that there exists a negative correlation between age and RSA.

Table 6.14 shows the results of RSA estimation with the Biosign data set using breathing amplitude to normalize RSA. To compare RSA with age in this case, the subjects were split into three age ranges and then the normalized RSA was compared. The three age ranges are subjects less than 35 years old, between 35 and 50 years old and more than 50 years old. The

mean age of all subjects was about 41 years. The mean of 35 years and 50 years is 42.5 years. These age ranges were set such that the mean was close to the mean of the demographic. Then, the mean RSA for all ages is found. For each demographic, the number of subjects with RSA higher or lower than the mean is computed. It is expected that subjects younger than the mean age of 41 should have a higher RSA and subjects above the mean age of 41 should have a lower RSA. The percentages shown in the table here represent the number of subjects with higher or lower RSA than the mean. From these tables, it can be observed that younger subjects in the less than 35 age range do have high RSA, while older subjects in the age range greater than 50 do have the low RSA. These results are consistent with literature. Subjects in the age range between 35 to 50 years old were split between high and low RSA. No clear pattern is discernable in this age range. This introductory work on RSA provides a starting point for the new applications that breathing can aid. It shows that extracting breathing signals from blood pressure recordings brings new novelty to oscillometric measurements.

	Normalized RSA	
Age	**Low**	**High**
< 35	33.16%	66.84%
35 – 50	48.57%	51.43%
> 50	61.18%	38.82%

Table 6.14. Results of RSA compared with age using amplitude to normalize.

Chapter 7 – Conclusion

7.1 Summary of Work

A variety of algorithms exist to determine the SBP and DBP from the oscillometric method. Although literature examines oscillometric devices from the perspective of a black box approach, no work has been done to examine the quality of the underlying algorithms. What is also missing is a survey of these existing algorithms to estimate blood pressure from oscillometric measurements. This includes various methods and sub-algorithms used in each step of oscillometric method. The work here first surveyed and evaluated the different algorithms to assess performance in the estimation of blood pressure. Various algorithms for oscillometric blood pressure estimation were implemented and validated on a data set provided by Biosign. This allowed for the algorithms to be evaluated after each step of the procedure. The algorithm which produced the lowest error between the estimated blood pressure and the reference readings here is to extract the OMW by filtering, and then use the area defined OPI. The preferred envelope cleaning method consists of a moving average filter, followed by Gaussian curve fitting.

Breathing effects in oscillometric blood pressure were also studied. Work here took advantage of the existing knowledge on breathing in blood pressure and ECG, such as the AM and FM effects and detection methods, to develop new algorithms that are applicable to oscillometric recordings. Methods for the detection and extraction of breathing in OMW were first developed. These take advantage of the well-known properties of the HF component in blood pressure and ECG. Adaptive filtering algorithms were then applied to suppress breathing effects when estimating SBP and DBP. The results obtained in Chapter 6 support the use of adaptive filtering to suppress breathing effects. Estimates of SBP and DBP after filtering and suppressing breathing effects are closer to the nurse reference values. They also exhibit less variation across five recording trials than before the filter was applied. Extracting breathing from the OMW also opens the door to a slew of new potential uses of oscillometric devices for obtaining more physiological markers of a subject's cardio-respiratory system. One such marker is RSA, which was extracted here across the 85 subjects. The work here confirmed the dependence of RSA on age. These methods can be

used to extend current blood pressure monitors. In addition, the novelty of blood pressure monitors can be expanded with an ECG signal as well.

7.2 Future Work

It is important to note that the algorithms here work particularly well for the data set provided by Biosign. Here, oscillometric recordings were performed using the UFIT device. Unfortunately, other oscillometric devices were unavailable so this thesis is limited to the waveforms and data sets provided by UFIT. It may be entirely possible that another device performs differently than the UFIT. This does not render the work done here useless, however. The work here provides a survey of many methods, which can be applied to any oscillometric recording device. Results here are tabulated for the UFIT, but the algorithms certainly are not restricted to the UFIT. The algorithms surveyed may be applied to any oscillometric device, but with potentially different results.

Out of the four algorithms evaluated here, one final algorithm used for estimation of SBP and DBP is difficult to choose since each them have its own advantages and disadvantages. Choosing one over another may neglect important physiological features. Future work proposed includes algorithm fusion or selection which can combine the advantages of the different fundamental approaches. This idea can also go beyond oscillometric measurements as well, in that it can combine different methods for blood pressure estimation altogether. For example, oscillometry can be fused with the auscultation or tonometric method to provide estimates of SBP and DBP that take advantage of the different underlying methods.

Obtaining a breathing signal from the OMW greatly extends the capabilities of oscillometric devices. This work extracted a normalized RSA from these signals, but a lot more potential work exists in this field. RSA is known to be an indicator of many physiological conditions such as diabetes, stress, hypertension, etc. Ongoing work is still being performed to prove the link between RSA and these physiological conditions, but if proven to be linked, indicators of these conditions can be extracted from oscillometry as well.

Appendix A: Ethics Approval Notice

File Number: H02-10-01 Date (mm dd yyyy): 06 09 2010

Université d'Ottawa University of Ottawa
Service de subventions de recherche et deontologie Research Grants and Ethics Services

Ethics Approval Notice

Health Sciences and Science REB

Principal Investigator / Supervisor / Co-investigator(s) / Student(s)

First Name	Last Name	Affiliation	Role
Hilmi	Dajani	Engineering SITE	Principal Investigator
Saif	Ahmad	Medicine Medicine	Co-investigator
Miodrag	Bolic	Engineering Computer Science	Co-investigator
Voicu	Groza	Engineering Computer Science	Co-investigator
Soojeong	Lee	Engineering Computer Science	Co-investigator
Karen	Soueidan	Engineering Computer Science	Co-investigator
Silu	Chen	Engineering Computer Science	Student Researcher
Mohamad	Forouzanfar	Engineering Computer Science	Student Researcher

File Number: H02-10-01

Type of Project: Professor

Title: Robust Noninvasive Blood Pressure Measurement

Approval Date (mm/dd/yyyy)	Expiry Date (mm/dd/yyyy)	Approval Type
06 09 2010	06 08 2011	Ia

(Ia: Approval, Ib: Approval for initial stage only)

Special Conditions / Comments:
N A

550, rue Cumberland 550 Cumberland Street
Ottawa (Ontario) K1N 6N5 Canada Ottawa, Ontario K1N 6N5 Canada
(613) 562-5841 • Telec. Fax (613) 562-5338
http: www.rges.uottawa.ca http: www.ssrd.uottawa.ca

File Number: H02-10-01 Date (mm dd yyyy): 06/09/2010

Université d'Ottawa University of Ottawa

Service de subventions de recherche et deontologie Research Grants and Ethics Services

This is to confirm that the University of Ottawa Research Ethics Board identified above, which operates in accordance with the Tri-Council Policy Statement and other applicable laws and regulations in Ontario, has examined and approved the application for ethical approval for the above named research project as of the Ethics Approval Date indicated for the period above and subject to the conditions listed the section above entitled "Special Conditions / Comments".

During the course of the study the protocol may not be modified without prior written approval from the REB except when necessary to remove subjects from immediate endangerment or when the modification(s) pertain to only administrative or logistical components of the study (e.g. change of telephone number). Investigators must also promptly alert the REB of any changes which increase the risk to participant(s), any changes which considerably affect the conduct of the project, all unanticipated and harmful events that occur, and new information that may negatively affect the conduct of the project and safety of the participant(s). Modifications to the project, information/consent documentation, and or recruitment documentation, should be submitted to this office for approval using the "Modification to research project" form available at: http://www.rges.uottawa.ca/ethics/application_dwn.asp

Please submit an annual status report to the Protocol Officer 4 weeks before the above-referenced expiry date to either close the file or request a renewal of ethics approval. This document can be found at: http://www.rges.uottawa.ca/ethics/application_dwn.asp

If you have any questions, please do not hesitate to contact the Ethics Office at extension 5841 or by e-mail at: ethics@uOttawa.ca.

Germain Zongo
Protocol Officer for Ethics in Research
For Dr. Daniel Lagarec, Chair of the Health Sciences and Sciences REB

550, rue Cumberland 550 Cumberland Street
Ottawa (Ontario) K1N 6N5 Canada Ottawa, Ontario K1N 6N5 Canada
(613) 562-5841 • Telec. Fax (613) 562-5338
http://www.rges.uottawa.ca http://www.ssid.uottawa.ca

References

[1] J.A. Cutler, P.D. Sorlie, M. Wolz, T. Thom, L.E. Fields and E.J. Roccella, "Trends in Hypertension Prevalence, Awareness, Treatment, and Control Rates in United States Adults Between 1988-1994 and 1999-2004," *Hypertension*, vol. 52, Nov. 2008, pp 818-827.

[2] S. Fox, *Human Physiology*, 8th ed. New York: McGraw-Hill, 2007.

[3] W.A. Littler, B. Komosuoglu, "Which is the Most Accurate Method of Measuring Blood Pressure?," *American Heart Journal*, vol. 117, Mar. 1989, pp. 723-728.

[4] K.G. Ng, C.F. Small, "Survey of Automated Noninvasive Blood Pressure Monitors," *Journal of Clinical Engineering*, vol. 33, Dec. 1994, pp. 452-475.

[5] E.J. Marey, Ecole Practique des Hautes Etudes, *Physiologie Experimentale*, vol. 6, 1876, pp. 307-343.

[6] M. Pagani, F. Lombardi, S. Guzzetti, O. Rimoldi, R. Furlan, P. Pizzinelli, G. Sandrone, G. Malfatto, S. Dell'Orto, E. Piccaluga, M. Turiel, G. Baselli, S. Cerutti, A. Malliani, "Power Spectral Analysis of Heart Rate and Arterial Pressure Variabilities as a Marker of Sympathovagal Interaction in Man and Conscious Dog," *Circulation Research*, vol. 59, Aug. 1986, pp. 178-193.

[7] A.C. Dornhost, P. Howard, G.L. Leathart, "Respiratory Variations in Blood Pressure," *Circulation*, vol. 6, Oct. 1952, pp. 553-558.

[8] S. Hales, *Statistical Essays*, vol. 2, London, W. Innys, 1733.

[9] M. Ramsey III, "Blood Pressure Monitoring: Automated Oscillometric Devices," *Journal of Clinical Monitoring and Computing*, vol. 7, Jan. 1991, pp. 55-67.

[10] K.M. Borrow, J.W. Newburger, "Noninvasive Estimation of Central Aortic Pressure using the Oscillometric Method for Analyzing Systemic Artery Pulsatile Blood Flow: Comparative Study of Indirect Systolic, Diastolic, and Mean Brachial Artery Pressure with Simultaneous Direct Ascending Aortic Pressure Measurements," *American Heart Journal*, vol. 103, May 1982, pp. 879-886.

[11] G.A. van Montfrans, "Oscillometric Blood Pressure Measurement: Progress and Problems," *Blood Pressure Monitoring*, vol. 6, Dec. 2001, pp. 287-290.

[12] M.A. Hasan, T.A. Thomas, C. Prys-Roberts, "Comparison of Automatic Oscillometric Arterial Pressure Measurement with Conventional Auscultatory Measurement in the Labour Ward," *British Journal of Anaeshesia*, vol. 70, Feb. 1993, pp. 141-144.

[13] T.K. Lee, D.R. Westenskow, "Comparison of Blood Pressure Measured by Oscillometry from the Supraorbital Artery and Invasively from the Radial Artery," *Journal of Clinical Monitoring*, vol. 14, Feb. 1998, pp. 113-117.

[14] A. Bur, M.M. Hirschl, H. Herkner, E. Oschatz, J. Kofler, C. Woisetschlagerm A.N. Laggner, "Accuracy of Oscillometric Blood Pressure Measurement According to the Relation Between Cuff Size and Upper-Arm Circumference in Critically Ill Patients," *Critical Care Medicine*, vol. 28, Feb. 2000, pp. 371-376.

[15] C.M. Masi, L.C. Hawkley, E.M. Rickett, J.T. Cacioppo, "Respiratory Sinus Arrhythmia and Diseases of Aging: Obesity, Diabetes Mellitus and Hypertension," *Biological Physiology*, vol. 74, Feb. 2007, pp. 212-223.

[16] L.A. Geddes, M. Voelz, C. Combs, D. Reiner, C.F. Babbs, "Characterization of the Oscillometric Method for Measuring Indirect Blood Pressure," *Annals of Biomedical Engineering*, vol. 10, Nov. 1982, pp. 271-280.

[17] H. Sorvoja, R. Myllyla, P. Karja-Koskenkari, J. Koskenkari, M. Lilja, A. Kesaniemi, "Accuracy Comparison of Oscillometric and Electronic Palpation Blood Pressure Measuring Methods Using Intra-Arterial Method as a Reference," *Molecular and Quantum Acoustics*, vol. 26, 2005, pp. 235-260.

[18] J.C.T.B. Moraes, M. Cerulli, P.S. Ng, "Development of a New Oscillometric Blood Pressure Measurement System," *IEEE Computers and Cardiology*, Hannover, Germany, Sep. 1999, pp. 467-470.

[19] V. Jazbinsek, J. Luznik, Z. Trontelj, "Non-Invasive Blood Pressure Measurements: Separation of the Arterial Pressure Oscillometric Waveform from the Deflation Using Digital Filtering,"*IFBME Proceedings of EMBEC'05*, Prague, Czech Republic, Nov. 2005.

[20] J.N. Amoore, "Extracting Oscillometric Pulses from the Cuff Pressure: Does it Affect the Pressures Determined by Oscillometric Blood Pressure Monitors?," *Blood Pressure Monitoring*, vol. 11, Oct. 2006, pp. 269-279.

[21] A. Ball-llovera, "An Experience in Implementing the Oscillometric Algorithm for the Non-Invasive Determination of Human Blood Pressure," *Proceeding of the 25th Annual International Conference of the IEEE Engineering in Medicine and Biology Society*, Cancun, Mexico, Sep. 2003.

[22] G. Gersak, V. Batagelj, J. Drnovsek, "Oscillometric Virtual Instrument for Blood Pressure Measurement," *XVIII Imeko World Congress*, Rio de Janeiro, Brazil, Sep. 2006.

[23] P. Shaltis, A. Reisner, H. Asada, "Calibration of the Photoplethysmogram to Arterial Blood Pressure: Capabilities and Limitations for Continuous Pressure Monitoring," *27th Annual International Conference of the IEEE/IMBS*, Shanghai, China, Sep. 2005.

[24] P.D. Baker, D.R. Westenskow, K. Kuck, "Theoretical Analysis of Non-Invasive Oscillometric Maximum Amplitude Algorithm for Estimating Mean Blood Pressure," *Medical and Biological Engineering*, vol. 35, May 1997, pp. 271-278.

[25] J.Y. Lee, J.K. Kim, G. Yoon, "Digital Envelope Detector for Blood Pressure Measurement Using an Oscillometric Method," *Journal of Medical Engineering & Technology*, vol. 26, May 2002, pp. 117-112.

[26] S. Colak, C. Isik, "Fuzzy Pulse Qualifier," *Proceeds of the 23rd International Conference of the North American Fuzzy Information Processing Society*, Banff, Canada, June 2004, pp. 850-853.

[27] C.T. Lin, S.H. Liu, J.J. Wang, Z.C. Wen,"Reduction of Interference in Oscillometric Arterial Blood Pressure Measurement Using Fuzzy Logic," *IEEE Transactions on Biomedical Engineering*, vol. 50, Apr. 2003, pp. 432-441.

[28] L.T. Hersh, B. Friedman, R. Medero, "Method for Oscillometric Blood Pressure Determination Employing Curve Fitting," US Patent 5 704 362, Jan. 6, 1998.

[29] H. Chunbao, L. Lingjiao, "Technique Research and System Design of Ambulatory Blood Pressure Monitoring," *8th Internation Conference on Electronic Measurement Instruments*, Xian, China, Jul.-Aug. 2007, pp. 669-672.

[30] C.H. Nelson, T.J. Dorsett, C.L. Davis, "Method for Noninvasive Blood-Pressure Measurement by Evaluation of Waveform-Specific Area Data," US Patent 4 889 133, Dec. 26, 1989.

[31] R. Medero, "Determination of Oscillometric Blood Pressure by Linear Approximation," US Patent 5 577 508, Nov. 26, 1996.

[32] J. Erlanger, "Studies in Blood Pressure Estimations by Indirect Methods I. The Mechanism of the Oscillatory Criteria," *American Journal of Physiology*, vol. 39, 1916, pp. 401-446.

[33] W.T. Link, "Method of and Appatus for Determining the Diastolic and Systolic Blood Pressure of a Patient," US Patent 4 712 563, Dec. 15, 1987.

[34] J. Jilek, "Physiology of Oscillometric Blood Pressure Measurement," unpublished.

[35] H. Sorvoja, R. Myllyla, "Noninvasive Blood Pressure Measurement Methods," *Molecular and Quantum Acoustics*, vol. 27, 2006, pp. 239-264.

[36] J. Jilek, T. Fukushima, "Oscillometric Blood Pressure Measurement: The Methodology, Some Observations and Suggestions," *Biomedical Instrumentation & Technology*, vol. 39, May. 2005, pp. 237-241.

[37] S. Hales, *Statistial Essays*, vol. 2, London, W. Innys, 1733.

[38] S. Iamratanakul, J. McNames, B. Goldstein, "Estimation of Respiration from Physiologic Pressure Signals," *Proceeding of the 25th Annual International Conference of the IEEE Engineering in Medicine and Biology Society*, Cancun, Mexico, Sep. 2003, pp. 2734-2737.

[39] S. Bruno, P. Scalart, "Estimation of Cardiac and Respiratory Rhythms Based on an AMFM Demodulation and an Adaptive Eigenvector Decomposition," *13th European Signal Processing Conference*, Antalya, Turkey, Sep. 2005.

[40] S. Tiinanen, M. Tulppo, T. Seppanen, "Reducing the Effect of Respiration in Baroreflex Sensitivity Estimation with Adaptive Filtering," *IEEE Transactions in Biomedical Engineering*, vol. 55, Jan. 2008, pp. 51-59.

[41] G.B. Moody, R.G. Mark, A. Zoccola, S. Mantero, "Derivation of Respiratory Signals from Multi-lead ECGs," *Computers in Cardiology*, vol. 12, 1985, pp. 113-116.

[42] M. Varanini, M. Emdin, F. Allegri, M. Raciti, F. Conforti, A. Macerata, A. Taddei, R. Francesconi, G. Kraft, A.L. Abbate, C. Marchesi, "Adaptive Filtering of ECG Signal for Deriving Respiratory Activity," *Proceedings in Computers in Cardiology 1990*, Chicago, IL, Sep. 1990, pp. 621-624.

[43] J. Felblinger, C. Boesch, "Amplitude Demodulation of the Electrocardiogram Signal (ECG) for Respiration Monitoring and Compensation during MR Examinations," *Magnetic Resonance in Medicine*, vol. 38, July 1997, pp. 129-136.

[44] J.M. Kim, J.H. Hong, N.J. Kim, E.J. Cha, T.S. Lee, "Two Algorithms for Detecting Respiratory Rate from ECG Signal," *World Congress on Medical Physics and Biomedical Engineering 2006*, Seoul, Korea, Aug. 2006, pp. 4069-4071.

[45] S. Chen, V. Groza, M. Bolic, H. Dajani, "Assessment of Algorithms for Oscillometric Blood Pressure Measurement," *IEEE Internation Instrumentation and Measurement Technology Conference I²MTC 2009*, Singapore, May 2009, pp. 1763-1767.

[46] S. Chen, M. Bolic, V. Groza, H. Dajani, I. Batkin, S. Rajan, "Improvement of Oscillometric Blood Pressure Estimates Through Suppression of Breathing Effects,"

IEEE International Instrumentation and Measurement Technology Conference I²MTC 2010, Austin, Texas, May 2010, pp. 1238-1243.

[47] S. Chen, M. Bolic, V. Groza, H. Dajani, I. Batkin, S. Rajan, "Extraction of Breathing Signal and Estimation of RSA from Oscillometric Blood Pressure Measurements," *IEEE Transactions on Instrumentation and Measurements* [submitted: June 20, 2010].

[48] K. Soueidan, S. Chen, H. Dajani, M. Bolic, V. Groza, "The Effect of Blood Pressure Variability on the Estimation of the Systolic and Diastolic Pressures," *International Workshop on Medical Measurements and Applications 2010*, Ottawa, Canada, Apr.-May. 2010, pp. 14-18.

[49] K. Soueidan, H. Dajani, M. Bolic, V. Groza, S. Chen, "Characterization of the Statistical Variability of Systolic and Diastolic Blood Pressure," *The 33rd Conference of the Canadian Medical and Biological Engineering Society*, Vancouver, Canada, June 2010.

[50] S. Ahmad, S. Chen, K. Soueidan, I. Batkin, M. Bolic, H. Dajani, V. Groza, "A Prototype of an Integrated Blood Pressure and Electrocardiogram Device for Multi-Parameter Physiologic Monitoring," *IEEE International Instrumentation and Measurement Technology Conference I²MTC 2010*, Austin, Texas, May 2010, pp. 1244-1249.

[51] ANSI/AAMI SP10: 2002/A1:2003/(R)2008/A2:2006/(R)2008, "Manual, Electronic or Automated Sphygomanometers," Association for the Advancement of Medical Instrumentation, 2008.

[52] D. Benitez, P.A. Gaydecki, A. Zaidi, A.P. Fitzpatrick, "The Use of the Hilbert Transform in ECG Signal Analysis," *Computers in Biology and Medicine*, vol. 31, Sep. 2001, pp. 399-406.

[53] H.S. Shin, C. Lee, M. Lee, "Adaptive Threshold Method for the Peak Detections of Photoplyethysmographic Waveform," *Computers in Biology and Medicine*, vol. 39, Dec. 2009, pp. 1145-1152.

[54] W.P. Holsinger, K.M. Kempner, M.H. Miller, "A QRS Preprocessor Based on Digital Differentiation," *IEEE Transactions on Bio-Medical Engineering*, vol. 3, May 1971, pp. 212-217.

[55] B.U. Kohler, C. Hennig, R. Orglmeister, "QRS Detection Using Zero Crossing Counts," *Progress in Biomedical Research*, vol. 8, Sep. 2003, pp. 138-145.

[56] P.G. Yong, L.A. Geddes, "The Effect of Cuff Pressure Deflation Rate on Accuracy in Indirect Measurement of Blood Pressure With the Auscultatory Method," *Journal of Clinical Monitoring*, vol. 3, July 1987, pp. 155-159.

[57] H.S. Choi, H.D. Park, K.J. Lee, "Motion Artifact Reduction in Blood Pressure Signals Using Adaptive Digital Filter with a Capacitive Sensor," *Proceedings of the 29th Annual International Conference of the IEEE Engineering in Medicine and Biology Society*, Cite Internationale, Lyon, France, Aug. 2009, pp. 3285-3284.

[58] S. Iamratanakul, J. McNames, B. Goldstein, "Estimation of Respiration from Physiologic Pressure Signals," *Proceedings of the 25th Annual International Conference of the IEEE Engineering in Medicine and Biology Society*, Cancun, Mexico, Sep. 2003, pp. 2734-2737.

[59] S. Bruno, P. Scalart, "Estimation of Cardiac and Respiratory Rhythms Based on an AMFM Demodulation and an Adaptive Eigenvector Decomposition," *13th European Signal Processing Conference*, Antalya, Turkey, Sep. 2005.

[60] A.C. Dornhorst, P. Howard, G.L. Leathart, "Respiratory Variation in Blood Pressure," *Circulation*, vol. 6, 1952, pp. 553-558.

[61] Doohan, James (1999, Sept. 17), "Lesson 4: Circulatory System" in *BioMed 108 – Human Physiology*, [Online]. Available: http://www.biosbcc.net/doohan/sample/htm/COandMAPhtm.htm.

[62] Nolan, Robert (2003), "Heart Rate Variability," *Behavioural Medicine Institute of Australia* [Online]. Available: http://www.behavioural-medicine.com/articles/hrv/001.html

[63] J.A. Hirsch, B. Bishop, "Respiratory Sinus Arrhythmia in Humans: How Breathing Pattern Modulates Heart Rate," *American Journal of Phyiology Heart and Circulatory Physiology*, vol. 241, Oct. 1981, pp. 620-629.

[64] G.G. Bernstson, J.T. Cacioppo, K.S. Quigley, "Respiratory Sinus Arrhythmia: Autonomic Origins, Physiological Mechanisms and Psychophysiological Implication," *Psychophysiology*, vol. 30, Mar. 1993, pp. 183-196.

[65] G. Parati, J.P. Saul, M. Di Rienzo, G. Mancia, "Spectral Analysis of Blood Pressure and Heart Rate Variability in Evaluating Cardiovascular Regulation," *Hypertension*, vol. 25, Feb. 1995, pp. 1276-1286.

[66] S.I. Ando, H. Dajani, F. Floras, "Frequency Domain Characteristics of Muscle Sympathetic Nerve Activity in Heart Failure and Healthy Humans," *American Journal of Phyioslogy – Regulatory, Integrative and Comparative Physiology*, vol. 273, July 1997, pp. 205-212.

[67] T.T. Shannon, J. McNames, M.S. Ellensy, B. Goldstein, "Modeling Respiration from Blood Pressure Waveform Signals: An Independent Component Approach," *Proceedings of the Second Joint EMBS/BMES Conference 2002*, Houston, Texas, Oct. 2002, pp. 200-201.

[68] R.E. De Meersman, A.S. Zion, S. Teitelbaum, J.P. Weir, J. Lieberman, J. Downey, "Deriving Respiration from Pulse Wave: A New Signal-Processing Technique," *American Journal of Phiosology – Heart and Circulatory Physiology*, vol. 270, May 1996, pp. 1672-1675.

[69] A. Johansson, C. Ahlstrom, T. Lanne, P. Ask, "Pulse Wave Transit Time for Monitoring Respiration Rate," *Medical and Biological Engineering and Computing*, vol. 44, June 2006, pp. 471-478.

[70] S. Haykin, Adaptive Filter Theory 4th ed. Upper Saddle River: Prentice Hall, 2001.

[71] D.V.B. Rao, S.Y. Kung, "Adaptive Notch Filtering for the Retrieval of Sinusoids in Noise," *IEEE Transactions on Acoustics, Speech, and Signal Processing*, vol. 32, Aug. 1984, pp. 791-802.

[72] V.K. Pandey, P.C. Pandy, "Cancellation of Respiratory Artifact in Impedance Cardiography," *Proceedings of the 27th Annual International Conference of the IEEE Engineering in Medicine and Biology Society*, Shanghai, China, Sep. 2005, pp. 5503-5506.

[73] M.V. Pitzalis, F. Mastropasqua, F. Massari, A. Passantino, R. Colombo, A. Mannarini, C. Forleo, P. Rizzon, "Effect of Respiratory Rate on the Relationships between RR Interval and Systolic Blood Pressure Fluctuations: A Frequency-Dependent Phenomenon," *Cardiovascular Research*, vol. 38, May 1998, pp. 332-339.

[74] P. Calabrese, H. Perrault, T.P. Dinh, A. Eberhard, G. Benchetrit, "Cardiorespiratory Interactions during Resistive Load Breathing," *American Journal on Physiolgy – Regulatory, Integrative and Comparative Physiology*, vol. 279, Dec. 2000, pp. 2208-2213.

[75] B.H. Taha, P.M. Simon, J.A. Dempsey, J.B. Skatrud, C. Iber, "Respiratory Sinus Arrhythmia in Humans: an Obligatory Role for Vagal Feedback from the Lungs," *Journal of Applied Physiology*, vol. 78, Feb. 1995, pp. 628-645.

[76] *IEEE Standard on Transitions, Pulses and Related Waveforms*, IEEE Std 181, 2003.

[77] B.H. McGhee, E.J. Bridges, "Monitoring Arterial Blood Pressure: What You May Not Now," *Critical Care Nurse*, vol. 22, Apr. 2002, pp. 60-78.

[78] V. Cizek, "Discrete Hilbert Transform," *IEEE Transactios on Audio and Electroacoustics*, vol. AU-18, Dec. 1970, pp. 340-343.

[79] T. Opthof, "The Normal Range and Deteminants of the Intrinsic Heart Rate in Man," *Cardiovascular Research*, vol. 45, Jan. 2000, pp. 177-184.

[80] B. Boashash, "Estimating and Interpreting the Instantaneous Frequency of a Signal. II. Algorithms and Applications," *Proceedings of the IEEE*, vol. 80, Apr. 1992, pp. 540-568.

[81] C.K. Peng, J.E. Mietus, Y. Liu, C. Lee, J.M. Hausdorff, H.E. Stanley, A.L. Goldberger, L.A. Lipsitz, "Quantifying Fractal Dynamics of Human Respiration: Age and Gender Effects," *Annals of Biomedical Engineering*, vol. 30, May 2002, pp. 683-692.

[82] B. Buttkus, "Homomorphic Filtering – Theory and Practice", *Geophysical Prospecting*, vol. 23, 1975, pp. 712-748.

[83] J. Choi, S. Hong, R. Nelesen, W.A. Bardwell, L. Natarajan, C. Schubert, J.E. Dimsdale, "Age and Ethnicity Differences in Short-Term Heart-Rate Variability," vol. 68, May 2006, pp. 421-426.

[84] Wolfram MathWorld (2010, Apr. 30), "Cauchy Distribution" in *Probability and Statistics*, [Online]. Available: http://mathworld.wolfram.com/CauchyDistribution.html.

[85] W.D. McArdle, F.I. Katch, V.L. Katch, *Exercise Physiology: Energy, Nutrition, and Human Physiology*, Lippincott Williams & Wilkins, 2006, pp. 270.

[86] R. Bailon, L. Sornmo, P. Laguna, "A Robust Method for ECG-based Estimation of the Respiratory Frequency During Stress Testing," *IEEE Transactions on Biomedical Engineering*, vol. 53, Jul. 2006, pp. 1273-1285.